1-1-2004

Morphologies and tensile properties of block copolymers with different molecular architectures.

Yuqing, Zhu
University of Massachusetts Amherst

MORPHOLOGIES AND TENSILE PROPERTIES OF BLOCK COPOLYMERS WITH DIFFERENT MOLEULCAR ARCHITECTURES

A Dissertation Presented

by

YUQING ZHU

Submitted to the Graduate School of the
University of Massachusetts Amherst in partial fulfillment
of the requirements for the degree of

DOCTOR OF PHILOSOPHY

February 2004

Polymer Science and Engineering

MORPHOLOGIES AND TENSILE PROPERTIES OF BLOCK COPOLYMERS WITH DIFFERENT MOLECULAR ARCHITECTURES

A Dissertation Presented

by

YUQING ZHU

Approved as to style and content by:

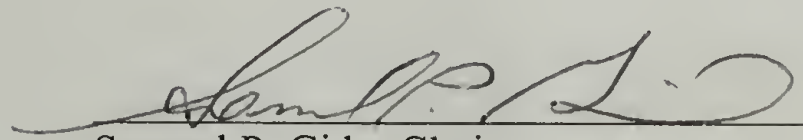

Samuel P. Gido, Chair

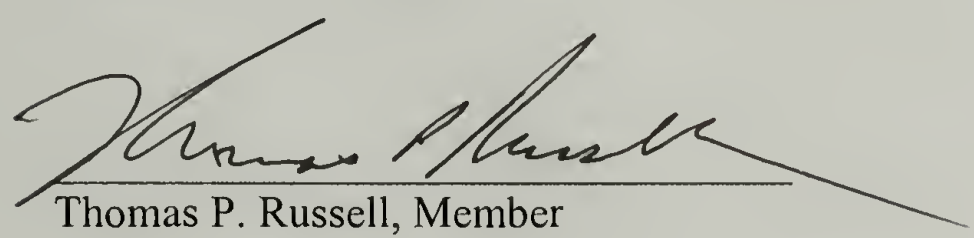

Thomas P. Russell, Member

H. Henning Winter, Member

Thomas J. McCarthy, Department Head
Polymer Science & Engineering

DEDICATION

To my parents, for their love and support.

ACKNOWLEDGEMENTS

It has been my greatest pleasure to work for my dissertation advisor, Prof. Samuel P. Gido. I have learned much from Sam in many aspects of scientific researches. I thank him for his kindness and patient guidance. Prof. Thomas P. Russell is not only my committee member but also my co-advisor in some extent. His guidance is not limited to polymer thin films, but to extend of all my research works. Prof. H. Henning Winter serves as my committee member during the course of my dissertation research, and I owe him many thanks for his valuable time and input.

A number of people have significant contribution to the studies described in this dissertation. Prof. Nikos Hadjichristidis, Prof. Hermis Iatrou, Dr. Gabriel Velis, and Maria Moshakou at the University of Athens, Greece, synthesized most of the block copolymer materials. Prof. Jimmy W. Mays and Dr. David Uhrig at the University of Tennessee, Knoxville, provided the multigraft copolymer samples. Finally, Dr. Roland Weidisch at the University of Dresden in Germany conducted the tensile testing on the block copolymer materials. Our collaboration extended to several other projects since then.

It has been a wonderful experience to work in this department and in Gido's research group. Dr. Ken Laverdure, who has been my officemate for years, taught me most of the fundamental techniques in morphological studies. Lou Raboin is a very skilled microscopist and I learned a lot of techniques from him during my Ph.D. study.

Friends supported me in various ways. I am grateful to Prof. Ted Atkins for the support and kindness he has bestowed upon me. Dr. Huiqing Zhang has been one of my close friends in UMass for all these years. Accompanied by these two friends, I climbed up to the top of Mountain Equinox (Vermont) in a cold Feburary morning in year 2002. Dr. Chuntao Cao has been the one to share some late-night discussions in my early years in PSE. A lot good time has been shared with my friends, Sungkyun, Jongyoung, and Shujun, to name a few of them.

Much gratitude is toward my parents. I appreciate their effort in bringing me up and educating me during their most difficult time. The effort has greatest impact on my life and encourages me to try harder. They are the few knowing that I can do it. I would also like to thank my sister Yucheng and my brother-in-law Kai. Their help has accompanied me every step of my life.

ABSTRACT

MORPHOLOGIES AND TENSILE PROPERTIES OF BLOCK COPOLYMERS WITH DIFFERENT MOLECULAR ARCHITECTURES

FEBRUARY 2004

YUQING ZHU, B.S., JILIN UNIVERSITY

Ph.D., UNIVERSITY OF MASSACHUSETTS AMHERST

Directed by: Professor Samuel P. Gido

The effects of molecular architecture on morphological behavior of block copolymers for four types of architectures have been investigated. In Chapter 2, the morphological behaviors of a group of polystyrene-polybutadiene $(PS\text{-}PBD)_C$ cyclic block copolymers and their corresponding linear polystyrene-polybutadiene-polystyrene (PS-PBD-PS) triblock copolymer precursors were investigated across a range of morphologies. The contour length and the volume fraction of the cyclic block copolymers obtained are essentially identical to that of their corresponding linear triblock copolymers. Therefore, morphological difference due to compositional mismatch between the cyclic and triblock copolymer pair is eliminated. It is found that when the cyclic and its triblock copolymer form the same morphology, microdomain periods of cyclic block copolymers are all smaller than those of the corresponding linear triblock copolymer precursors. This is resulted from the portion of chain segments that adopts their trajectory parallel to the interface in cyclic block copolymers and thus does not contribute to domain spacing. When different morphologies are formed between the

cyclic and triblock pairs, the interface tends to curve away from the linked end-block side in cyclics compared to their triblock copolymers.

In Chapter 3, lamellar spacings of a series of $(PS)_n(PI)_n$ star block copolymers, with n = 1, 2, 4, 16, were studied. Among the series, all the PS blocks are of same length and all the PI blocks have the same molecular weight. Lamellar spacings of the stars (n = 2, 4, 16) were compared directly with that of the diblock copolymer (n = 1). A significant increase in lamellar spacing with increasing junction point functionality (n) was found in this series of materials and can be attributed to molecular crowding near the junction point.

Chapter 4 and chapter 5 discussed the effect of chain architecture on the morphological and tensile properties of series of multigraft copolymers. By applying the "constituting block copolymer concept", the physical behavior of these molecules was compared with the existing theories. It is found that morphological behavior of grafted copolymers can be well predicted using this theoretical approach. The material property, however, is controlled by both the chain architecture and the morphologies thus formed.

TABLE OF CONTENTS

LIST OF TABLES

LIST OF FIGURES

CHAPTER 1

INTRODUCTION

1.1 Block copolymers and molecular architectures

Block copolymers are created by joining two immiscible homopolymers together. The presence of the junction point restricts phase separation in nanometer scales. As a result, a veriety of periodic nanostructures emerges.[1,2] This is the result of energy balance between the energy required to create an interface between the two microdomains, and the energy from the stretching of polymer chains away from the interface. Depending upon the volume fractions of the constituent blocks in the copolymer, lamellae, cylinders and spheres are formed.[2] More complex morphologies have also been experimentally observed.[3-6]

Linear AB diblocks represent the simplest structures among various block copolymers. With the advance in the synthetic techniques, block copolymers with well-defined but more complex architectures have been synthesized. Molecular architecture of block copolymers strongly influences their morphological properties, and consequently influences the material properties. Studying the effect of architecture toward material physical behaviors of block copolymer materials has been one of the continuing interests for years. Recently, both experimental results and theoretical calculations have been reported on block copolymers with various complex architectures, such as linear ABC triblock copolymers,[7-10] simple graft copolymers,[11,12] A_nB_n star block copolymers,[13-16]

multigraft copolymers[17,18] etc.. These studies will undoubtedly shed light on designing polymeric materials with desired properties.

1.2 Theoretical background

1.2.1 Self-assembly of linear AB diblock copolymers

Linear AB diblock copolymers represent the simplset yet well-studied system in polymer physics. Figure 1.1 is the morphology diagram calculated by Matsen and Bates.[1] This diagram predicts linear AB diblock copolymer morphology as a function of volume fraction f, and the segregation strength between the two blocks, χN, where χ is the Flory-Huggins segmental interaction parameter and the N is the total degree of polymerization of the block copolymers. Polymers A and B in this case have identical conformational behavior. It predicts the formation of the "classical" morphologies, alternating lamellae (L), hexagonally packed cylinders (H), body-centered cubic spheres (S), as well as more complicated morphologies such as the "gyroid" cubic bicontinuous morphology ($Q_{Ia\bar{3}d}$). Below a critical level of $\chi N = 10.5$ for a block copolymer with equal volume fractions of A and B, a diblock copolymer is predicted to be homogenous or disordered. The symmetry of this diagram is strongly affected by the conformational asymmetry due to the difference in space filling characteristics between the two blocks.[19-21] When one of the blocks is beyond certain stiffness, the diblock will no longer behave as *Gaussian coil* as usual amorphous diblock copolymers. The system becomes more complicated to elucidate.

Three regimes in Figure 1.1 are commonly defined. These are the weak

segregation limit (WSL, $\chi N < 15$), the intermediate segregation limit (ISL, $15 < \chi N < 100$), and the strong segregation limit (SSL, $\chi N > 100$). The divisions between these regimes are based on the change in scaling behavior of mesophase period with degree of polymerization, wich is also accompanied by the change in the mass distribution around interface.[22] For the purposes of most block copolymer morphology studies, samples that fall in the SSL are preferred as their behavior has been most extensively modeled and examined. In the SSL, the interface between the microphase-separated domains is sharp between essentially pure domains of components A and B. This condition, utilized by Helfand as the narrow interphase approximation[23] is only possible when the unfavorable enthalpic interactions dominate the free energy of the system.

1.2.2 Self-assembly of AB cyclic copolymers

The morpholgical behavior of the cyclic block copolymer melts is almost the same as that of the linear AB diblocks.[24,25] However, the mean-field critcal point for cyclic block copolymers is $\chi N = 17.8$.[26] The higher critical point is resulted from the close contour shape, which supresses the random thermal fluctuation. Thus, cyclic block copolymers still show a mean-field behavior at the temperature at which the linear diblock copolymers do not obey the mean-field prediction. Another difference is a big compositional rane $f = 0.33 - 0.67$, where direct transition from disordered to hexagonal cylinders occurs in the cyclyc block copolymer systems. Phase diagram of AB cyclic block copoylmers is shown in Figure 1.2. With increase of the *N* parameter the following sequence of transitions takes place: DIS fcc(0.24), BCC(0.33), HEX, GYR(0.39), LAM. The number in brackets indicates the compositional limit of stability of the corresponding

phase.

1.2.3 Self-assembly of linear ABA triblock copolymers

The ABA triblock copolymers can be considered to be the result of linking two AB diblocks together. Morphological behavior of such ABA triblock is slightly different to that of AB diblocks at low segregation limit, and gradually become identical in SSL.[27,28] The diagram for an ABA triblock with degree of polymerization at 2N is shown in Figure 1.3. The critical χN for such ABA triblocks is around 18.0, and shifts slightly to the lower volume fraction of the end-blocks. The higher value of χN is due to the increase of degree of polymerization in ABA triblocks comparing to AB diblocks with half of the molecular weight.[29] Entropically it is more difficult to confine two A blocks into microdomains than a single B block. As the matrix component, the central B blocks must deform more to accommodate the A blocks into A domains.

Confinement of the two junction points around interface leads to the bridged and/or single-looped chain conformation in ABA triblocks. The bridged conformation allows coupling between different microdomains and thus enhances energy transfer among them. It has been found that about 40% of the molecules adopt bridged conformation in lamellar morphologies over a wide range of χN.[30,31]

1.2.4 Milner's theory

For simple graft copolymers, where two A polymer blocks and one B block are connected at one central junction point, their morphological behaviors are predicted by

Milner's theory.[32] Figure 1.4 shows the morphological diagram generated using Milner's theory for A_nB_m type of block copolymers characterized by volume fraction, ϕ_B, and the unified molecular asymmetry parameter, ε. The molecular asymmetry comprises the information of molecular architecture and elastic asymmetry that are inherent in both polymer blocks. The molecular asymmetry parameter is defined as:

$$\varepsilon = \left(\frac{n_A}{n_B}\right)\cdot\left(\frac{l_A}{l_B}\right)^{1/2} = \left(\frac{n_A}{n_B}\right)\cdot\left(\frac{\frac{V_A}{R_A^{\,2}}}{\frac{V_B}{R_B^{\,2}}}\right)^{1/2} = \left(\frac{n_A}{n_B}\right)\cdot\left(\frac{\frac{v_A}{b_A^{\,2}}}{\frac{v_B}{b_B^{\,2}}}\right)^{1/2}$$

where n_i is the number of arms of component *i*, and l_i is a material parameter describing the conformational behavior of component *i*. This material parameter is defined as $l_i = V_i/(R_i^2)$, where V_i is the volume of component *i* having radius of gyration, R_i. Both terms are proportional to chain length, N, and the equation defining ε reduces to a function of arm number, n_i, segmental volume, v_i, and statistical segment length, b_i.

The model predicts that the volume fraction range in which a given morphology is predicted to emerge shift to higher volume fraction with increasing molecular asymmetry. This arises from the effect of confining multiple arms to one side of an interface. Hence, nonlinear copolymers are capable of producing microstructures that cannot be obtained by linear diblock copolymers at similar volume fractions.

1.2.5 Constituting block copolymer concept

While various morphology diagrams are helpful in predicting microstructures formed by block copolymers with respective architectures, they are unable to render

information directly to copolymers with more complicated structures. One of the approaches to study morphological behavior of materials with complex structures is to utilize the "*constituting block copolymer hypothesis*".[13,14,18,33-35] This approach proposes that the morphological behavior of the material can be estimated by their building blocks associated with each junction points. These building blocks, also called constituting block copolymer units (CBU), are mapped onto appropriate morphology diagrams according to their molecular characteristics. Graphically, these building blocks can be obtained by cutting the polymer backbones at the middle of the adjacent junction points. If the junction points are regularly placed along the backbone, the half of the backbone spacer (backbone length between adjacent junction points) is used for calculating the molecular characteristics of the CBU. However, if the placement of junction points is random, the averaged backbone spacer is employed for calculation. Figure 1.5 illustrates such approach on a multigraft copolymer with random placement of the tetrafunctional junction points.

1.3 General procedures in morphological characterization of block copolymers

Solutions of about 3-5 weight percent copolymers in toluene were prepared. Bulk films about 1 mm thick were obtained by slowly evaporating the solvent from these solutions over 14 days at room temperature. The dried films thus obtained were annealed at 120 °C under vacuum for 7 days to promote equilibrium structures. All samples for transmission electron microscopy (TEM) study were microtomed using a Leica Ultracut UCT cryoultramicrotome. Thin sections 40 - 80 nm in thickness were cut with a Diatome diamond knife at a sample temperature of -110 °C and a knife temperature of -100 °C.

These sections were collected on TEM grids and stained in OsO_4 vapor for 6 hours. TEM was performed on a JEOL 100 CX, operated at an accelerating voltage of 100 kV.

Small angle X-ray scattering (SAXS) data was collected, at the University of Massachusetts-Amherst (UMass), using Ni-filtered Cu-K_α radiation (1.54 Å wavelength) from a Rigaku rotating anode operated at 40 kV, 200 mA. The primary beam was collimated by a set of three pinholes. A gas-filled area detector (Siemens Hi-Star), located 87.52 cm from the sample, was used to record scattering patterns. The flight path between the sample and the detector was evacuated.

1.4 General procedures of tensile testing on block copolymers

Tensile testing was performed using a universal-testing machine Instron 1123 with a 1000 N load cell at a crosshead speed of 15 mm/min. Dogbone specimens of 0.7 mm thick were stamped from the same pieces of cast and annealed film that were used for TEM and SAXS studies with a standard die having 20 mm gauge length. Crosshead separation was used to quantify strain. Material Stress vs. Strain curves were produced by utilizing engineering stresses, based on the measured initial cross-section dimensions of these specimens. For each material, at least 10 tests were performed.

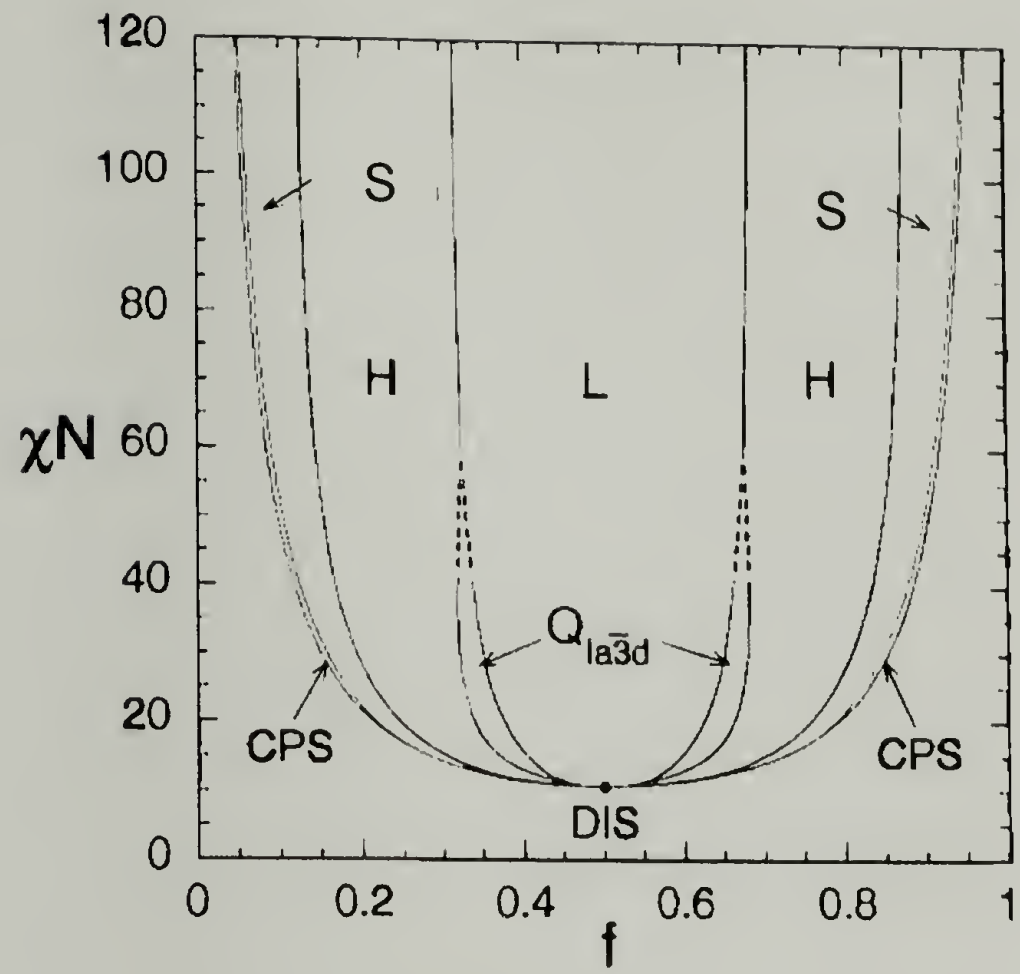

Figure 1.1 Morphology diagram of linear AB diblock copolymers.

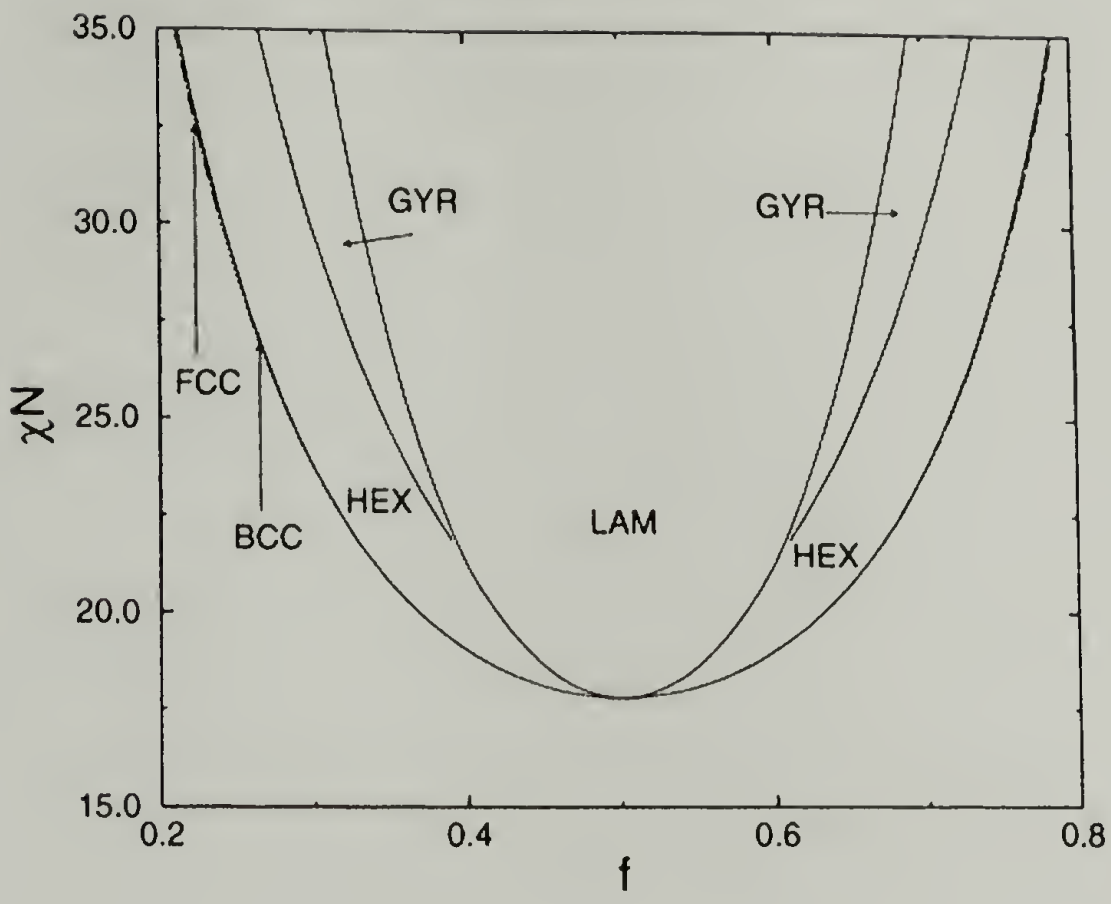

Figure 1.2 Phase diagram of cyclic block copolymers.

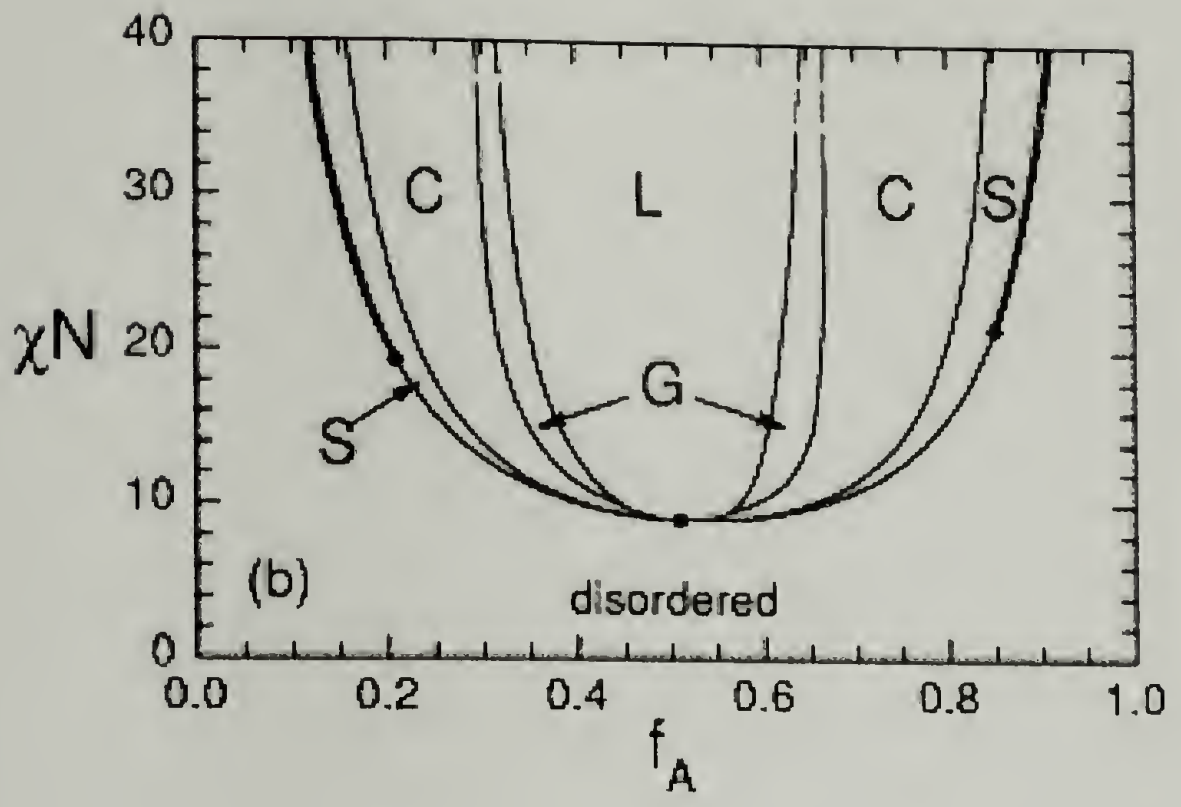

Figure 1.3 Mean-field phase diagram for melts of symmetric ABA triblock copolymers with the degree of polymerization of 2N. Segregation strength χN is plotted against volume fraction of the end-blocks A.

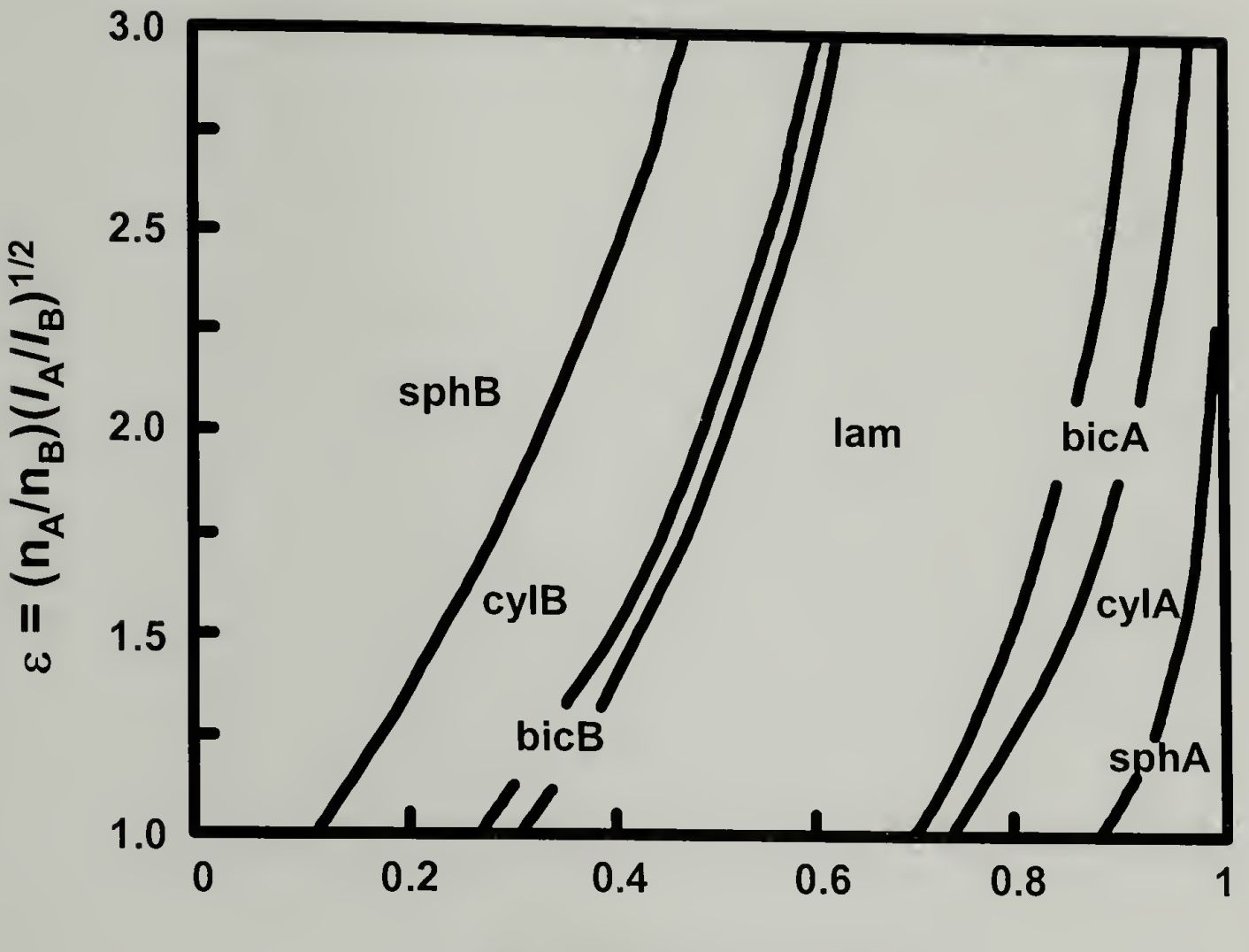

Figure 1.4 Milner's phase diagram in the strong-segregation limit for A_nB_m star block copolymers with n arms of A block, and m arms of B. Morphology is given for the volume fraction of the B component, ϕ_B, and molecular asymmetry parameter, ε.

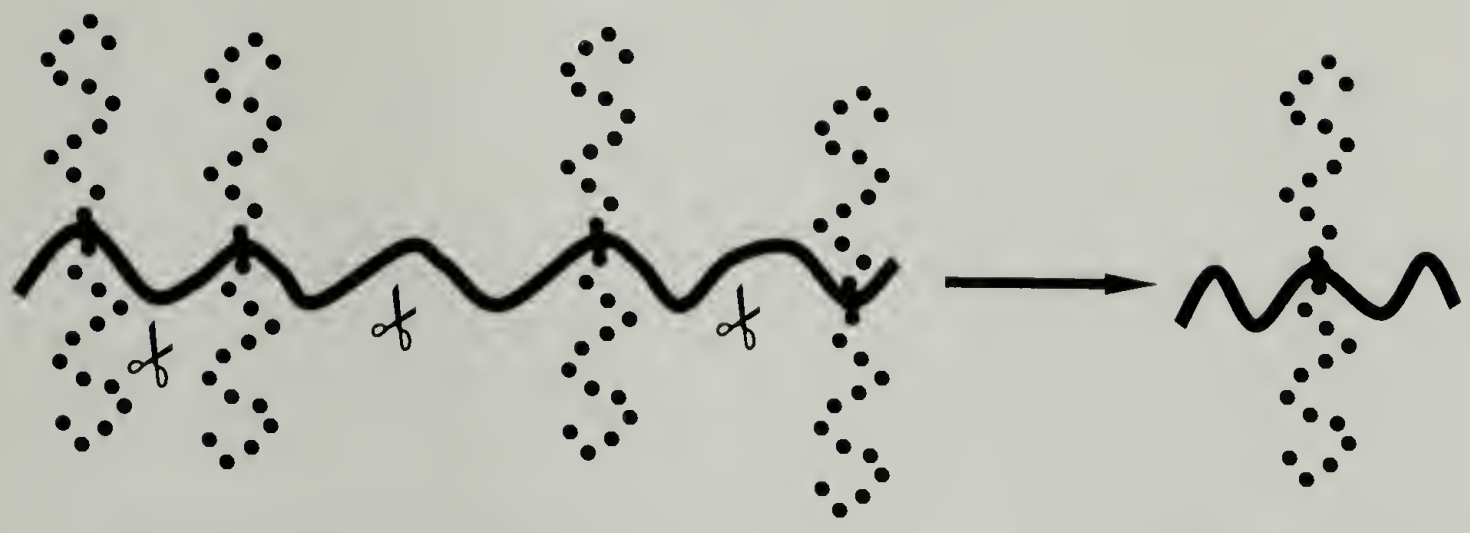

Figure 1.5 Illustration of "*constituting block copolymer concept*" approach on a multigraft copolymer with randomly placed junction points along the polymer backbone.

CHAPTER 2

MORPHOLOGICAL BEHAVIORS OF AB CYCLIC BLOCK COPOLYMERS AND THEIR LINEAR ABA TRIBLOCK COPOLYMER PRECURSORS

2.1 Abstract

A series of five cyclic block copolymers of styrene and butadiene, having essentially the same molecular weight (52 ± 5 Kg/mol) and PS volume fraction varying from 11 to 70%, were synthesized by cyclization of α,ω-dilithium polystyrene-polybutadiene-polystyrene triblock copolymers with bis(dimethylchlorosilyl)ethane. The cyclic block copolymers thus obtained have practically the same molecular weight and composition as their corresponding linear triblock copolymers. All materials were investigated via transmission electron microscopy (TEM) and small angle X-ray scattering (SAXS) techniques. In three cases where the cyclic and the corresponding linear block copolymer had the same morphology, the domain spacings of the cyclic block copolymers are found to be 84% - 89% of those of their respective linear triblock copolymers. In the other two cases different morphologies are found in the cyclic and its corresponding triblock copolymer. Comparing to their linear triblocks, the interfaces are curved away from the connected end blocks.

2.2 Introduction

When the two chain ends of a linear ABA triblock copolymer are linked to each other, a cyclic AB block copolymer is formed. The molecular architectures of the ABA

triblock and AB cyclic block copolymers are illustrated in Figure 2.1. Due to their unique closed contour shape, cyclic block copolymers possess distinctively different solution properties[36,37] and microdomain-forming properties[24,25,38-40] than linear block copolymer counterparts.

In the microphase-separated states, because of their molecular architecture, an AB cyclic block copolymer can only adopt a double-looped conformation, where both polymer blocks form loops in their respective domains and the two junction points between the blocks reside at the same interface. On the other hand, ABA triblock copolymers can form either single-loops and/or bridged conformations.[38] Therefore, an ABA triblock copolymer may have its junction points confined at one same interface (loops) or at two different interfaces (bridges). It has been found that,[30,31,41] the percentage of triblock copolymers forming bridges in the lamellar morphology is around 40% over a wide range of χN, where χ is the *Flory-Huggins* interaction parameter and N the total degree of polymerization.

Cyclic block copolymers have been found to have smaller lamellar long periods than their corresponding linear copolymers. *Marko* discussed the microphase separation of cyclics and diblock copolymers of the same composition and molecular weight, and concluded that the lamellar spacing ratio of a cyclic to its corresponding diblock copolymer is about 0.67 in the strong segregation limit.[26] More recently *Jo and Jang*,[24] by using Monte Carlo simulations, found that the ratio of the domain spacing between the cyclic diblock copolymer and the corresponding linear diblock is 0.7. The lamellar

spacing ratio was predieted, by *Thomas et al,*[38] to be weakly dependent on χN and to vary between 0.60 and 0.62 for dibloek copolymer and between 0.90 and 0.98 for the triblock eounterparts. Their experimental results on eyelie PS-PDMS and PS-P2VP and the eorresponding triblocks agree well with the prediction. Since the cyclie bloek eopolymers possess a double-looped eonformation, a non-negligible fraetion of chain segments must have their trajeetories parallel to the lamellar layers in both mierodomains. Thus, this fraction of the segments does not eontribute to lamellar long period in the normal dirceion of lamellar and consequently a decrease in lamellar long period is expected.

Previous research eomparing the domain spacings of the eyclie and triblock eopolymers has been limited in lamellar morphologies. The foeus of this study is to probe the influenee of moleeular arehiteeture on their mierophase separation bchavior aeross a range of morphologies. A group of α,ω-dilithium polystyrene-polybutadiene-polystyrene (PS-PBD-PS) tribloek eopolymers were synthesized anionieally. The eyelization reaction was achieved by linking the two living ehain ends of the difunctional tribloek eopolymer preeursor under high dilution eonditions with an appropriate ehlorosilane. By this approach, the eontour length and the volume fraetions of the eyclic bloek eopolymers obtained is essentially identieal to that of its eorresponding linear tribloek eopolymers. Therefore, any morphologieal differenee due to compositional mismateh between the eyelie and eorresponding triblock eopolymers is climinated.

2.3 Experimental

2.3.1 Synthesis of the linear and cyclic block copolymers

The synthesis of the cyclic and their corresponding triblock copolymers has been presented in details elsewhere.[42] The molecular characteristics are given in Table 2.1. The materials are the same as those in ref. 42, but a different nomenclature is used here. The subscript "c" used in this study refers to cyclic block copolymer. For example, (PS-PBD)$_C$-11 represents the cyclic block copolymer with 0.11 PS volume fraction, while the PS-PBD-PS-11 refers to its corresponding linear triblock. As indicated in Table 1, cyclics and their corresponding triblock copolymers with 0.40, 0.51, and 0.70 PS volume fractions have deuterated PS blocks while the other materials have protonated PS blocks.

2.3.2 Morphological characterization

The morphological characteristics of these cyclic and triblock copolymers based on TEM and SAXS can be found in Table 2.2.

2.4 Results

As shown in Table 2.2, at PS volume fractions of 0.11, 0.24, and 0.51, the cyclics and their triblock copolymer counterparts form the same morphology. On the other hand, comparison of the morphologies of the cyclics and their corresponding triblock copolymers at 0.40 and 0.70 PS volume fractions reveals different microstructures.

PS-PBD-PS-11 and (PS-PBD)$_C$-11 both form the same morphology. The TEM image of (PS-PBD)$_C$-11 in Figure 2.2a, shows PS spheres in an osmium stained PBD

matrix. These microphase separated PS spheres appear to lack long-range lattice order. Figure 2.2b shows the small angle X-ray scattering data of PS-PBD-PS-11 and $(PS\text{-}PBD)_C$-11. Both profiles exhibit the primary reflection and one higher order scattering vector maximum. The primary scattering peak q^* suggests average correlations length of 32.7 nm for $(PS\text{-}PBD)_C$-11 and 36.8 nm for PS-PBD-PS-11. The higher q reflections in both materials are consistent with form factor scattering maxima from the spherical domains.[43] For comparison the form factor from spherical domains of the same PS volume fraction as PS-PBD-PS-11 is plotted as a solid line in Figure 2.2b.

Both PS-PBD-PS-24 and $(PS\text{-}PBD)_C$-24 form hexagonally packed PS cylinders in a PBD matrix. The TEM image of cyclic $(PS\text{-}PBD)_C$-24 is shown in Figure 2.3a, where a projection down the axes of the PS cylindrical domains is visible. SAXS data for these two samples in Figure 2.3b exhibit two Bragg reflections: a primary peak at q^* and a higher order reflection at $\sqrt{7}q^*$. As also shown in Figure 2.3b, a cylindrical form factor minimum at the volume fraction of these samples was found to attenuate the expected reflections at $\sqrt{3}$ and $\sqrt{4}$. From this SAXS data, the (100) interplanar spacing is calculated to be 34.6 nm for $(PS\text{-}PBD)_C$-24 and 41.0 nm for PS-PBD-PS-24.

Lamellae are observed in TEM images of $(PS\text{-}PBD)_C$-51 and PS-PBD-PS-51. Figure 2.4a shows a TEM image of $(PS\text{-}PBD)_C$-51. Small angle X-ray scattering data for $(PS\text{-}PBD)_C$-51 and PS-PBD-PS-51 in Figure 2.4b display the primary reflection q^*, and one higher order reflection at $3q^*$. The absence of the 2^{nd} order reflections indicates that the volume fractions of both blocks are nearly identical, which is in good agreement with

the near symmetric volume fractions. The lamellar long period of $(PS\text{-}PBD)_c$-51 and PS-PBD-PS-51 determined by the scattering primary peak q^* are 38.4 nm and 40.3 nm respectively.

At PS volume fractions of 0.40 and 0.70, the cyclics and their corresponding triblocks were found to form different morphologies. At 0.40 PS volume fraction, the cyclic $(PS\text{-}PBD)_c$-40 forms lamellae, while the triblock PS-PBD-PS-40 forms PS cylinders in a PBD matrix. Figure 2.5a shows a TEM image of $(PS\text{-}PBD)_c$-40, and Figure 2.5b shows a TEM image of PS-PBD-PS-40. Figure 2.5c shows the SAXS data for to two samples at 0.40 PS volume fraction. For $(PS\text{-}PBD)_c$-40 the observation of integrally spaced Bragg reflections at q^*, $2q^*$, and $3q^*$ is consistent with the lamellar morphology observed via TEM. For PS-PBD-PS-40 reflections at q^*, $\sqrt{7}q^*$, and $3q^*$ are consistent with the TEM observation of hexagonally packed cylinders.

A TEM image of $(PS\text{-}PBD)_C$-70 in Figure 2.6a shows a hexagonally packed PI cylindrical morphology. The SAXS data for $(PS\text{-}PBD)_C$-70, shown in Figure 2.6c, displays a higher order peak at $\sqrt{7}$ of the primary reflection q^* consistent with the cylindrical morphology observed with TEM. Figure 2.6b shows a TEM image of PS-PBD-PS-70. Figure 2.6b shows a TEM image of PS-PBD-PS-70. The image indicates a gyroid structure with poor long-range order. Small angle scattering data of PS-PBD-PS-70 in Figure 6c were only able to give the primary reflection peak. Although this gyroid structure is poorly ordered a number of characteristic TEM projections were observed. In Figure 2.6b poorly ordered versions of the "serpentine" and "wagon wheel" projections

are visible.[44]

2.5 Discussions

In the three cyclic-triblock material pairs in which the cyclic and its triblock copolymer form the same morphology, microdomain periods of cyclic block copolymers were found to be all smaller than those of the corresponding linear triblock copolymers. This result was found consistently across the three different morphologies observed: PS spheres, PS cylinders, and lamellae at PS volume fractions of 0.11, 0.24, and 0.51 respectively. These findings not only support the previous results on lamellar morphologies[38] but also extend this phenomenon to the cylindrical and spherical structures. The domain spacing ratios of cyclic to corresponding triblock copolymer (D_C/D_T) found in this study are given in Table 2.2. The ratios observed here, between 0.84 and 0.89, are lower than observed or theoretically predicted in the previous study of *Thomas et al.*[38] where all values exceeded 0.90. The error for SAXS determination of the microdomain spacings is ± 0.3 nm, resulting in an uncertainty in the D_C/D_T ratios of ± 0.02. The discrepancies between the current results and those of *Thomas et al.* are beyond the range of this uncertainty.

Series of cyclic and corresponding triblock copolymers used in this study have χN values in the range of 52-81 at room temperature and 40 - 61 at sample annealing temperature of 120 °C. Actually, the structure observed at room temperature probably reflects the state of the material at the last temperature where there is considerable sample mobility during cooling from the annealing temperature, *i.e.* the T_g of the PS blocks.

However, the χN at the annealing temperature was reported for the PS-PDMS and PS-P_2VP cyclic and triblock copolymers in Reference 3, and thus we use equivalent conditions for the comparison of our results. The ratios of D_C/D_T obtained in this study are still lower than the theoretical prediction.

When different morphologies are formed by the cyclic and corresponding triblock copolymers, there is a consistent change in the interfacial curvatures with respect to the PS end-blocks. The interface curves away from the PS end blocks when they become connected to form a cyclic analog. In PS-PBD-PS-40, the end blocks stay on the concave side of the interface in the PS cylindrical structure, while the interfaec in the lamellae of $(PS\text{-}PBD)_C$-40 becomes flat. This means that the tendency of the interface to curve away from the PS side is increased by linking the two PS end-blocks together. The same effect was also been found in triblock PS-PBD-PS-70 which forms a gyroid structure PS in the matrix and cyclic $(PS\text{-}PBD)_C$-70 which forms PBD cylinders in a PS matrix. The interfacial curvature of gyroid is intermediate between those of cylinders and lamellae. Viewed from the PS (convex) side of the interface, the lower curvature interface of the gyroid in the triblock copolymer changes into the more curved cylindrical interface in the cyclic block copolymer. It is postulated that the same chain trajectory effect that underlies the decrease in domain spacing when going from triblock to cyclic morphologies within the same morphology (PS volume fractions 0.11, 0.24, and 0.51) is also responsible for the change in interfacial curvature that drives morphology changes in samples with PS volume fractions of 0.40, and 0.70. The cyclic requires a PS block chain trajectory component parallel to the interface. This requires more PS chain volume to be

located closer to the interface and thus results in a slightly increased tendency for the interface to curve away from the PS side.

2.6 Conclusions

The morphological behavior of a series of cyclic block copolymers and their corresponding PS-PBD-PS triblock copolymers has been investigated. The architectural difference of a cyclic and its corresponding triblock copolymers leads to differences in domain spacing. The cyclic morphology always has smaller domain spacing compared to its corresponding triblock copolymer. When cyclic and triblock analogs form different morphologies, it was found that connecting the end blocks of the triblock to form the cyclic tends to increase the tendency for the interface to curve away from the connected end-blocks.

Table 2.1 Moleeular charaeteristies of the eyelic and their triblock copolymer preeursors.

Sample	$M_n \times 10^3$ [b] (PBD)	$M_n \times 10^3$ [b] (Copolymer)	M_w/M_n [c] (Copolymer)	%PS (w/w) [e] (Copolymer)	% PS (w/w) [f] (Copolymer)
$(PS\text{-}PBD)_C$-11	42.0	47.2	1.06	12	14
PS-PBD-PS-11	42.0	47.5	1.06	14	15
$(PS\text{-}PBD)_C$-24	41.5	56.5	1.07	28	32
PS-PBD-PS-24	41.5	55.9	1.07	29	30
$(PS\text{-}PBD)_C$-40*	32.0	53.5	1.09	d	44
PS-PBD-PS-40*	32.0	55.1	1.08	d	43
$(PS\text{-}PBD)_C$-51*	23.0	53.4	1.11	d	55
PS-PBD-PS-51*	23.0	53.0	1.10	d	54
$(PS\text{-}PBD)_C$-70*	16.1	58.0	1.16	d	73
PS-PBD-PS-70*	16.1	56.9	1.15	d	70

a: Polystyrene bloek is perdeuterated.
b: Membrane osmometry in toluene at 37 °C.
c: Size exelusion chromatography in THF at 25 °C with a DRI deteetor.
d: N/A, deuterated polystyrene.
e: Obtained from ^1H NMR results in $CDCl_3$ at 25 °C.
f: Size exelusion ehromatography in THF at 25 °C with a UV deteetor.
*: Deuterated PS bloeks.

Table 2.2 Morphological results of the cyclics and their corresponding triblock copolymers.

	M_n ($\times 10^{-3}$) [a]	fPS [b]	D (nm) [c]	D_C/D_T [d]	Morphology
$(PS\text{-}PBD)_C$-11	47.5	10.8	32.7		Random PS Spheres
PS-PBD-PS-11	47.6	10.6	36.8	0.89 ± 0.02	Random PS Spheres
$(PS\text{-}PBD)_C$-24	55.9	24.0	34.6		PS Cylinders
PS-PBD-PS-24	56.0	23.9	41.0	0.84 ± 0.02	PS Cylinders
$(PS\text{-}PBD)_C$-40	55.1	37.8	38.4		Lamellae
PS-PBD-PS-40	53.5	39.5	40.3		PS Cylinders
$(PS\text{-}PBD)_C$-51	51.7	51.2	29.9		Lamellae
PS-PBD-PS-51	51.4	51.4	34.6	0.86 ± 0.02	Lamellae
$(PS\text{-}PBD)_C$-70	56.9	69.6	32.7		PI Cylinders
PS-PBD-PS-70	58.0	70.2	55.2		Gyroid

a: Size exclusive chromatography in THF at 30 °C.
b: Determined from 1H NMR results.
c: Determined based the primary reflection of the respective SAXS data. . The error for the measurement is ± 0.3 nm.
d: Microdomain spacing ratio of that of cyclic to that of its corresponding triblock copolymer.

(a)

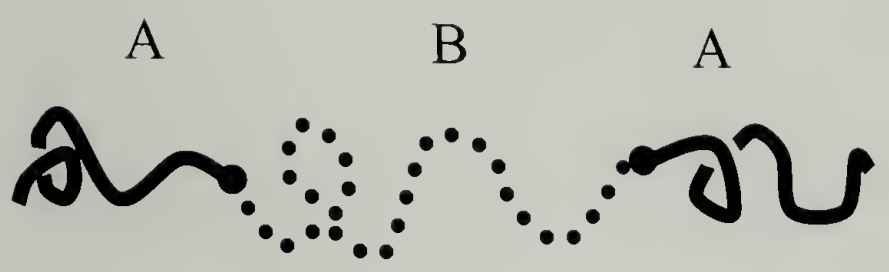

(b)

Figure 2.1 Illustration of an ABA triblock copolymer (a) and an AB cyclic block copolymer (b).

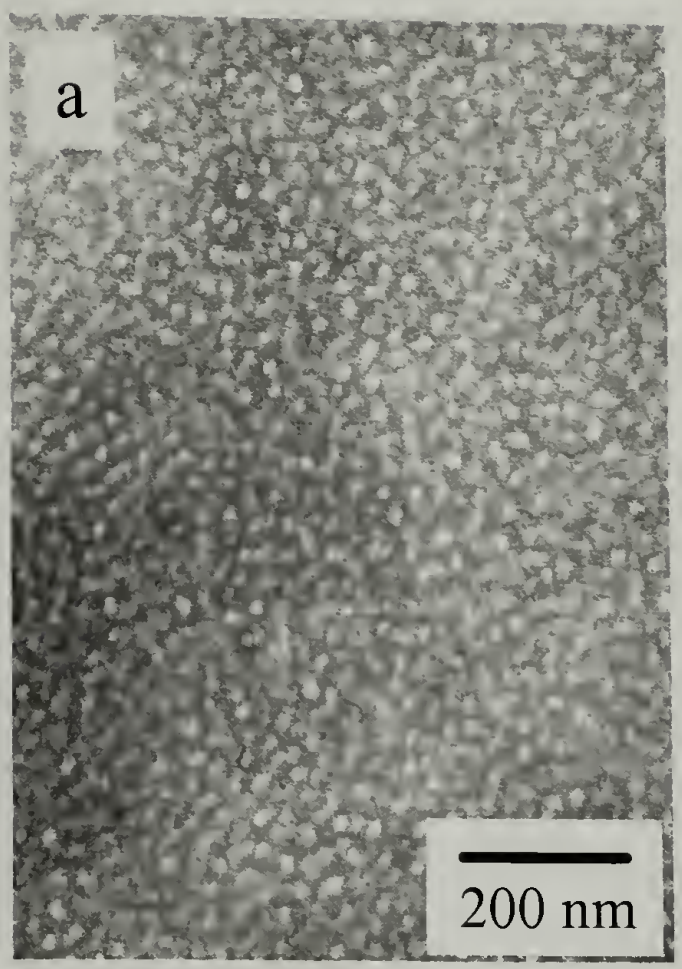

Figure 2.2 (a) TEM image for (PS-PBD)$_C$-11 cyclic block copolymer; (b) Small angle X-ray scattering data for cyclic (PS-PBD)$_C$-11(▲), PS-PBD-PS-11 triblock copolymers (●), and the form factor from spherical domains (—).
Continued next page.

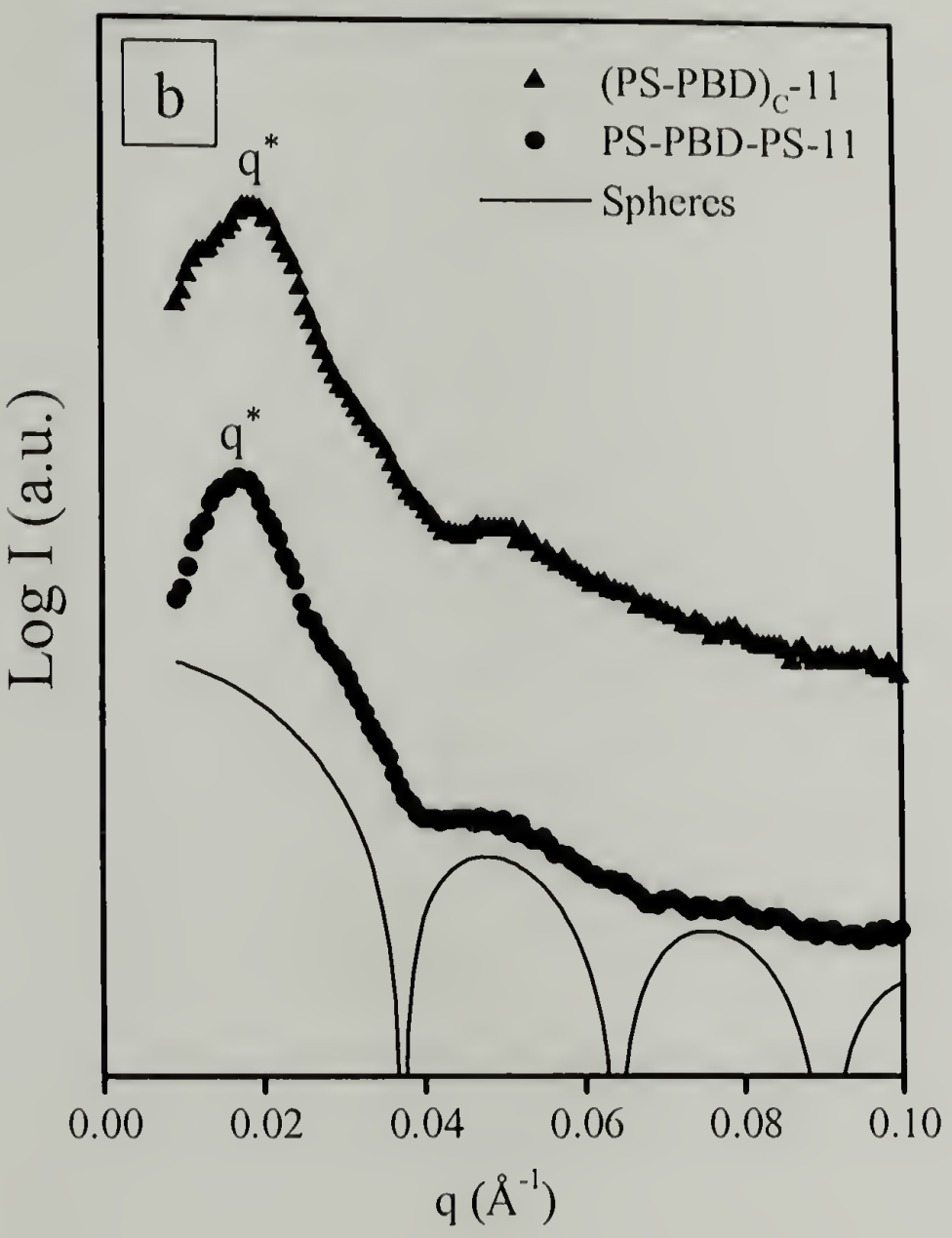

Figure 2.2 Continued.

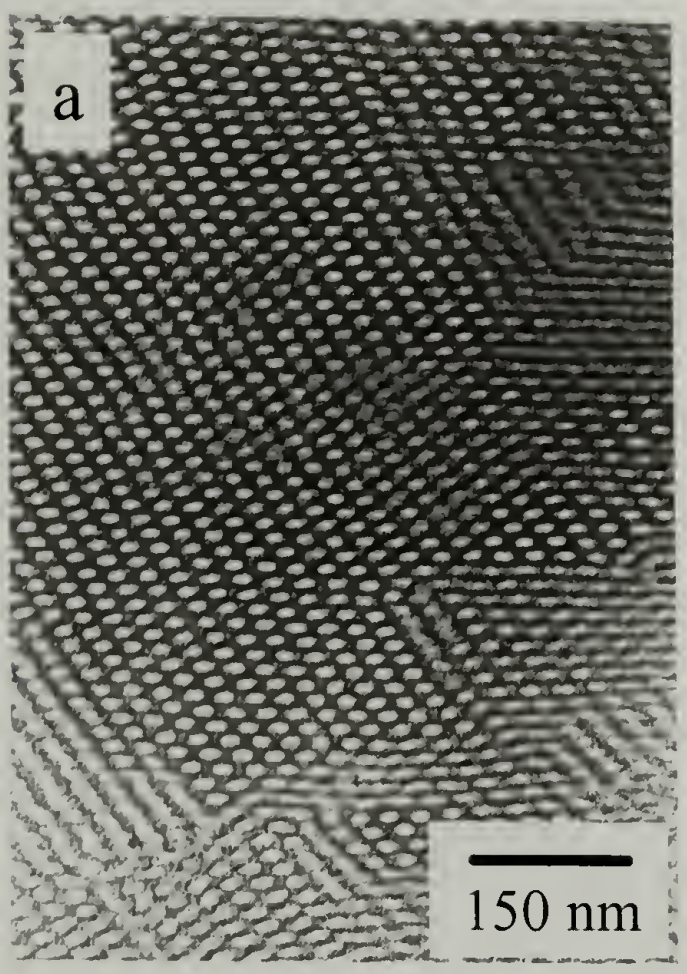

Figure 2.3 (a) TEM micrograph for $(PS\text{-}PBD)_C$-24 cyclic block copolymer; (b) Small angle X-ray scattering data for cyclic $(PS\text{-}PBD)_C$-24 (▲) and PS-PBD-PS-24 triblock copolymers (●), and the form factor for cylindrical domains (—). Continued next page.

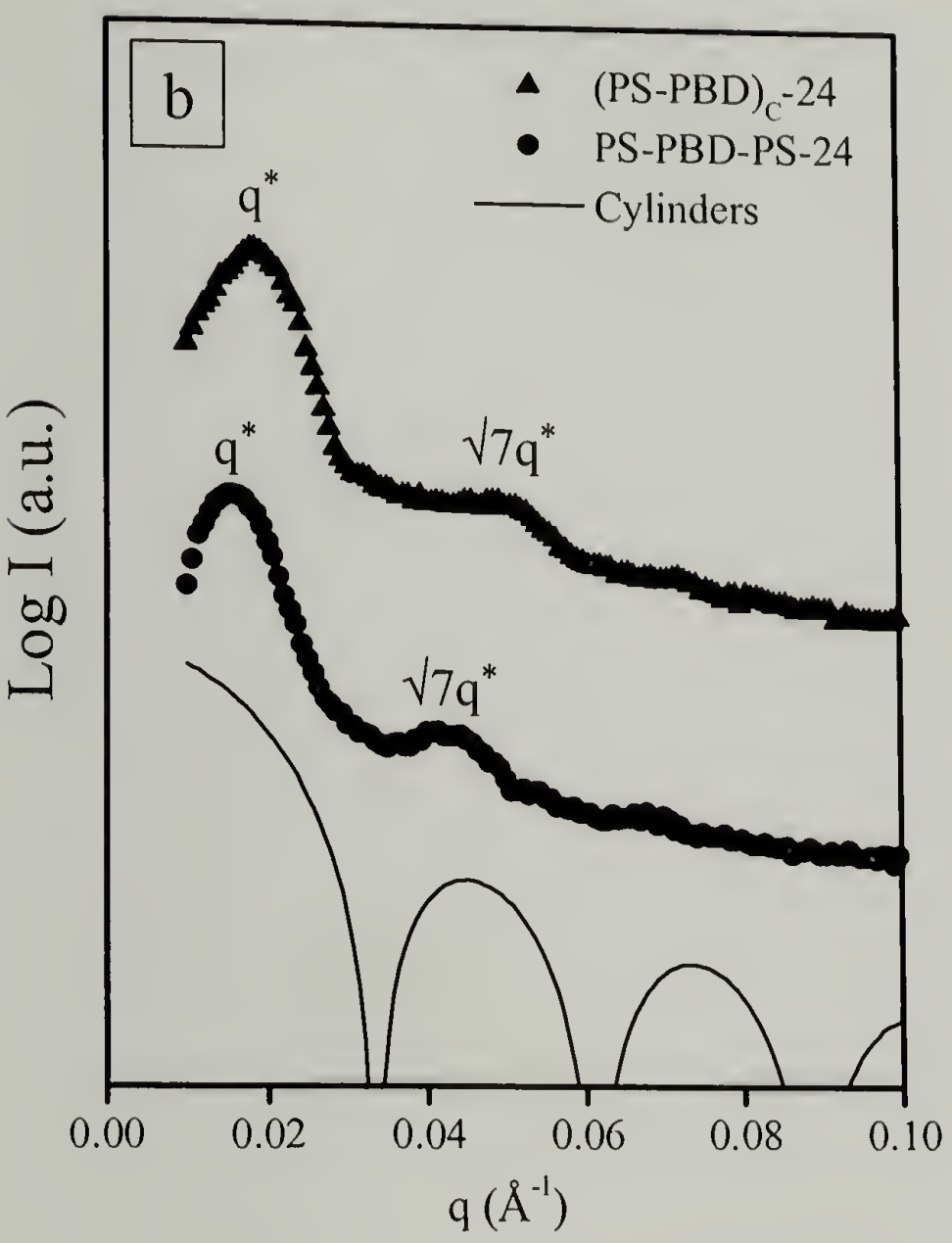

Figure 2.3 Continued.

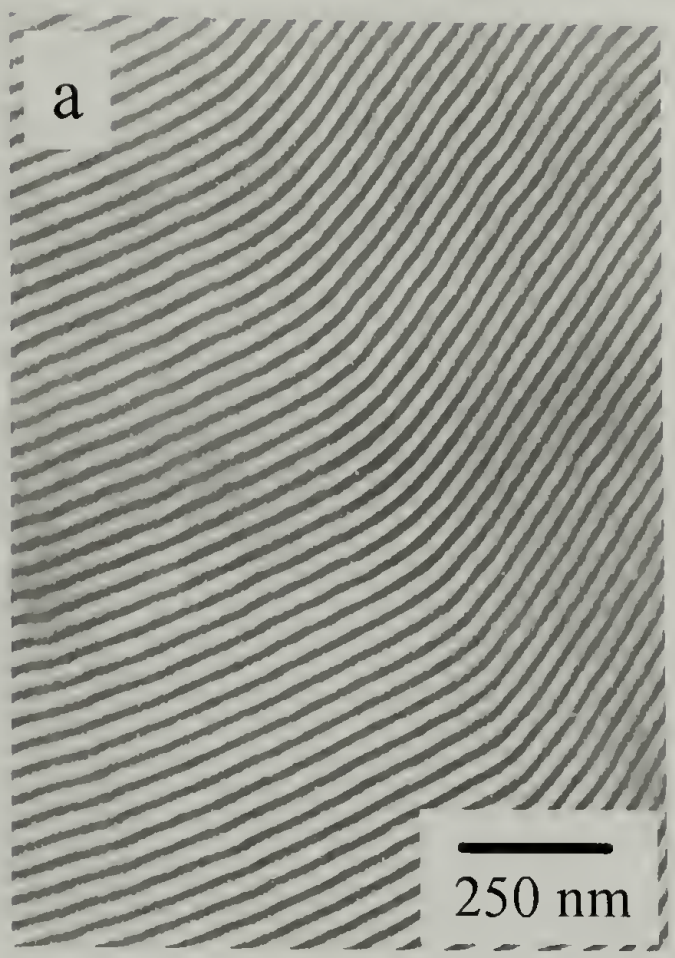

Figure 2.4 (a) TEM micrograph for $(PS\text{-}PBD)_C$-51 cyclic block copolymer; (b) Small angle X-ray Scattering profiles for cyclic $(PS\text{-}PBD)_C$-51 (▲) and PS-PBD-PS-51 triblock copolymers (●). Continued next page.

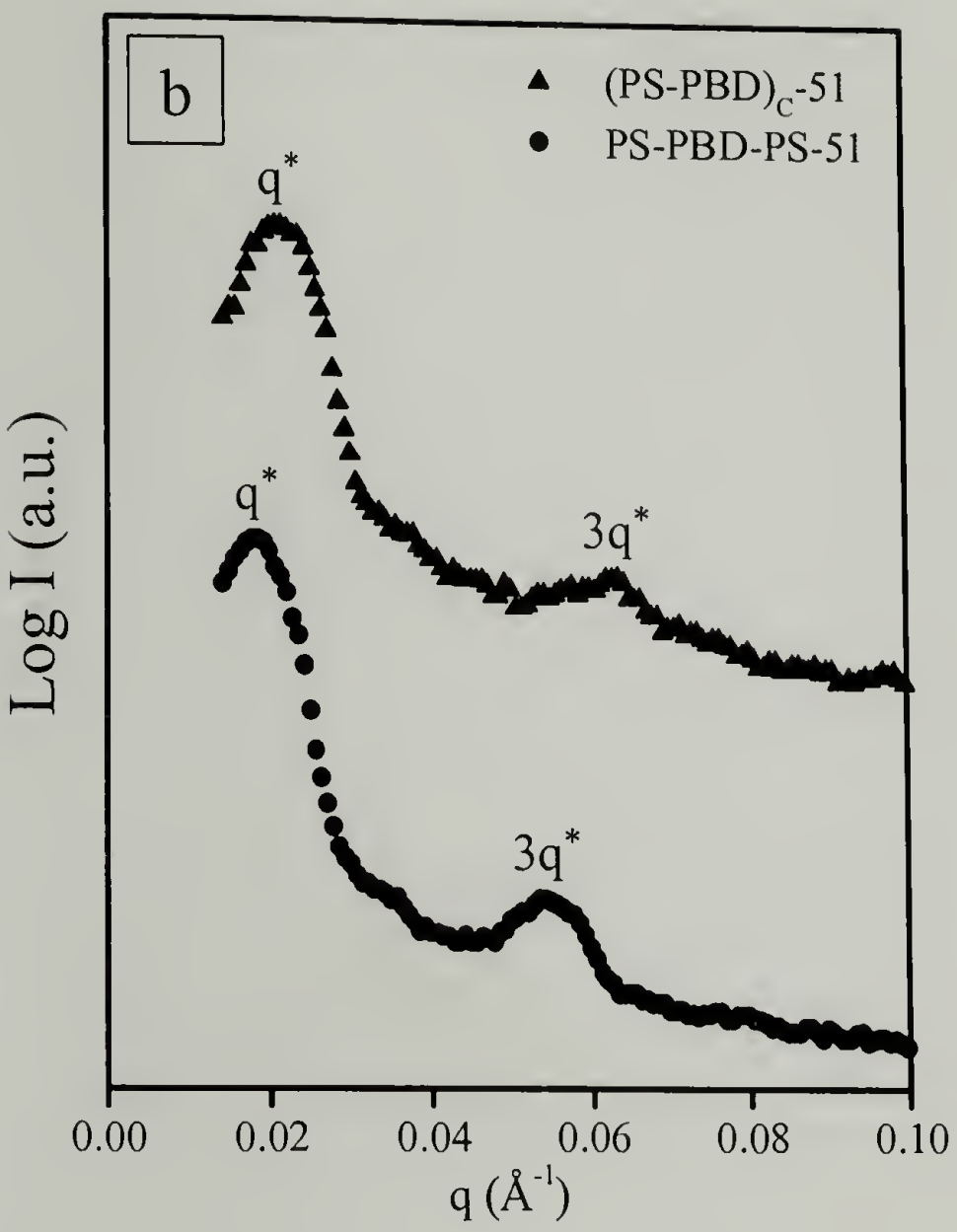

Figure 2.4 Continued.

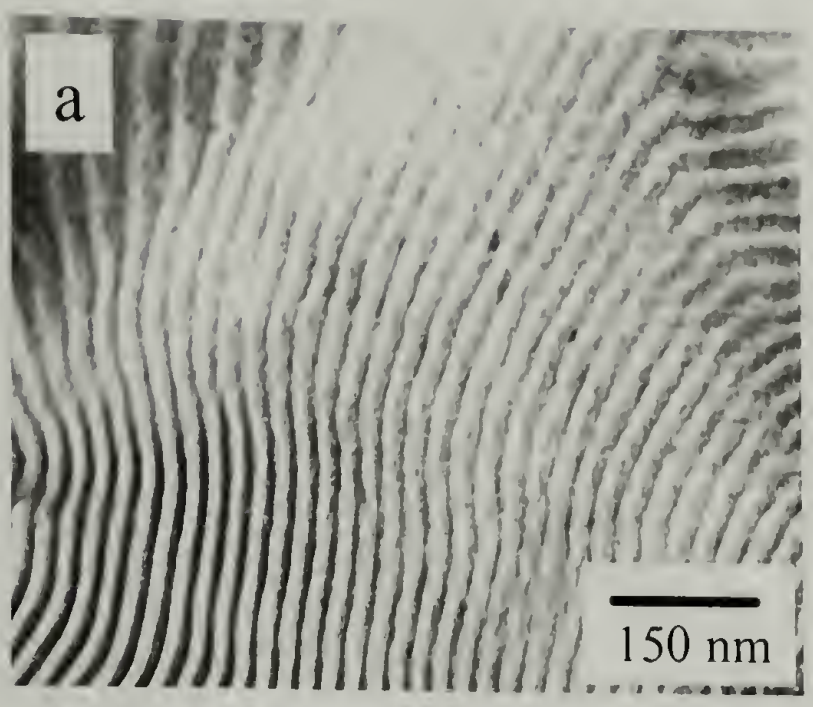

Figure 2.5 (a) TEM images for $(PS\text{-}PBD)_C$-40; (b) PBD-PS-40; and (c) SAXS data for $(PS\text{-}PBD)_C$-40 (▲) and PS-PBD-PS-40 (●).

Continued next page.

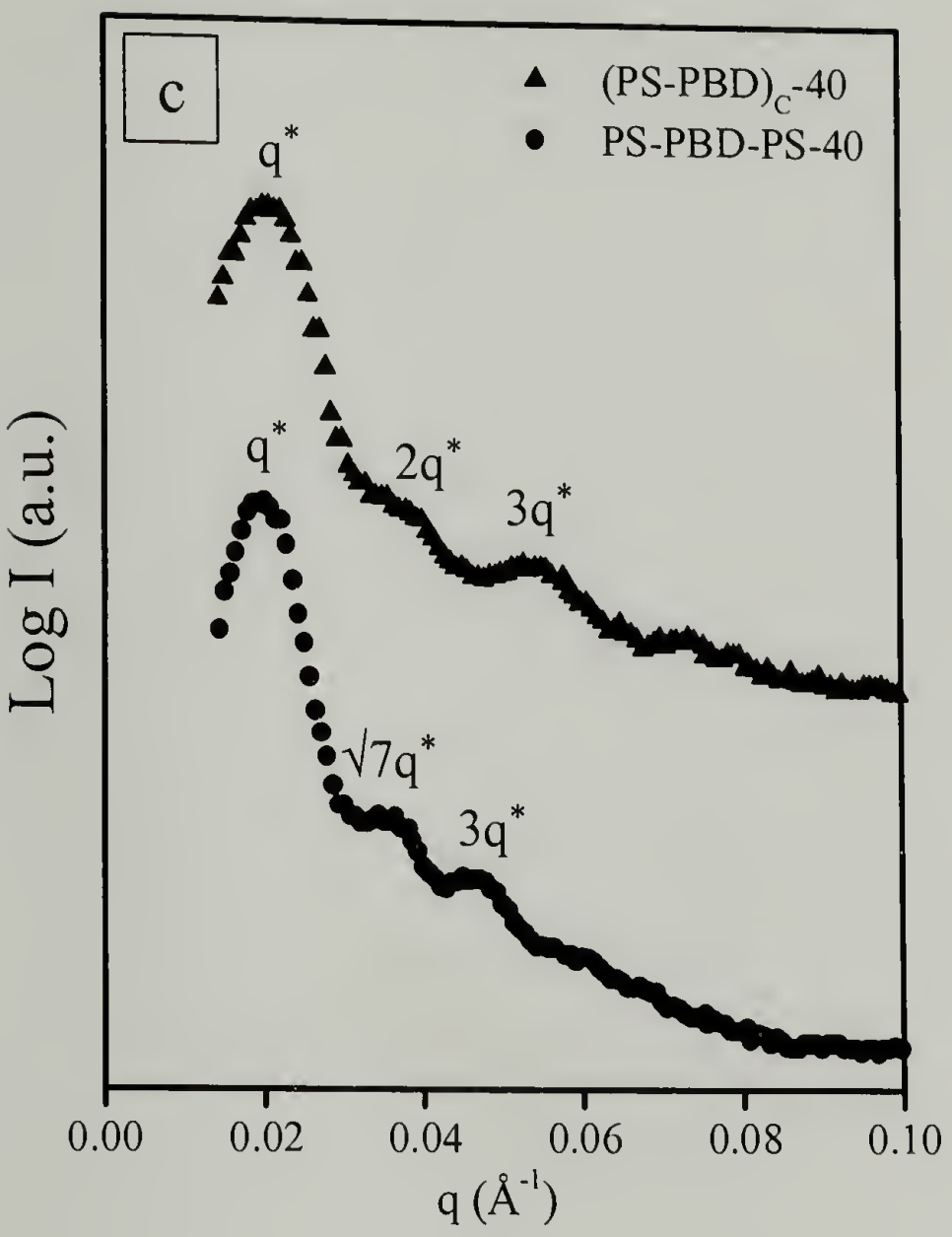

Figure 2.5 Continued.

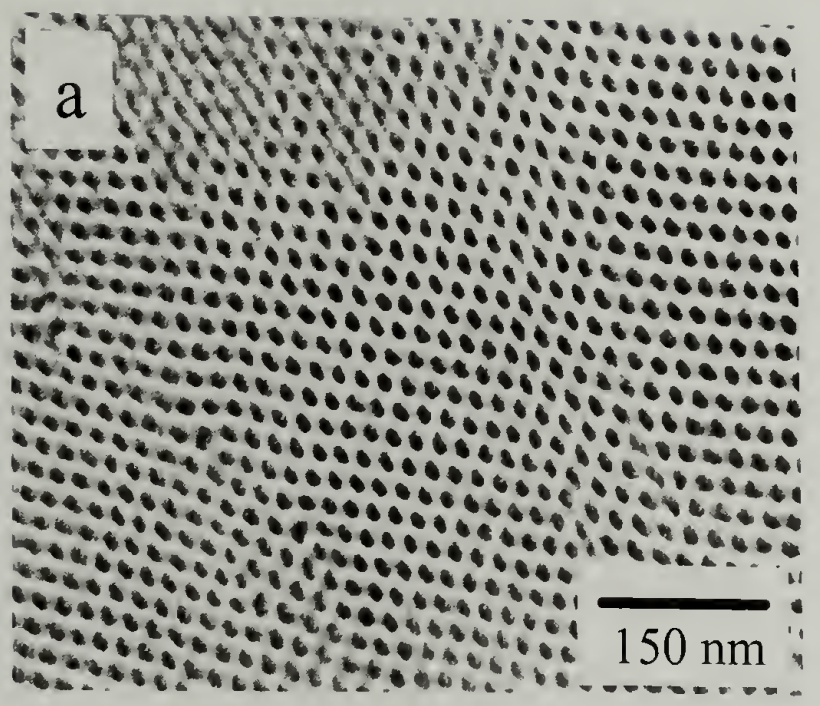

Figure 2.6 (a) TEM images for $(PS\text{-}PBD)_C$-70; (b) PS-PBD-PS-70; and (c) SAXS data for $(PS\text{-}PBD)_C$-70 (▲) and PS-PBD-PS-70 (●).

Continued next page.

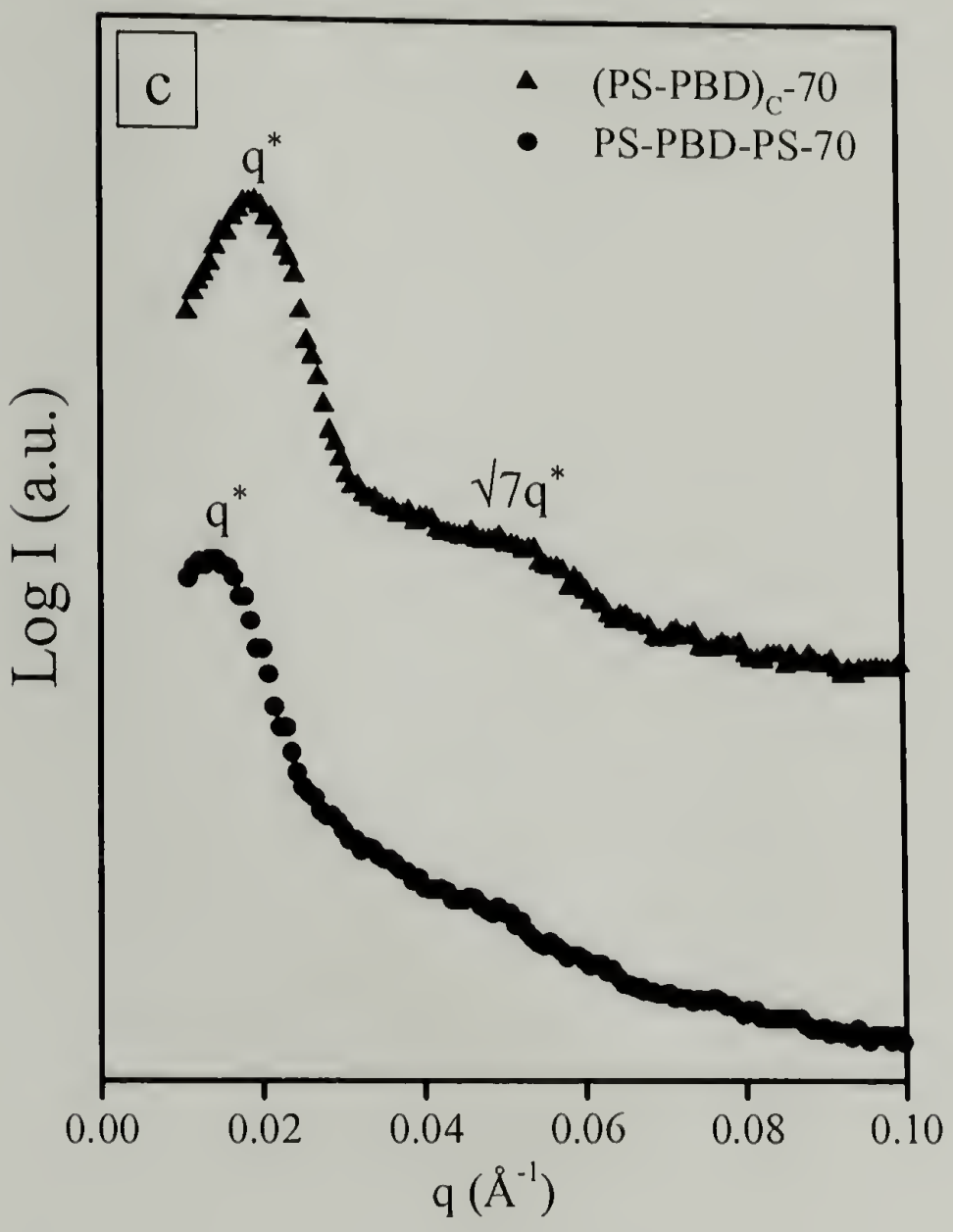

Figure 2.6 Continued.

CHAPTER 3

LAMELLAR SPACINGS AND THE JUNCTION POINT FUNCTIONALITY IN MIKTOARM STAR BLOCK COPOLYMERS

3.1 Abstract

To probe the effect of junction point functionality in miktoarm star block copolymer architecture on chain conformation and morphology, a series of A_nB_n miktoarm star copolymers where A arms are PS blocks and B arms are PI blocks were investigated. The overall series including a diblock and the star block copolymers can be represented by A_nB_n where n = 1, 2, 4 and 16. These materials were produced by synthesizing a single batch of living PS arms and a single batch of living PI arms and then linking them together with chlorosilane coupling agents of different functionality. Thus all PS arms are identical and all PI arms are identical across the entire series of materials. All stars in the series have equal numbers of PS and PI arms and the volume fractions of all the samples in the series (nearly 0.50 PS by volume) are identical within experimental error. All the materials were found, via small angle X-ray scattering (SAXS) and transmission electron microscopy (TEM), to form lamellar morphologies. A significant increase in lamellar spacing with increasing junction point functionality (n) was found in this series of materials and can be attributed to molecular crowding near the junction point.

3.2 Introduction

Miktoarm star block copolymers with the A_nB_n architecture, illustrated in Figure 3.1, have n arms of polymer A and n arms of polymer B connected at one central junction point. AB diblocks can be viewed as a special case of A_nB_n star block copolymers where n is equal to 1. *Olvera de la Cruz and Sanchez*[35] have predicted that near 0.5 component volume fractions, the Order-Disorder Transition temperatures (ODT) of A_nB_n star copolymers are independent of n and the length scales of the microphase separated morphologies in the weak segregation limit are also independent of n. Additionally, the strong segregation limit theory of *Milner*[32] for the morphologies of *miktoarm* star copolymers neglects the details of the junction point effects on chain conformation, and thus predicts that A_nB_n *miktoarm* stars of all n values behave identically to the A_1B_1 diblock copolymer with the same A arm and the same B arm.

Contrary to these early predictions, recent experimental results have shown that the lamellar long periods of A_nB_n *miktoarm* star copolymers are larger than their corresponding diblock copolymers.[13,14,16,45,46] Comparison among the results from different groups of A_nB_n star block copolymers [13] indicates that domain spacing increases with increasing values of n. The lamellar spacing discrepancy between the A_nB_n stars and their corresponding AB diblocks results from chain crowding near the central core, where multiple arms converge on the same junction point. For any A_nB_n architecture, we define the corresponding diblock to consist of one A and one B arms. The polymer chain segments near the junction point have to adopt a stretched trajectory away from the junction points, as in the case of a star molecule,[47] to minimize this chain crowding. This

leads to an increase in lamellar spacing of star block copolymers compared to a corresponding diblock copolymer.

It has been established that the discrepancy between AB diblock and A_2B_2 stars can be predicted by a self-consistent mean-field theory, and it is due to a reduction in the translational entropy of the junction point.[15] By adding this entropy term into the free energy equation, a strong segregation theory has been derived to explain the increase in domain spacing of A_2B_2 as compared to AB diblock copolymers. It has also been pointed out that the lamellar spacing difference between A_2B_2 and the corresponding AB diblock decreases with the increasing χN_0, where the N_0 is the degree of polymerization of the corresponding diblock copolymer and the χ is the *Flory-Huggins* interaction parameter. This supports the earlier observations[13,32] that this influence from the central core vanishes when the molecular weight of the corresponding diblock copolymer (or N_0) becomes very large. For molecules with high value of N_0, the lamellar spacing is larger because of the high molecular weight, but the increase in the spacing over that of the corresponding AB diblock decreases with increasing molecular weight. This trend has been proven by comparing the microdomain properties of three pairs of A_2B_2 stars and their corresponding AB diblocks.[45] The lamellar spacing ratio of the A_2B_2 stars to their corresponding AB diblocks decreases from 1.10 to 1.05 as the value of χN_0 increases from 12 to 73. A theoretical model was recently proposed to describe this extra stretching effect of star block copolymers with small to intermediate arm length based on the assumption of segmental mixing in an oblate ellipsoid volume located at the interface and centered on the junction point. It is predicted that the lamellar period for *miktoarm*

stars increases as $f^{1/6}N^{2/3}\chi^{1/12}$, where $f\ (=2n)$ is the total number of both A and B arms.[16] Based on the previous research, it is clearly suggested that the lamellar spacing of A_nB_n stars is controlled by two independent parameters: the molecular weight of the corresponding AB diblock, which determines the segregation strength of the polymer segments, and the functionality (number of arms connected) at the central core.

However, for most of the systems studied, the corresponding AB diblock copolymers were either not available for direct comparison, or synthesized in a different batch. The spacing differences between *miktoarm* star copolymers and diblocks were usually obtained by comparing experimental data from A_nB_n stars with the spacings of the calculated corresponding diblock copolymers based on their molecular weights and previously determined scaling relationships.[48] The objective of current work is to experimentally isolate the influence of functionality (n) on the lamellar morphologies of A_nB_n copolymers while holding the variables, such as arm molecular weight and composition, constant. To achieve this end, a series of $(PS)_n(PI)_n$ *miktoarm* star copolymers (n = 1, 2, 4, and 16) were synthesized utilizing anionic polymerization and chlorosilane coupling chemistry. The n equal to 1 case is the corresponding diblock copolymer for all the stars with higher n in this series. All the PS arms used in all the samples were obtained from the same anionically synthesized batch and thus were characteristically the same. Likewise, all the PI arms were also from the same batch. These arms were then linked together in different symmetric numbers using different cholorsilane coupling agents. To within experimental error, all samples have the same component volume fractions and differ only in the junction point functionality, allowing

us to isolate the effect of the junction point on lamellar morphology.

3.3 Experimental

All reagents used were purified using standard techniques.[49,50] Manipulations were performed under high vacuum in glass vessels, washed with *n*-BuLi and rinsed with benzene. Additions of reagents were made through breakseals and removals of materials were performed through heat-sealing of constrictions.[49,51,52] *s*-BuLi was prepared under vacuum from *s*-butyl chloride and lithium dispersion and was used for initiating polymerization of PS and PI arms. The coupling agents - liquid chlorosilanes with 2 and 4 Si-Cl groups (for n = 1, 2) were purified by fractional distillation on the vacuum line, diluted with benzene, and then subdivided into breakseal equipped ampoules. The synthesis of chlorosilane coupling agents with 8 and 32 Si-Cl groups (n = 4, 16) was accomplished according to methods reported previously.[53]

The general reactions used for the synthesis of PS-PI diblock copolymer are given in the following scheme:

Styrene + s-BuLi $\rightarrow$ PSLi

Isoprene + s-BuLi $\rightarrow$ PILi

PSLi + excess $SiCl_2(CH_3)_2 \rightarrow (PS)SiCl(CH_3)_2 + LiCl + SiCl_2(CH_3)_2\uparrow$

$(PS)SiCl(CH_3)_2$ + excess PILi $\rightarrow (PS)(PI)Si(CH_3)_2 + LiCl + PILi\downarrow$

A benzene solution of the living PSLi was added to a large amount of dichlorodimethylsilane (ratio of Si-Cl groups to PSLi was about 100). This resulted in

chlorosilane end-capped with a minimum of PS-PS block coupling. Excess linking agent was removed by extensive pumping on the vacuum line and by repeatedly dissolving the polymer and removing the solvent. Finally, a slight excess amount of living PILi chains was added to the macromolecular linking agent $(PS)Si(CH_3)_2Cl$. The step-by-step synthetic procedure was monitored by size exclusion chromatography (SEC). While this is an unusually complicated procedure for the synthesis of a diblock copolymer, it was necessary in order to preserve structural consistency with the other materials in our A_nB_n series.

The synthesis of $(PS)_2(PI)_2$ stars was accomplished using the following reactions:

$$PSLi + PSSiCl_3 \xrightarrow{\text{titration}} (PS)_2SiCl_2 + LiCl$$
$$PSLi + SiCl_4 \rightarrow PSSiCl_3 + LiCl$$

$$(PS)_2SiCl_2 + \text{excess } PILi \rightarrow (PS)_2Si(PI)_2 + 2LiCl + PILi\downarrow$$

A PSLi benzene solution was added into a solution of $SiCl_4$ in a ratio of $(SiCl_4)/(PSLi) = 3:1$. The resulting mixture of $(PS)_2SiCl_2$ and $PSSiCl_3$ were titrated with PSLi until nearly all the $PSSiCl_3$ was transformed into $(PS)_2SiCl_2$. The reaction is deterred from proceeding to the formation of $(PS)_3SiCl$ or $(PS)_4Si$ through the steric hindrance of the polystyryl lithium anions. Finally an excess of living PILi chains was added to the macromolecular linking agent $(PS)_2SiCl_2$ in order to react with the two remaining chloride functionalities, which leads to the formation of $(PS)_2Si(PI)_2$.

The syntheses of the remaining materials in the A_nB_n series were accomplished

using the following reactions:

$$n\ PSLi + SiCl_{2n} \rightarrow (PS)_nSiCl_n + nLiCl$$

$$(PS)_nSiCl_n + \text{excess } PILi \rightarrow (PS)_nSi(PI)_n + nLiCl$$

The chlorosilane coupling agent $Si[CH_2CH_2Si(CH_3)Cl_2]_4$ was used for the synthesis of the $(PS)_4(PI)_4$ and $Si[CH_2CH_2Si(CH_3)\{CH_2CH_2Si(CH_3)[CH_2CH_2Si(CH_3)Cl_2]_2\}_2]_4$ for $(PS)_{16}(PI)_{16}$ respectively. These multifunctional chlorosilanes were prepared by using tetravinylsilane as the initial core molecule, methyldichlorosilane as the propagating units, and vinylmagnesium bromide for the transformation of the silicon chloride to the silicon vinyl group as described elsewhere.

An appropriate quantity of living PSLi was added to the benzene solutions of the different chlorosilane coupling agents [(Si-Cl)/(PSLi) = 2:1.1] to insure the formation of the $(PS)_nSiCl_n$ stars. The progress of the formation of $(PS)_nSiCl_n$ was monitored using SEC and Membrane Osmometry (MO). As before, there is a sterically directed tendency for the reaction to stop after addition of one PS chain to each difunctional chlorosilane group of the linking agent. As an example, the SEC curves of the $(PS)_4(PI)_4$ *miktoarm* star copolymer, its precursor arms and its intermediate product $(PS)_4SiCl_4$ are given in Figure 3.2. These reactions usually were completed in 1-2 days and then an excess amount of PILi benzene solution was added to the reactor. Depending upon the number of arms, coupling reactions were completed in 1.5 to 2 months. Excess living PSLi and PILi arms were terminated by addition of degassed methanol. All the $(PS)_n(PI)_n$ star

block copolymers were purified by fractionation.

SEC experiments were carried out at 25 °C in THF, using a Waters 410 SEC with a differential refractometer detector, a UV detector, and six columns with porosity ranges from 10^2 to 10^6 Å. Number average molecular weights (M_n) of the precursor arms, the intermediates, and the final products were also measured with a Jupiter Model 231 Recording Membrane Osmometer (MO) at 35 °C. Weight average molecular weights (M_w) of the $(PS)_n(PI)_n$ star copolymers were measured at 25 °C using a Chromatix KMX-6 Low Angle Laser Light Scattering (LALLS) photometer at a wavelength of 633 nm. Molecular information of all the materials is listed in Table 1. PS weight fractions were determined by ^{1}H-NMR analysis using a Bruker AC 200 instrument in $CDCl_3$ at 30 °C. PS volume fractions were calculated based on ^{1}H NMR and GPC-UV results. The experimental error for ^{1}H NMR or GPC-UV analysis is about ± 2%, which leads to ± 2% error in the calculated PS volume fractions.

The successful establishment of the scale law of lamellar spacing on the functionality of the star block copolymers relies on the successful synthesis of the $(PS)_n(PI)_n$ star copolymers, without serious contamination by star block copolymers with other component combinations, such as $(PS)_{n+1}Si(PI)_{n-1}$ or $(PS)_{n-1}Si(PI)_{n+1}$ or other combinations. In order to probe this composition fluctuation in the materials we studied, temperature gradient liquid chromatography (TGLC) was carried out on a typical HPLC system equipped with a C18 bonded silica column (Alltech, Platinum EPS C18, 100 Å pore, 53 x 7.0 mm I.D., 3 μm particle size). The mobile phase was 1,4-dioxane and the

temperature of the column was linearly raised from 15 °C to 45 °C throughout the experiment as shown in Figure 3.3 for star block copolymers with n = 2, 4 and 16. Gaussian peak deconvolution was used to calculate the percentage of each structure in the HPLC chromatogram. The purity of $(PS)_2(PI)_2$ is determined to be 74% with some contamination of PS and PI homopolymers, while that of $(PS)_4(PI)_4$ is 57% with 16% of $(PS)_4(PI)_3$ and 20% of $(PS)_3(PI)_4$ as major side products. The molecular weight of $(PS)_{16}(PI)_{16}$ is too high to be analyzed using the TGLC method. Based on these analyses, we conclude that there is inherent contamination resulting from the synthesis of *miktoarm* stars of this type. These contamination species are resistant to detection via standard SEC and to separation by standard methods such as solvent-nonsolvent fractionation. All previous results reported in the literature regarding miktoarm stars obtained by methods were produced by similar synthetic routes and thus these materials most likely had similar contamination.

3.4 Results and discussion

All the $(PS)_n(PI)_n$ *miktoarm* star copolymers (n = 1, 2, 4 and 16) form lamellar morphologies. Figure 3.4 shows a TEM micrograph of the lamellar structure observed in the $PS_{16}PI_{16}$ star copolymer. The SAXS plot in Figure 3.5 shows several higher order reflections in all materials, indicating that these materials are well ordered. The different sets of SAXS data have been offset vertically for clarity. The second-order reflections of the three star block copolymers with low number of arms (n = 1, 2, 4) are suppressed, which indicates that the volume fractions of both blocks in these materials are nearly identical in the microphase separated state. The copolymer with 32 arms is slightly more

asymmetric in component volumes as the second reflection is readily seen in the profile. Determination of peak positions and thus lamellar spacing was conducted on *Lorentz* corrected Iq^2 vs. q plots. The scattering vectors divided by the orders of the respective peaks (q/n) were averaged over the primary and higher order peaks. This produced an average value for the scattering vector of the primary peak, q^*, from which an average lamellar long period was calculated. The average q^* values and the corresponding lamellar long periods (D_n) are listed in Table 2. These results show that the lamellar spacing increases with increasing star functionality from 256 Å for the PS-PI diblock to 287 Å for the $(PS)_{16}(PI)_{16}$ star block copolymer. Standard deviations (σ) of the mean for the values of the q/n for the series of reflections can also be found in this table.

When comparing the spacings of lamellar morphologies across the A_nB_n series, we must consider the fact that the chlorosilane linking agent for higher n members has a significantly larger molecular diameter than for lower n members of the series. We must address the question of whether the increasing size of this linking agent contributes significantly to the increase in lamellar spacing with increasing n. In order to properly take the core size into account, the observed domain spacings are normalized by the unperturbed radius of gyration of a diblock consisting of one PS block, one PI block and the average number of bonds linking these two arms through the core, $R_{g,n}$. For n = 1, and 2, this number of extra bonds to traverse the core is constant for any combination of one PS and one PI arm. However, for n = 4 and 16, there are different possible paths across the core that lead to different numbers of extra bonds. Table 2 lists the extra number of bonds in the core including averages over all combinations of PS and PI block

locations for the n =4 and 16 case. The table also lists the values of $R_{g,n}$; these values clearly do not increase significantly even when comparing the n = 1 case to the n = 16 case.

Figure 3.6 is a plot of the lamellar long periods of $(PS)_n(PI)_n$ star copolymers normalized with respect to the corresponding diblock radius of gyration including the core size ($D_n/R_{g,n}$) vs. n. This value is further normalized by ($D_1/R_{g,1}$), the value of this ratio for the corresponding diblock of the series. After the correction from the increased size of the coupling agent, it is clearly shown in Figure 3.6 that the lamellar spacing increases with the functionality of the center core and the curve plateaus at higher n. The experimental data were also mapped onto the log-log plot of lamellar period vs. $f_B^{1/4}N_B$ as described by Grayer *et al*,[16] which is shown in Figure 3.7. We conclude that the data from current series falls in a similar range as previous data. However, the limited range of $f_B^{1/4}N_B$ covered by our data makes it impossible to evaluate our data agreement with the *Grayer* theory.

3.5 Conclusions

Lamellar morphologies of a series of $(PS)_n(PI)_n$ star block copolymers (n = 1, 2, 4 and 16) with identical PS arms and identical PI arms, prepared by anionic polymerization and controlled chlorosilane chemistry, have been investigated. The materials were in the intermediate segregation regime and had nearly 50/50 volume fractions. Lamellar long periods of structures formed by the star copolymers (n > 1) were found to exceed that of the corresponding diblock copolymer (n = 1) and to increase with increasing number of

arms at the central core. The relationship between the lamellar long period of these star copolymers and star functionality has been studied via SAXS results. However, the presence of side products with unintended A or B arm numbers appears to be an unavoidable consequence of the synthetic coupling strategy. Thesis side products are often not completely separable by solvent-nonsolvent fractionation. These caveats apply not just to the materials of the current study but also to materials from previous reported work on A_nB_n stars in which the materials were synthesized by similar approaches. Although the data from this study and the previous studies generally follows the theoretical prediction for crowding near the star junction point, it is questionable as to whether a true test of the theory can be achieved until a cleaner synthesis of A_nB_n materials is available.

Table 3.1 Molecular characterization of the $(PS)_n(PI)_n$ star block copolymers.

Sample	$(PS)_nCl_n$ intermediate			$(PS)_n(PI)_n$ star block copolymers				
	M_n[a] Kg/mol	M_w/M_n[e]	# PS arms /junction	M_n[a] Kg/mol	M_w[b] Kg/mol	M_w/M_n[d]	Wt% PS	
							^{1}H NMR	UV[c]
PS arms	19							
PI arms	15							
PS-PI	19	1.04	1.0	36.2	36.3	1.05	55 ± 2	54 ± 2
$(PS)_2(PI)_2$	38	1.04	2.0	64	66	1.04	56 ± 2	55 ± 2
$(PS)_4(PI)_4$	67.3	1.04	3.5	121	127.5	1.04	54 ± 2	52 ± 2
$(PS)_{16}(PI)_{16}$	301.2	1.03	15.8	e	533	1.07	59 ± 2	58 ± 2

a Number averaged molecular weight measured using membrane osmometry (MO) in toluene at 35 °C.
b Weight averaged molecular weight measured using low angle laser light scattering (LALLS) in THF at 25 °C.
c Results measured using size exclusion chromatography in THF at 25 °C (UV detector).
d Determined via size exclusion chromatography in THF at 25 °C (DRI detector).
e The molecular weight of the molecule is too high to be measured by MO.

Table 3.2 Morphological characterization of the $(PS)_n(PI)_n$ *miktoarm* star block copolymers based on TEM and SAXS analyses.

	PS Vol%[a]	Average q^* ($Å^{-1}$)	σ of (q/n)[b]	D_n (Å)[c]	# of Si-C at core[d]	# of C-C at core[d]	N_n [e] (core)	$R_{g,n}$ (Å)[f]	$(D_n/R_{g,n})/(D_1/R_{g,1})$
PS-PI	51 ± 2	0.0246	0.0013	256	2	0	0.67	56.2	1
$(PS)_2(PI)_2$	52 ± 2	0.0234	0.0010	269	2	0	0.67	56.2	1.05
$(PS)_4(PI)_4$	50 ± 2	0.0231	0.0004	271	5	0	2.33	56.3	1.06
$(PS)_{16}(PI)_{16}$	55 ± 2	0.0219	0.0008	287	10.6	4.3	4.97	56.5	1.12

a PS volume fraction, calculated based on the average results of ^1H NMR and SEC-UV analyses.
b Standard deviation of the mean for q/n values.
c Lamellar long period, calculated based on average q^*.
d Extra bonds provided by the core structure. The number is averaged among all the probabilities of the arm combinations.
e Degree of polymerization of the core structure. It is calculated from N = [(# of Si-C bond) + (# of C-C bond)]/3.
f Radius of gyration of star block copolymers. $Rg_n^2 = [a_{av}(N_a + N_b + N_n)^2]/6$, where the a_{av} is the averaged *kuhn* length of PS and PI in this series $a_{av} = (a_aN_a + a_bN_b)/(N_a + N_b)$. The a_a and a_b, N_a and N_b are the *kuhn* length and the degree of polymerization of PS and PI arm respectively.

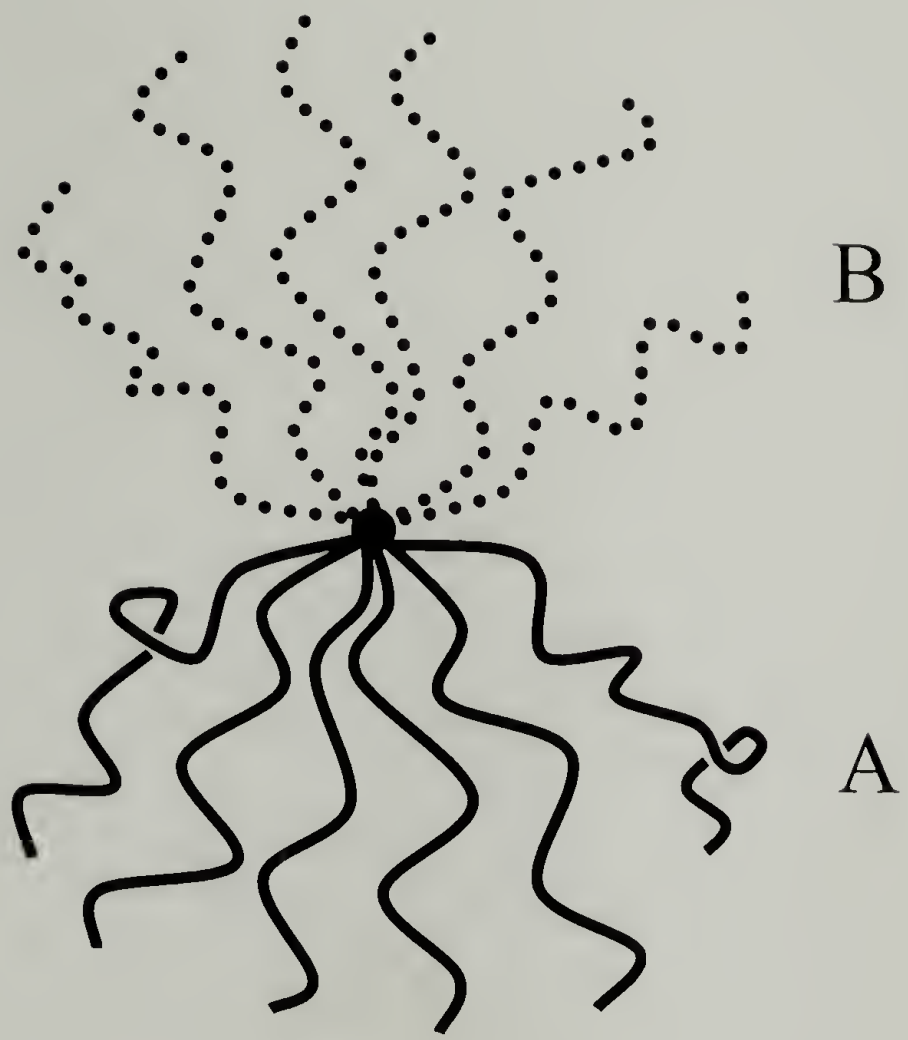

Figure 3.1 Illustration of a *miktoarm* star block copolymer with 6 arms of block A and 6 arms of block B connected at one central junction point.

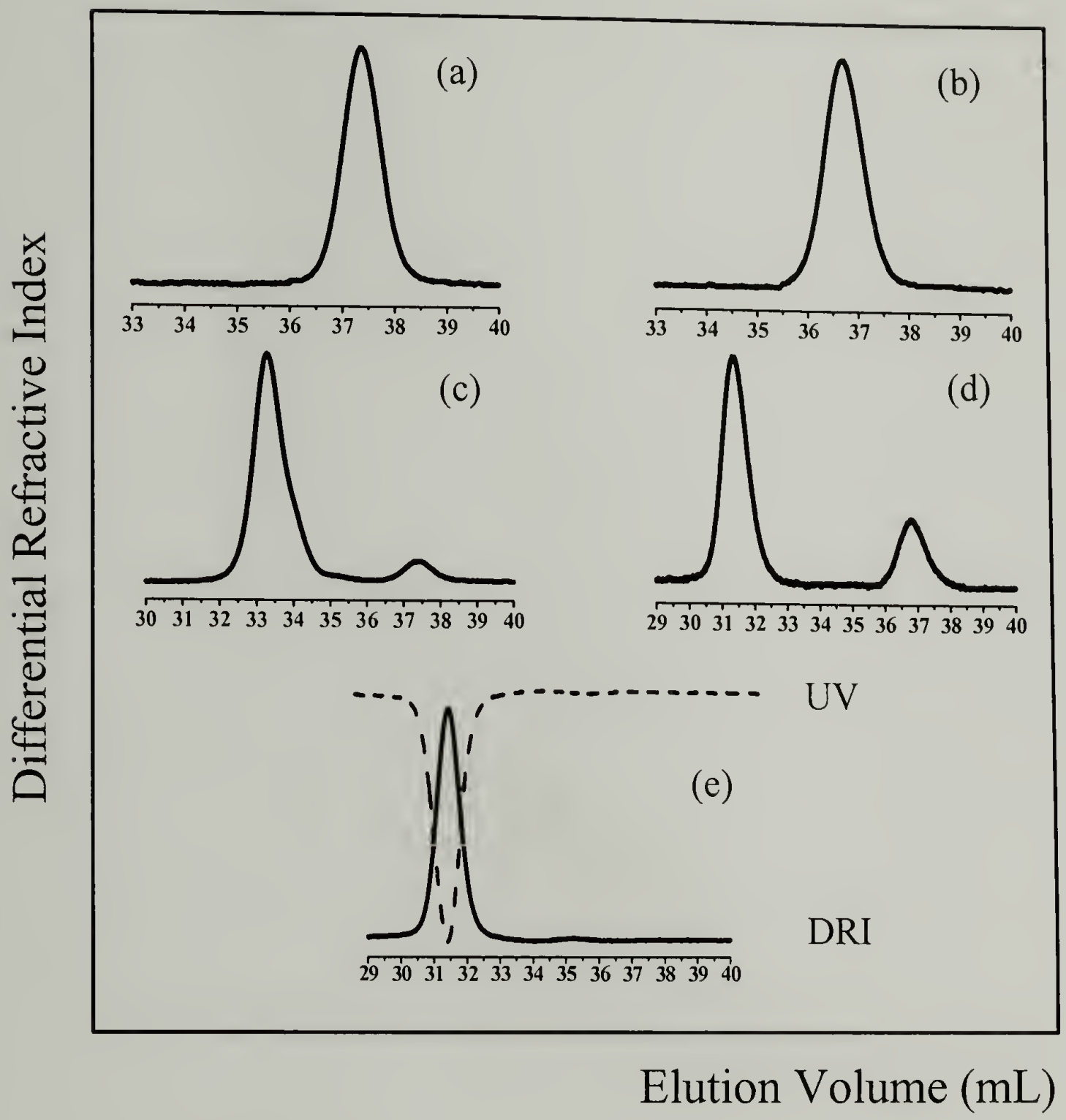

Figure 3.2 SEC chromatograms during the synthesis of the $(PS)_4(PI)_4$ miktoarm star copolymer. (a): PS arm, (b): PI arm, (c): $Si[CH_2CH_2Si(CH_3)(PS)Cl]_4$ intermediate macromolecule, (d) Unfractionated $(PS)_4(PI)_4$ star block copolymer, (e) Fractionated $(PS)_4(PI)_4$ copolymer.

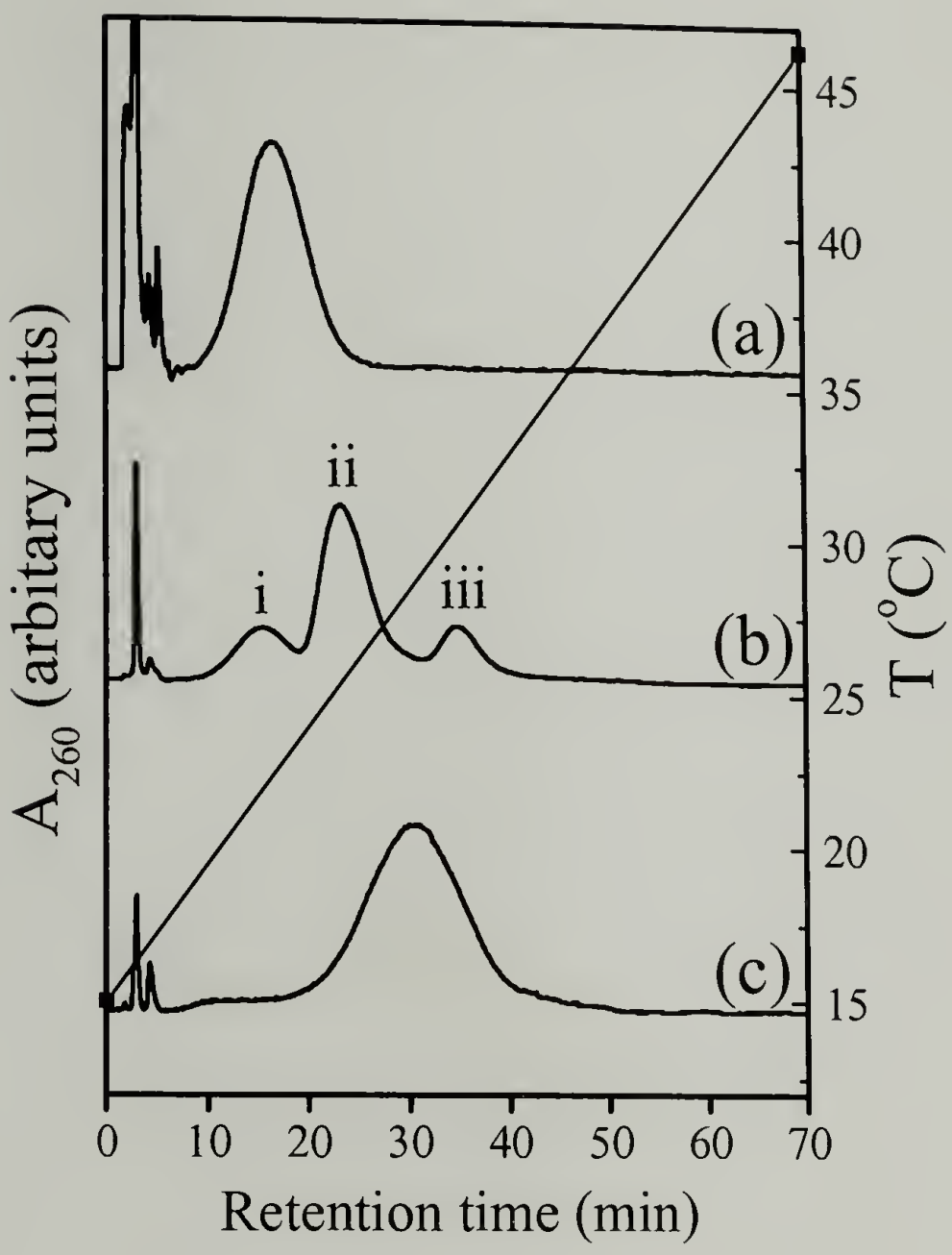

Figure 3.3 Temperature gradient liquid chromatography (TGLC) analyses of the star block copolymers (n = 2, 4, 16). (a): $(PS)_2(PI)_2$, with $(PS)_2(PI)_2$ at 74%; (b) $(PS)_4(PI)_4$, i) 16% of $(PS)_3(PI)_4$, ii) 57% of $(PS)_4(PI)_4$, and iii) 20% of $(PS)_4(PI)_3$; (c) $(PS)_{16}(PI)_{16}$, whose composition can not be resolved by TGLC method.

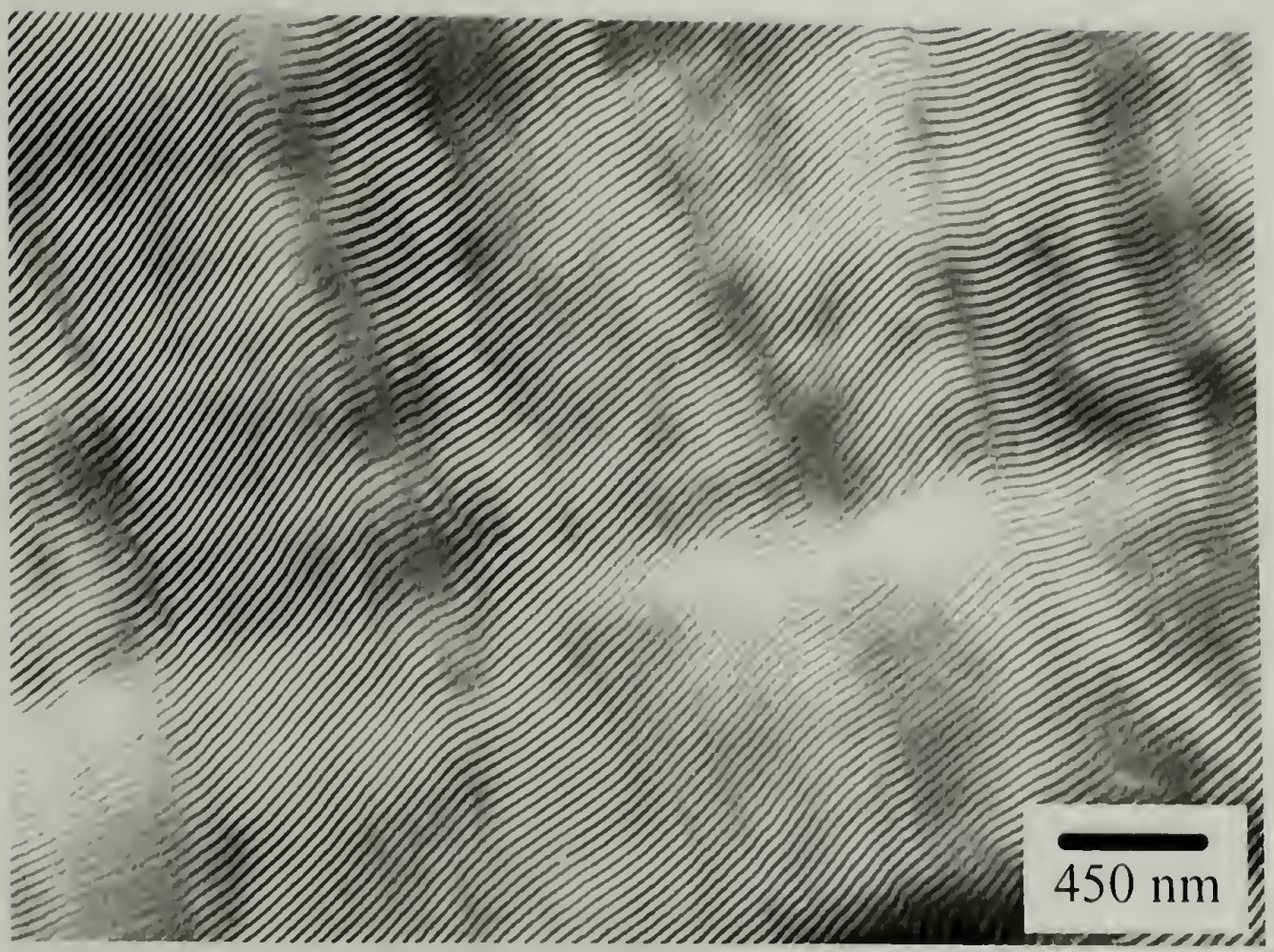

Figure 3.4 TEM image of $(PS)_{16}(PI)_{16}$ star block copolymer.

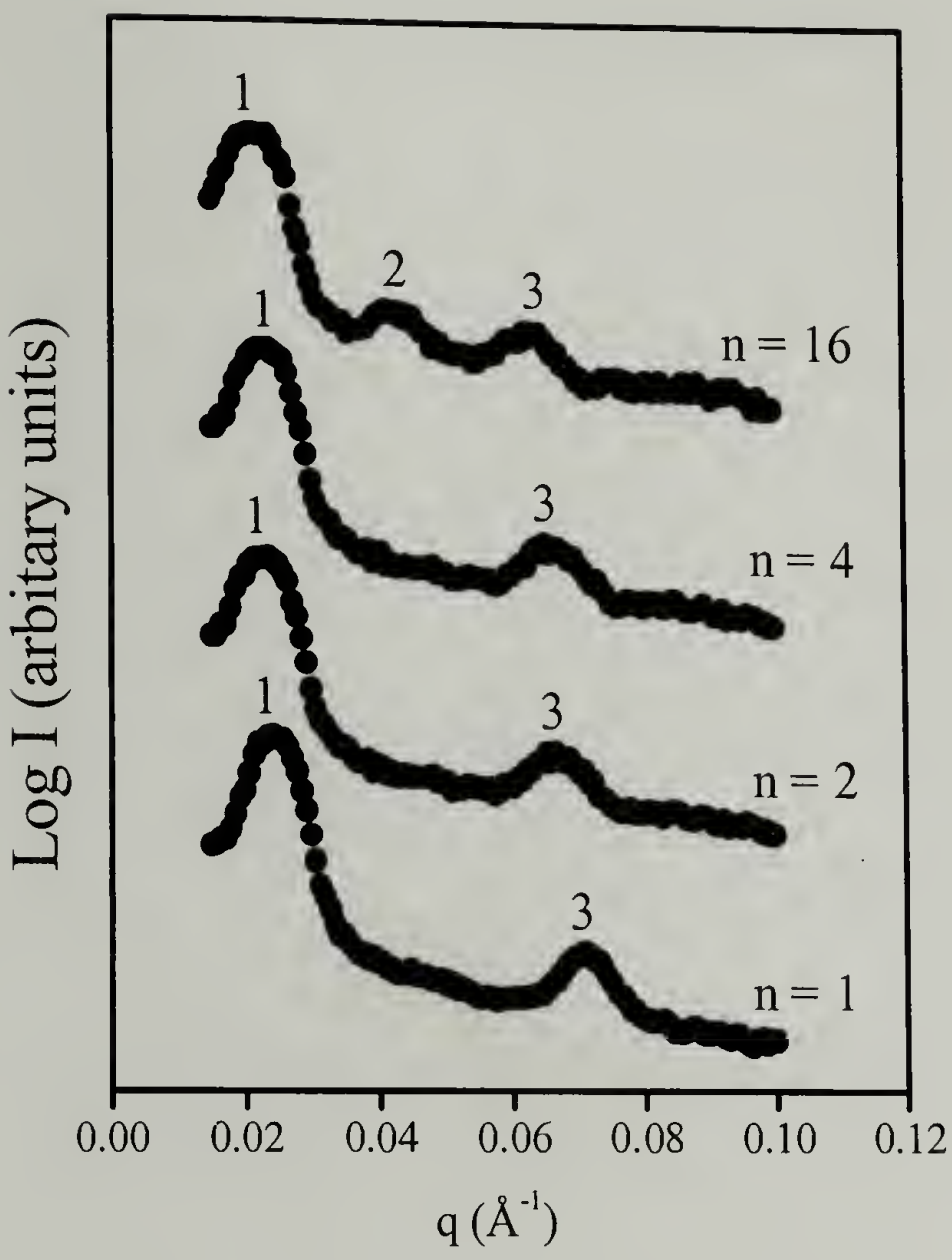

Figure 3.5 Small angle X-ray scattering profiles of the $(PS)_n(PI)_n$ star block copolymers, where n equals 1, 2, 4, and 16 respectively.

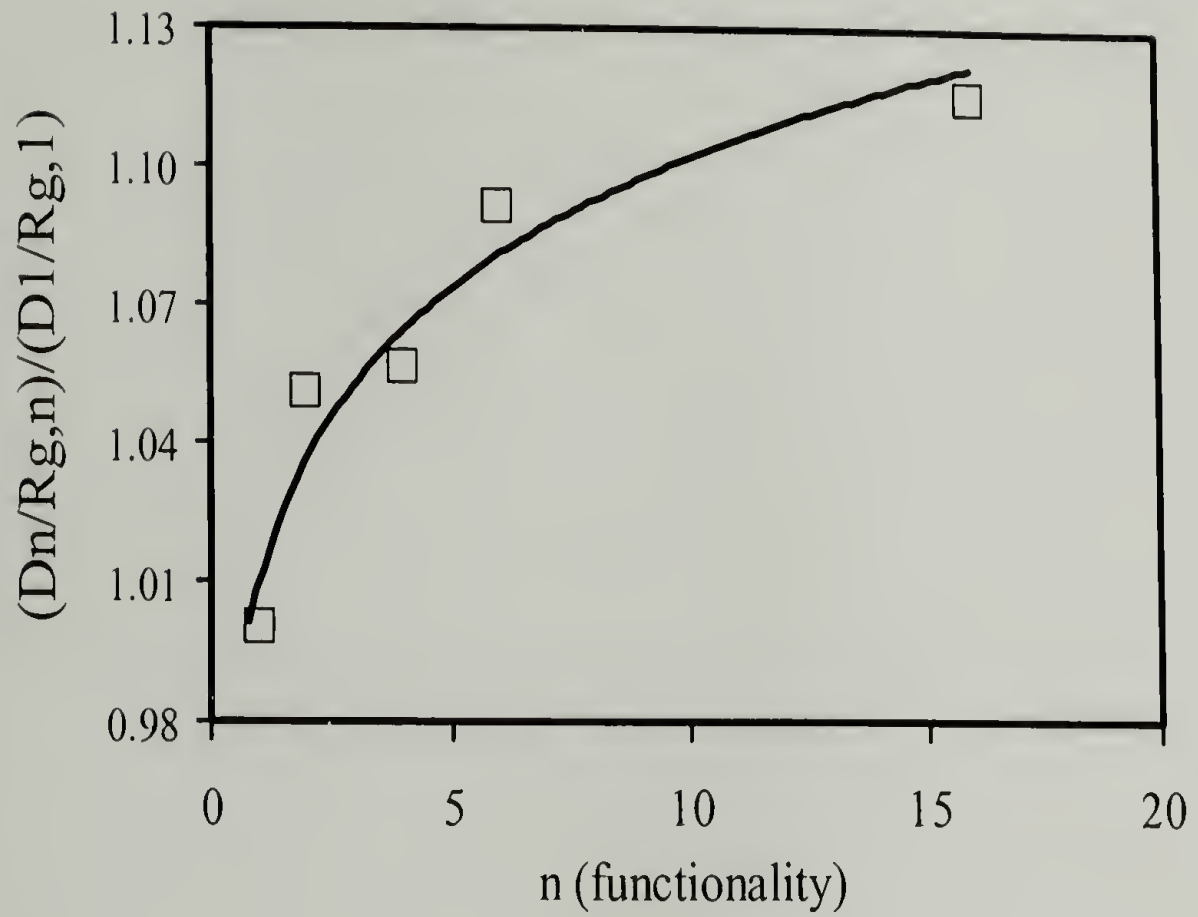

Figure 3.6 Plot of the normalized lamellar long periods ($D_n/R_{g,n}$) of $(PS)_n(PI)_n$ star copolymers (n = 1, 2, 4, 16) divided by that of the diblock member of the series ($D_1/R_{g,1}$) against the respective star functionality (n).

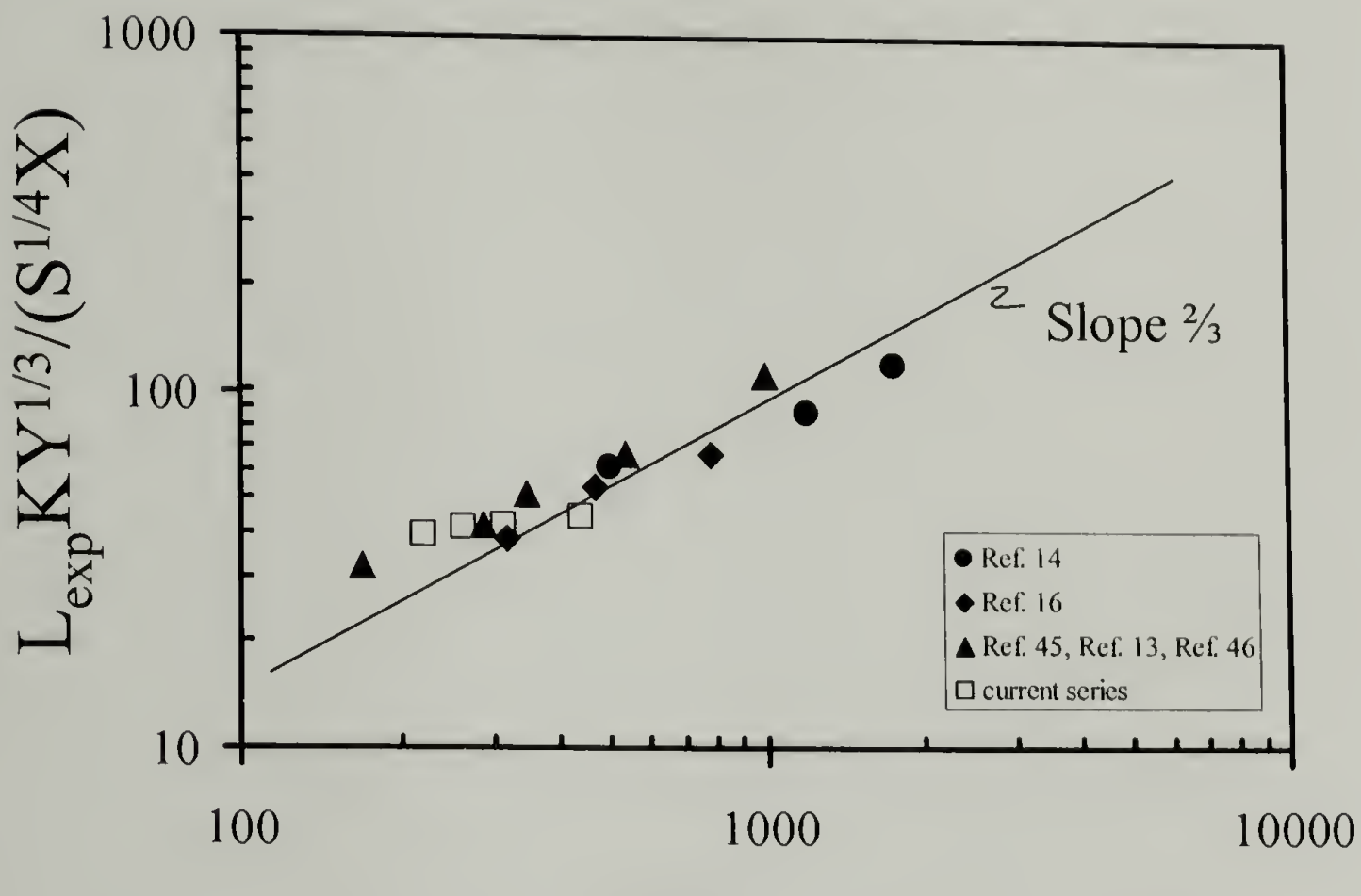

Figure 3.7 The experimental data mapped onto the log-log plot of modified lamellar period $[L_{exp}KY^{1/3}/(S^{1/4}X)]$ vs. $f_B^{1/4}N_B$ as described in reference 16.

CHAPTER 4

MORPOLOGICAL BEHAVIORS OF MUTILGRAFT COPOLYMERS WITH HEXAFUNCTIONAL AND TERTRAFUNCTIONAL JUNCTION POINTS

4.1 Abstract

The effect of chain architecture on the morphological and tensile properties of a series of regularly spaced multigraft copolymers, with tetrafunctional and hexafunctional junction points have been investigated using transmission electron microscopy (TEM), small angle X-ray scattering (SAXS), and tensile testing. The materials were synthesized by coupling difunctional PI spacer and living PS branches with chlorosilane of different functionality. Fractionation technique was used to separate each material into three fractions of low polydispersity, all of which have the same composition unit but different average number of composition units. By applying the "constituting block copolymer concept", the physical behavior of these molecules was compared with the current theories. It is found that morphological behavior of these grafted copolymers can be predicted using this theoretical approach. The number of the junction points, however, greatly influences the long-range order of microphase separation. Additionally, it is found that the tensile properties of these materials are also greatly affected by the molecular architecture and microstructures thus obtained.

4.2 Introduction:

It has long been recognized that molecular architecture of block copolymers is an

important parameter in designing materials with desired properties. Changing from simple diblock copolymers to graft copolymers, the dependence of the morphological behaviors on the volume fraction of the respective block is greatly altered.[1,6,19,27,32] Study of the morphological behavior of materials with novel molecular architectures can help the understanding on how variations in the molecular architecture of block and graft copolymers can be manipulated in order to develop materials with exceptional mechanical, transport, and optical properties, etc. With the development of synthetic approach, materials with more complicated architectures have been synthesized and their physical and mechanical properties have also been studied.[7,8,17,18,54] One of the approaches to probe the morphological behavior of materials with these complex structures is to apply the "*constituting block copolymer concept*".[17,18,35,54] According to this concept, the morphologies of some complicated graft copolymers can be approximated by the constituting block copolymer unit (CBU) associating with each junction points. Thus, in each material, the number of the CBUs is the same as the number of junction points. These CBUs are characteristically the same for each material, and can be described in a general formula A_nB_m, where the A and the B are the two respective blocks of the copolymer, while the n and m represent the number of arm A and arm B at central junction point. The morphological behavior of these materials can be mapped onto their respective morphological diagrams.[1,19,20,32]

Previously, morphological behaviors of multigraft copolymers with randomly spaced trifunctional and tetrafunctional, and regularly spaced tetrafunctional junction points along the backbone have been studied.[17,18] It is found that the number of junction

points greatly affects the long-range of the microstructures. Quantitative study on the grain size of the lamellar morphology shows that the correlation length $\kappa \sim n^{-2.0}$, where n is the number of the junction points in each molecule.[18] The tensile property study on multigraft copolymer with regularly spaced tetrafunctional junction points and 21% of PS shows very higher elongation and comparable stress at break as the commercial materials.[55] It is also found that the stress at break and the strain at break in this multigraft material increase with the increase of number of the junction points, from 5 to 7 and to 10.

The present study, however, concentrates on the effect of chain architecture on the morphological behavior of two series of multigraft copolymers. The two series have regularly spaced either hexafunctional or tetrafunctional junction points with polyisoprene (PI) as backbones and polystyrene (PS) as branches and the PS compositions of these materials cover the whole range of morphological diagram. Figure 4.1 illustrates the molecular architectures of these two groups of materials. The copolymers are synthesized by coupling living PS branches and difunctional PI spacers using chlorosilane linking agent. Material thus formed contains multigraft copolymers having the same building block - CBU but a distribution of molecular weights and accordingly a distribution of the numbers of CBUs. Solvent-fractionation method was employed so that each material is divided into three fractions, all of which have relatively narrow polydispersity (< 1.2). Thus, the distribution of the molecular weight for each fraction is narrow enough to for morphological studies. Additionally, the molecular weights of all the fractions among these multigraft copolymers are over 250 kg/mole,

where molecular weight dependence of mechanical properties is eliminated

4.3 Synthesis and characterization

Details of the synthesis and characterization of these multigraft copolymers can be found elsewhere.[56] The synthetic strategy employs anionic polymerization techniques and utilizes a modular approach in which the branches polystyryllithium, and the spacer poly(1,4-isoprenyl)dilithium are sequentially incorporated into chlorosilane linking centers.

Molecular characterizations of the multigraft copolymers with hexafunctional junction points, the PS branches and the PI spacers are listed in Table 4.1. Molecular characteristics of the tetrafunctional series and their PS branches and PI spacers can be found in Table 4.2. Multiple detection size exclusive chromatography (SEC) methods, combining refractive index (SEC-RI), ultraviolet (SEC-UV), and multiangle laser light scattering (SEC-MALLS) were used to characterize the materials. SEC-RI was performed using a Waters model 510 pump, Waters Ultrastyragel columns (with a continuous porosity range from 106 to 103 Å), and a Waters model 410 differential refractometer. Multidetector SEC analyses (SEC-UV and SEC-MALLS) were performed using a Waters Alliance separations module 2690, Waters Ultrastyragel columns (HR-4, HR-5E, HT-3, HT-6E with a continuous porosity range from 106 to 103 Å), a Waters refractive index detector 2410, a Waters photodiode array detector 996, and a Wyatt Technology Dawn DSP laser photometer. THF solutions were chromatographed at 30 °C and detected at 25 °C. SEC-MALLS and SEC-UV were accomplished using dried and

distilled THF. Weight fractions of PS in these two series of materials are calculated based on ^{1}H NMR measurements in $CDCl_3$, using a Bruker 300 MHz instrument.

Due to the fractionation method employed,[56] the average number of junctions per molecule differs among the fractions of each material. For easy identification, a general nomenclature for these multigraft copolymers is MG-n-ϕ-β. The "n" is the number of polymer blocks associated at each junction points, which is also called "the functionality of the junction points" and the "ϕ" represents the total PS volume fraction. The "β" refers to the averaged number of junction points per molecule in that fraction, which is sometimes omitted to represent all three fractions in the same group. Thus, MG-6-11-5.2 refers to the fraction of the multigraft copolymer (MG) with hexafunctional junction points, 0.11 of PS volume fraction and an average of 5.2 junction points per molecule. These labels can be found in Table 4.1 for hexafunctional multigraft copolymers and in Table 4.2 for tetrafunctional multigraft copolymers.

4.4 Morphological characterization

Morphological characterizations of these two series of materials are listed in Table 4.1 and Table 4.2 respectively.

Tensile testing of these specimens is describe in section 1.4.

4.5 Results and discussion:

Figure 4.2 displays a series of images, where microstructure ordering is

improving with decreasing average number of junction points per molecule in the three fractions of MG-6-21. In MG-6-21-5.2, shown in Figure 4.2a, the material is microphase separated with no long range order. Some poorly ordered lamellae were found in the MG-6-21-3.6, as those shown in Figure 4.2b. Shown in Figure 4.2c is the fairly well ordered lamellar morphology found in sample MG-6-21-2.7. Ordering of lamellar morphology is greatly improved compared to the other two factions with higher number of CBUs. Thus, as the number of branch points per molecule increases, the ability to form long range order is dramatically reduced. The scattering data of the three fractions in MG-6-21 series are shown in Figure 4.3. For all three fractions, the profiles yield only the primary reflection q^*. The average domain sizes are calculated to be 34.9 nm based on this primary reflection.

Lamellar morphologies are found in all three fractions of MG-6-35. Figure 4.4 shows the TEM image of sample MG-6-35-2.3 as a representative of these well-ordered structures. Scattering data of all three fractions in this group can be found in Figure 4.5. Multigraft copolymer MG-6-35-2.3 and MG-6-35-1.9 show three orders of reflections at ratios of 1:2:4 of primary reflection q^*, while that of MG-6-35-3.0 only gives the primary reflection peak q^* and one higher reflection at $2q^*$. This result directly supports the TEM observation in these three fractions that lamellae ordering increases with decreasing number of junction points. Based on the primary scattering vector q^* of the three fractions, lamellar spacing is calculated to be 46.4 nm for MG-6-35-3.0, 44.1 nm for MG-6-35-2.3, and 38.4 nm for MG-6-35-1.9.

All fractions of MG-4-14 form minor PS in a PI matrix. Shown in Figure 4.6 is the TEM image of MG-4-14-2.5. The shape of the PS domains indicates the coexistence of spheres and cylinders. However, their scattering profiles displayed in Figure 4.7 do not have any reflection other than the primary q^* to compare with the form factor of either spherical or cylindrical morphology.[43,57]

Samples from MG-4-23 all form hexagonally packed PS cylinders in PI matrix. Figure 4.8 shows the micrograph of MG-4-23-2.3. Scattering data of all the fractions in Figure 4.9 have a primary q^* and one higher order Bragg's reflections. These higher order reflections are consistent with the form factor of cylinders.[57] For comparison, the form factor from cylindrical domains of the same PS volume fraction as MG-4-23 is plotted as a solid line in Figure 4.9.

All materials in MG-4-41 form lamellae. Figure 4.10 shows the TEM micrograph of MG-4-41-4.4. Figure 4.11 illustrates the scattering profiles of all fractions in MG-4-41. Higher order reflections of SAXS are found in sample MG-4-41-4.4, which has the lowest number of junction points per molecule.

As described previously, the morphological behavior of the multigraft copolymers can be predicted by applying the "*constituting block copolymer concept*". For the multigraft copolymers with regularly placed hexafunctional junction points, the constituting block copolymer unit (CBU) is a I_2S_4 copolymer, whose morphology can be approximated by that of IS_2 copolymers. Each PI block in the CBU is half of the PI

spacer while the PS block is the same as the living PS arms used in the synthesis. The morphological diagram of such materials with a single junction point is predicted by *Milner*[32] whose analysis predicts morphology as a function of composition and molecular architecture asymmetry.

In order to map the CBU onto Milner's phase diagram, the asymmetry parameter, $\varepsilon = (n_A/n_B)(l_A/l_B)^{1/2}$, for current system is calculated. The n_i is the number of arms of each block at each central junction point, while the l_i is a material parameter and $l_i = V_i/R_i^2$. V_i and R_i are the volume and radius gyration of one arm of polymer block i. For our current system, $\varepsilon = 2.01$, where A block is chosen to be PS and the B block is the PI.

According to *Milner*'s diagram and the "*constituting block copolymer concept*", all the multigraft copolymers with hexafunctional junction points are expected to form lamellar morphology. Experimental results of multigraft copolymers in MG-6-35 match well with theoretical prediction. Higher order reflections from lamellae were observed in the scattering data of fractions with fewer numbers of average junction points per molecule. The finding, that the long range order of multigraft copolymers decreases with higher number of junction points, is consistent with previous results of multigraft copolymers with trifunctional and tetrafunctional junction points,[17,18] and is constantly observed throughout the materials in this study. Similarly, MG-6-21-5.2 has very poor ordering comparing to the ones with fewer number of junction points in the same series. It is possible that when the number of junction points per molecule is beyond certain limit, these junction points are kinetically trapped at different interface and thus hinder the

formation of ordered microdomains. Higher number of junction points may not only be able to decrease the long-range order of the material, but may also completely disrupt the formation of the recognizable morphology.

Stress-strain curves for the three fractions MG-6-21 are displayed in Figure 4.12. Clearly, increasing the number of hexafunctional junction points results in an increase in strength with small loss in extensibility. These trends are similar to those reported and published earlier for multigraft copolymers with tetrafunctional junction points.[55]

For multigraft copolymers with tetrafunctional junction points, the CBU is I_2S_2, whose morphological behavior can be approximated by that of PS-PI diblock with the same PS block as the living PS arms and the half of the PI spacer used in synthesizing the copolymers. The mapping of these multigraft copolymers onto the morphology diagram calculated by *Matsen*[6,19] indicates that the theory and experimental results match well for fractions in multigraft copolymers MG-4-23 and MG-4-41. The fact that the TEM observation of MG-4-14 indicates the coexistence of cylinder and spheres is consistent with its mapping on the diagram, on which the data point is on the boundary of spheres and cylinders. In addition, the increase of long-range order with decrease of the number of junction points per molecule phenomenon is also observed in the multigraft copolymers with tetrafunction junction points.

Figure 4.13 compares the stress vs. strain behavior of 5 branch points, 21% of PS multigraft materials of MG-4-21-5 and MG-6-21-5.2. These two materials have identical

PS composition and the same number of junction points per molecule. The only difference between them is the junction point functionality. However, the multigraft copolymer with hexafunctional junction points result in an approximately 2.5x increase in strength with a modest about 20% reduction in ultimate strain. This shows that the MG materials with hexafunctional junction points provide significantly more robust mechanical reinforcement than do the one with tetrafunctional junction points. The microscopic foundation between the discrepancies is that the MG material with hexafunctional junction points forms lamellar morphology while the one with tetrafunctional junction points forms PS cylinders. This manifests the influence on the mechanical properties from morphology, which is due to the change in chain architecture, other than the change in PS composition.

Table 4.1 Molecular and morphological characterization of multigraft copolymers with regularly spaced hexafunctional junction points.

		Mw [a] ($\times 10^3$g/mol)	# junctions /molecule	PS Vol% [b]	Morphology	D [c] (nm)
MG-6-21	PS branch	8.2				
	PI spacer	86.8				
MG-6-21-5.2		705	5.2	21.8	Microphase separated	34.6
MG-6-21-3.6		515	3.6	21.6	Lamellae	34.6
MG-6-21-2.7		411	2.7	21.4	Lamellae	34.6
MG-6-35	PS branch	13.0				
	PI spacer	63.3				
MG-6-35-3.0		409	3.0	35.6	Lamellae	46.4
MG-6-35-2.3		328	2.3	35.4	Lamellae	44.1
MG-6-35-1.9		287	1.9	35.6	Lamellae	38.4

a: Weight average molecular weight measured using SEC-MALLS (multi-angle laser light scattering).
b: PS volume fraction Calculated based on the averaged mass percentage from ^{1}H NMR and SEC-UV analyses.
c: Domain spacing $D = 2\pi/q^*$, where q^* is the primary Bragg's reflection.

Table 4.2 Molecular and morphological characterization of multigraft copolymers with regularly spaced tetrafunctional junction points.

		Mw [a] ($\times 10^3$g/mol)	# junctions /molecule	PS Vol% [b]	Morphology	D [c] (nm)
MG-4-14	PS branch	11.1				
	PI spacer	97.2				
MG-4-14-5.5		691	5.5	14.2	Spheres and Cylinders	28.5
MG-4-14-3.5		475	3.5	14.2	Spheres and Cylinders	28.5
MG-4-14-2.5		372	2.5	14.0	Spheres and Cylinders	31.5
MG-4-23	PS branch	16.8				
	PI spacer	87.6				
MG-4-23-6.6		891	6.6	23.3	PS Cylinders	31.5
MG-4-23-4.4		624	4.4	22.8	PS Cylinders	31.5
MG-4-23-3.2		472	3.2	22.7	PS Cylinders	33.9
MG-4-41	PS branch	26.6				
	PI spacer	63.6				
MG-4-41-7.4		930	7.4	40.8	Lamellae	38.4
MG-4-41-5.3		681	5.3	41.0	Lamellae	38.4
MG-4-41-4.4		572	4.4	41.0	Lamellae	41.0

a: Weight average molecular weight measured using SEC-MALLS (multi-angle laser light scattering).
b: PS volume fraction Calculated based on the averaged mass percentage from ^{1}H NMR and SEC-UV analyses.
c: Domain spacing $D = 2\pi/q^*$ where q^* is the primary bragg's reflection.

(a)

(b)

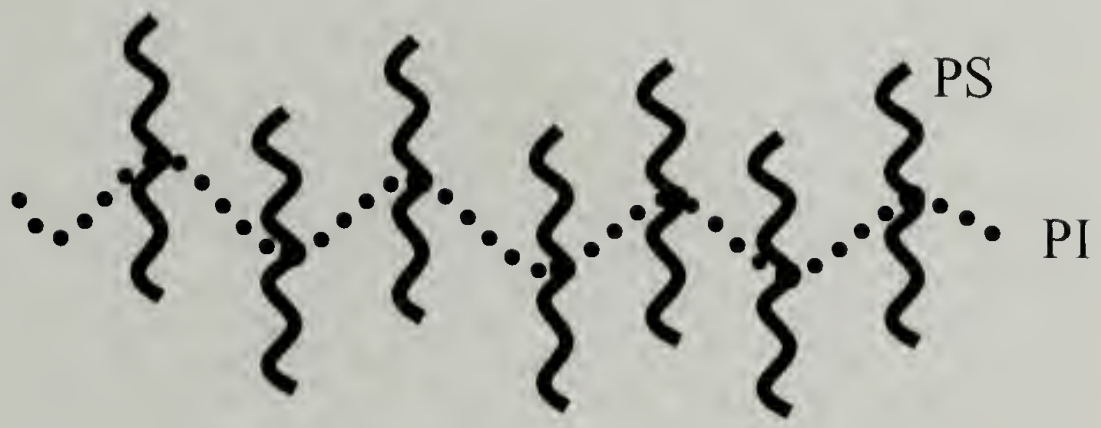

Figure 4.1 Illustration of two types of multigraft copolymers used in this study with regularly spaced (a) hexafunctional and (b) tetrafunctional junction points.

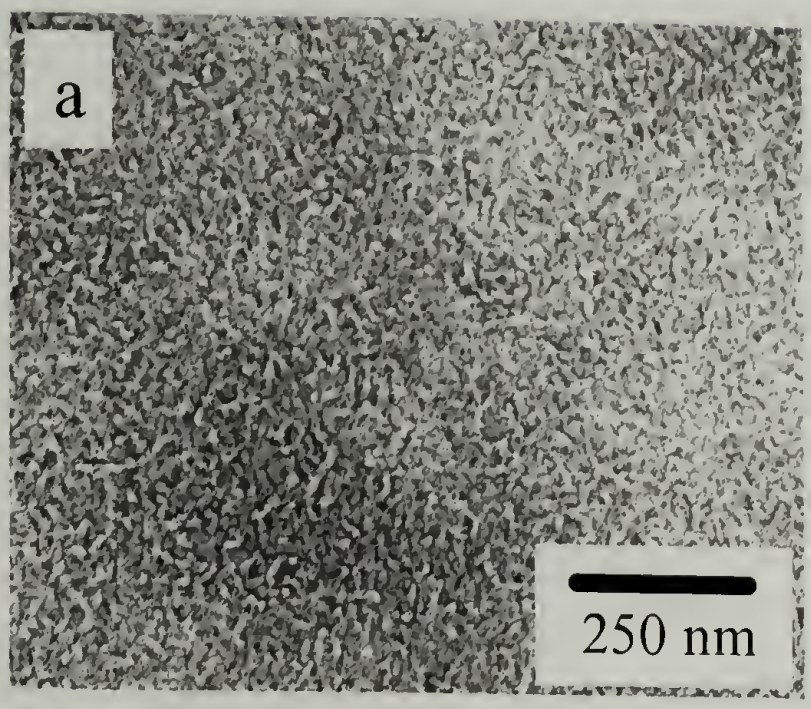

Figure 4.2 TEM images of multigraft copolymers (a) MG-6-21-5.3, (b) MG-6-21-3.6, and (c) MG-6-21-2.7. Continued next page.

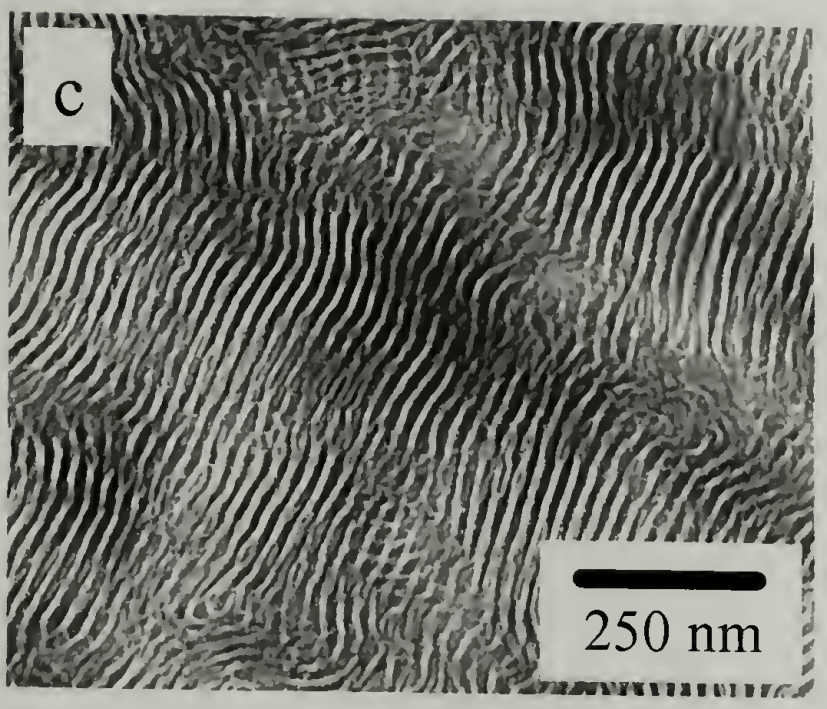

Figure 4.2 Continued.

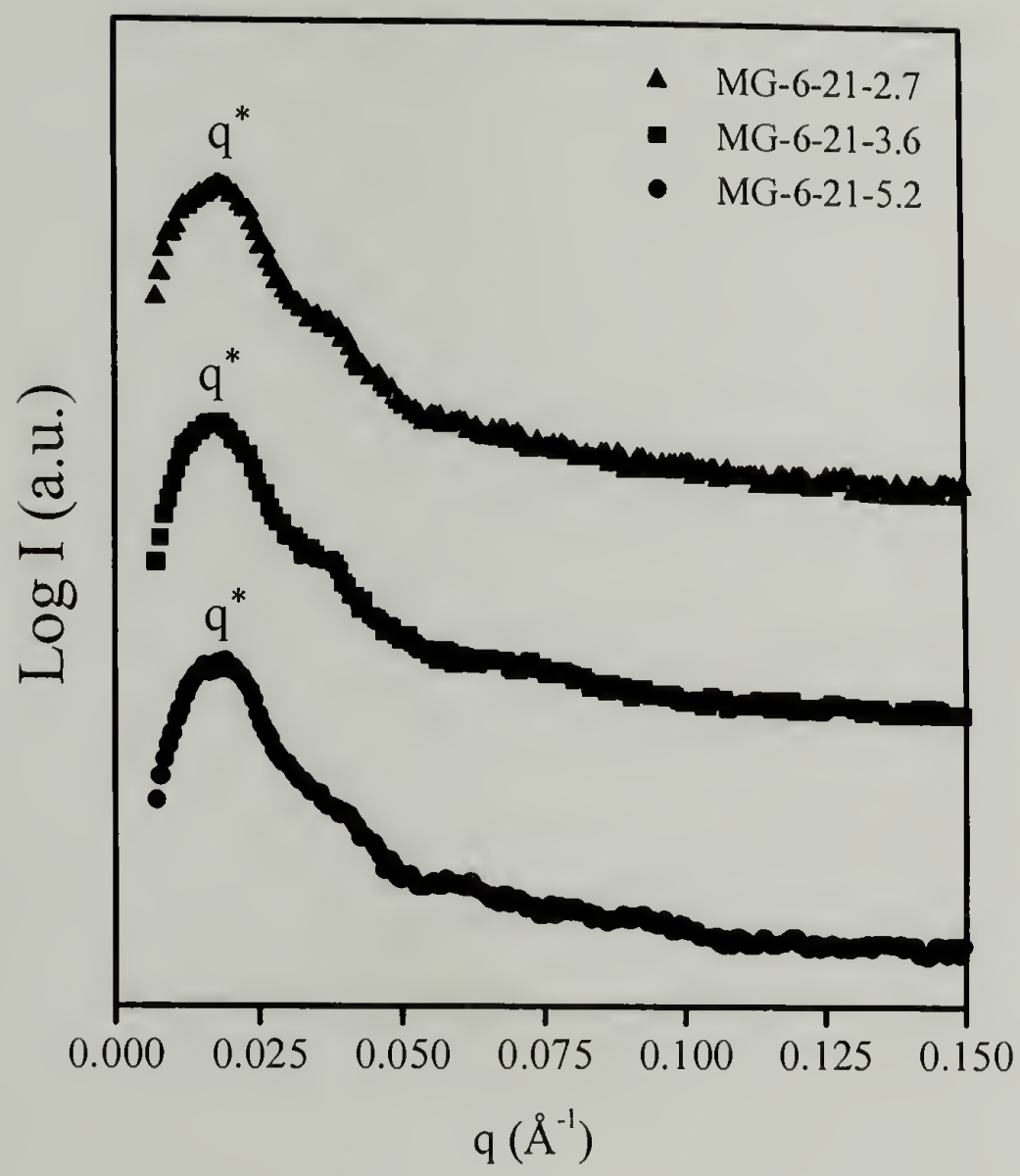

Figure 4.3 Small-angle X-ray scattering profiles of MG-6-21 samples.

Figure 4.4 TEM micrograph of sample MG-6-35-1.9 showing lamellar structure.

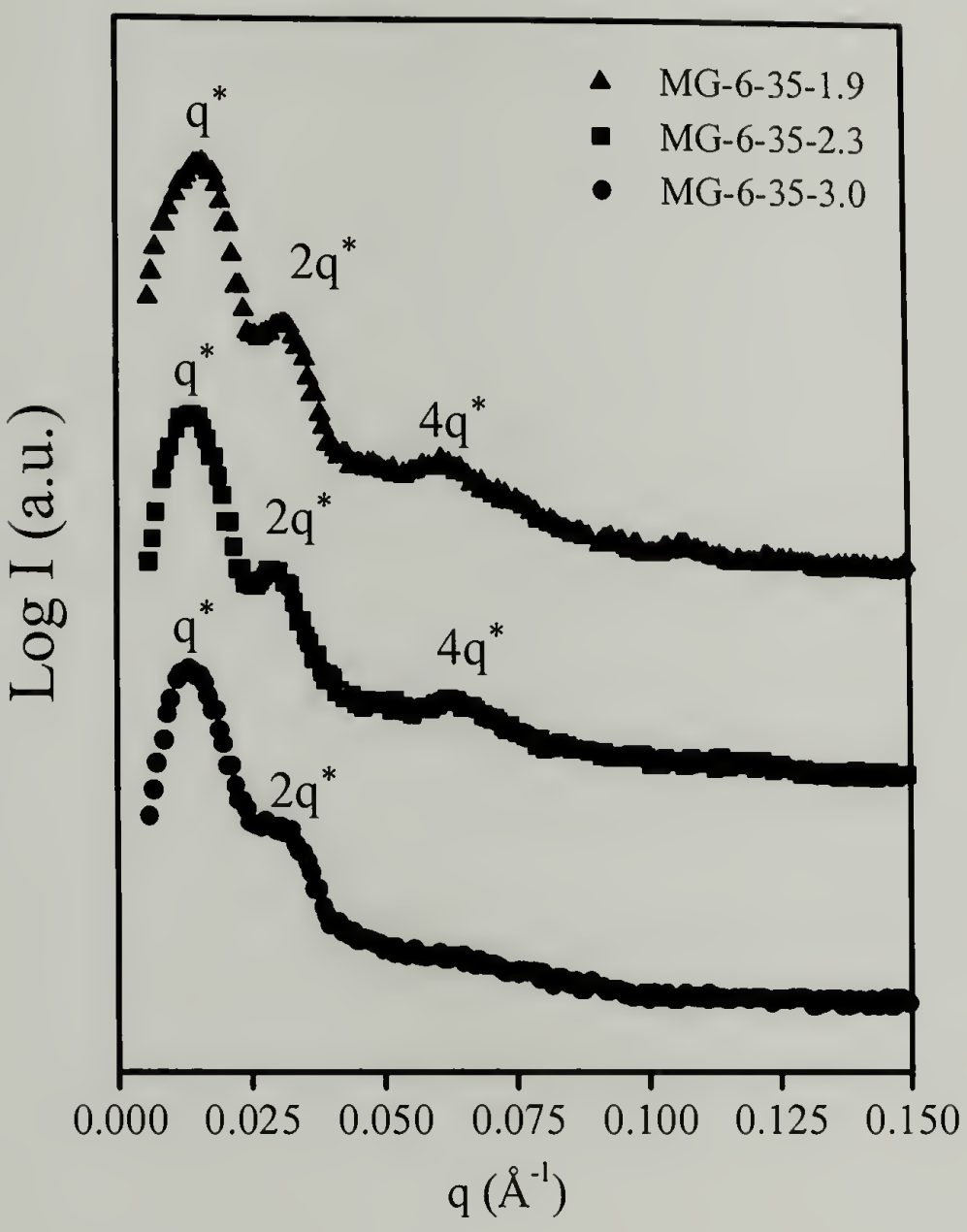

Figure 4.5 Small-angle X-ray scattering of all fractions in MG-6-35.

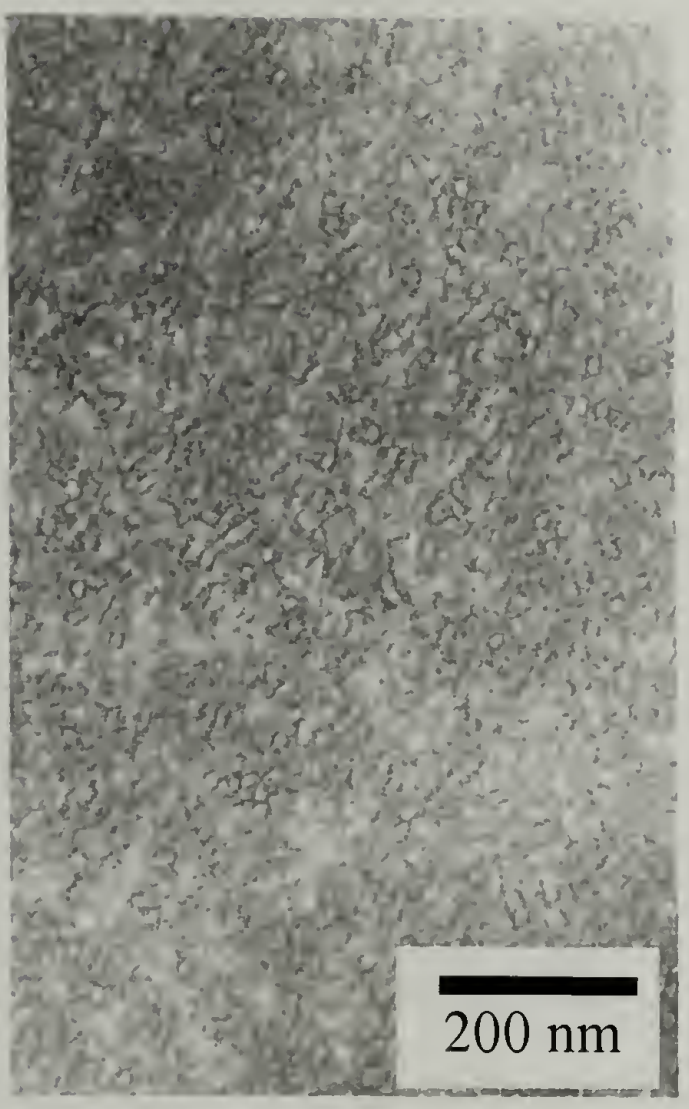

Figure 4.6 TEM observation of tetrafunctional multigraft copolymer MG-4-14-2.5.

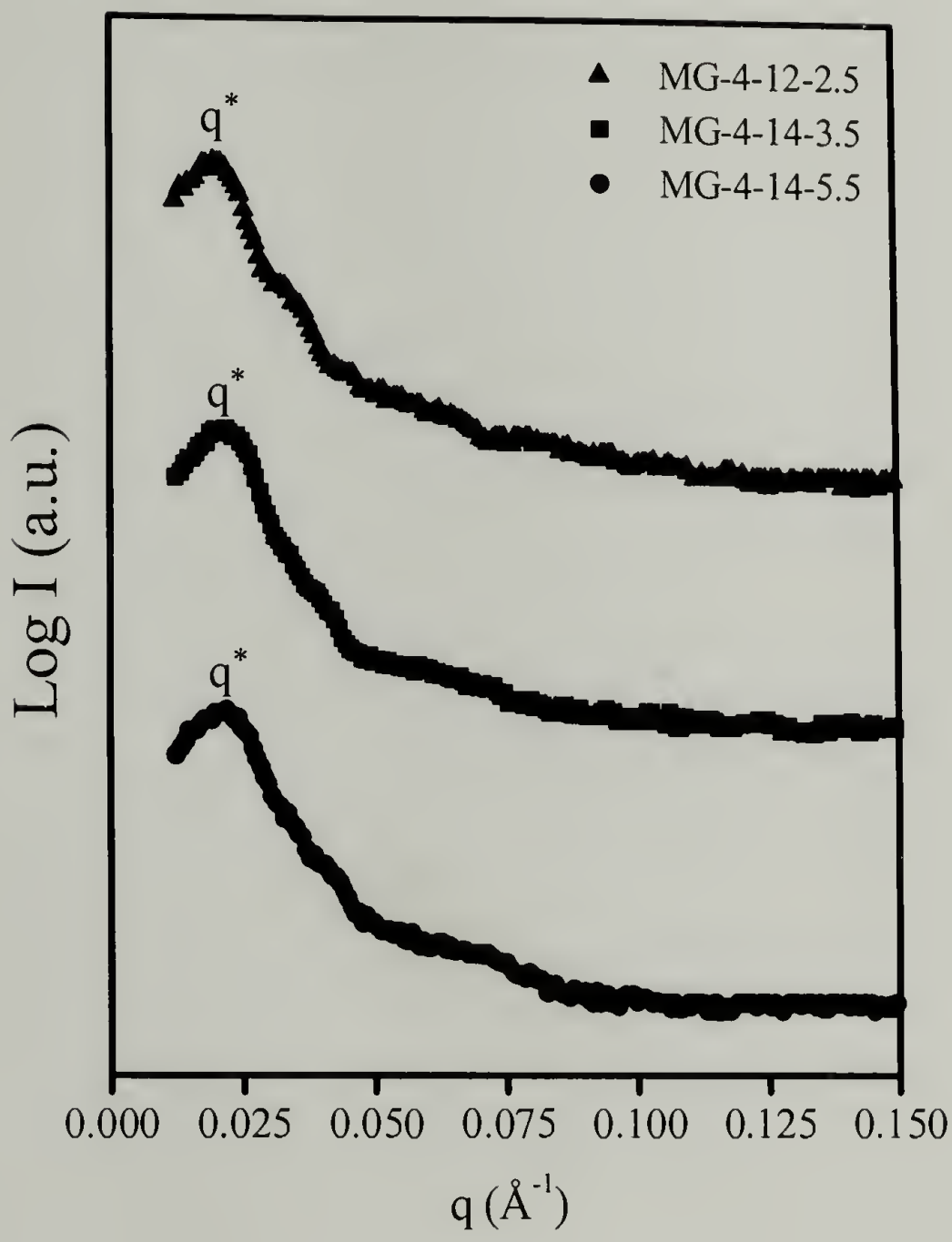

Figure 4.7 SAXS data of the three fractions in material MG-4-14.

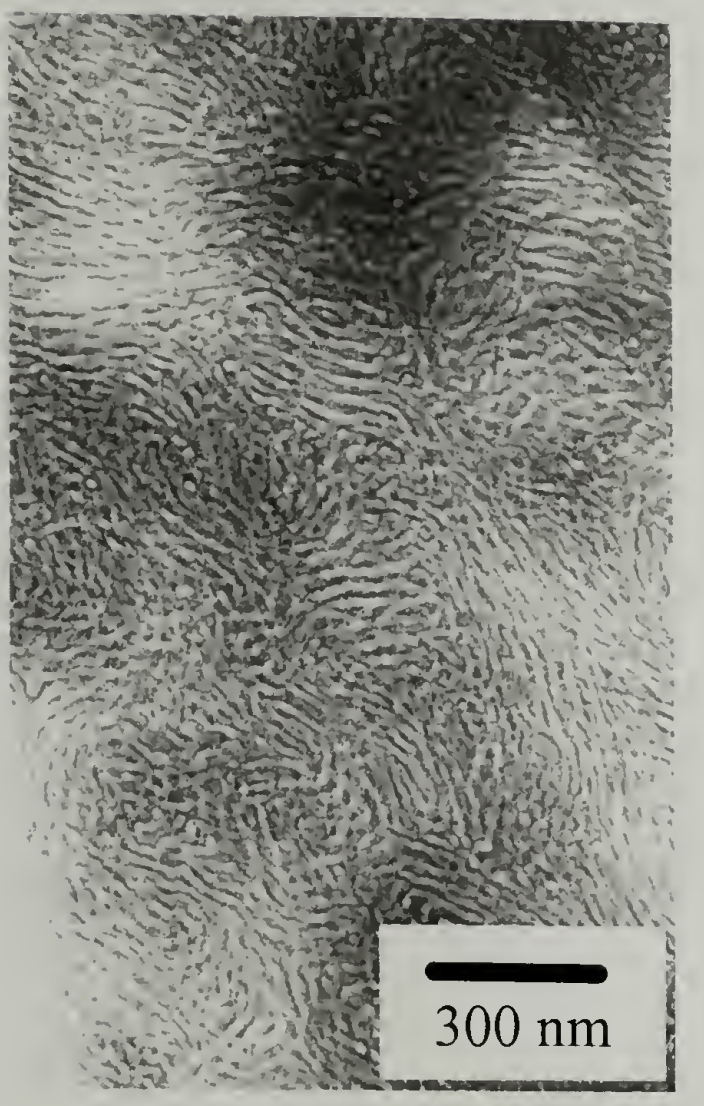

Figure 4.8 Cylindrical structures found in MG-4-23-3.2 with PS as the minority domain.

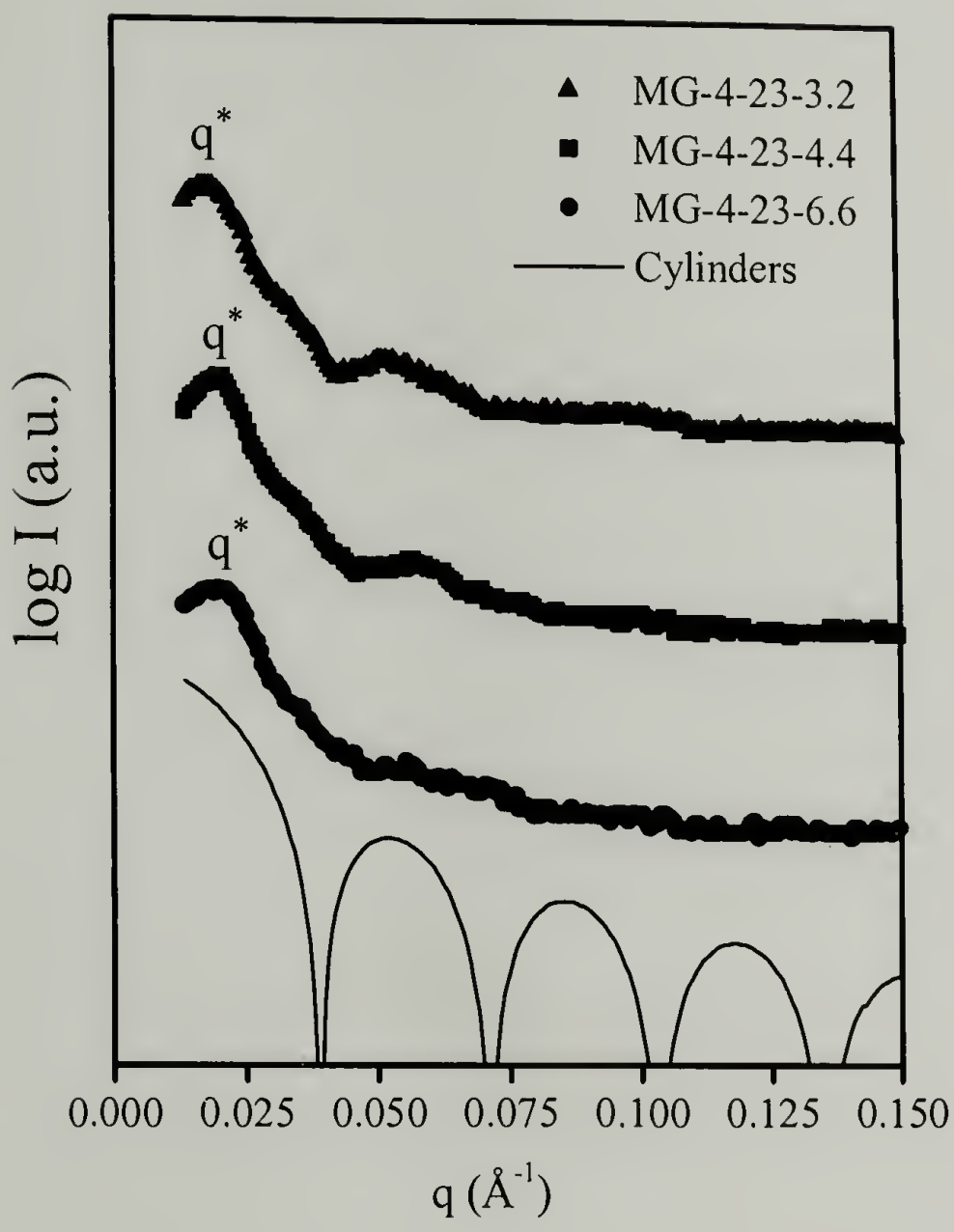

Figure 4.9 Scattering profiles of multigraft samples in MG-4-23.

Figure 4.10 TEM image of multigraft copolymer MG-4-41-4.4.

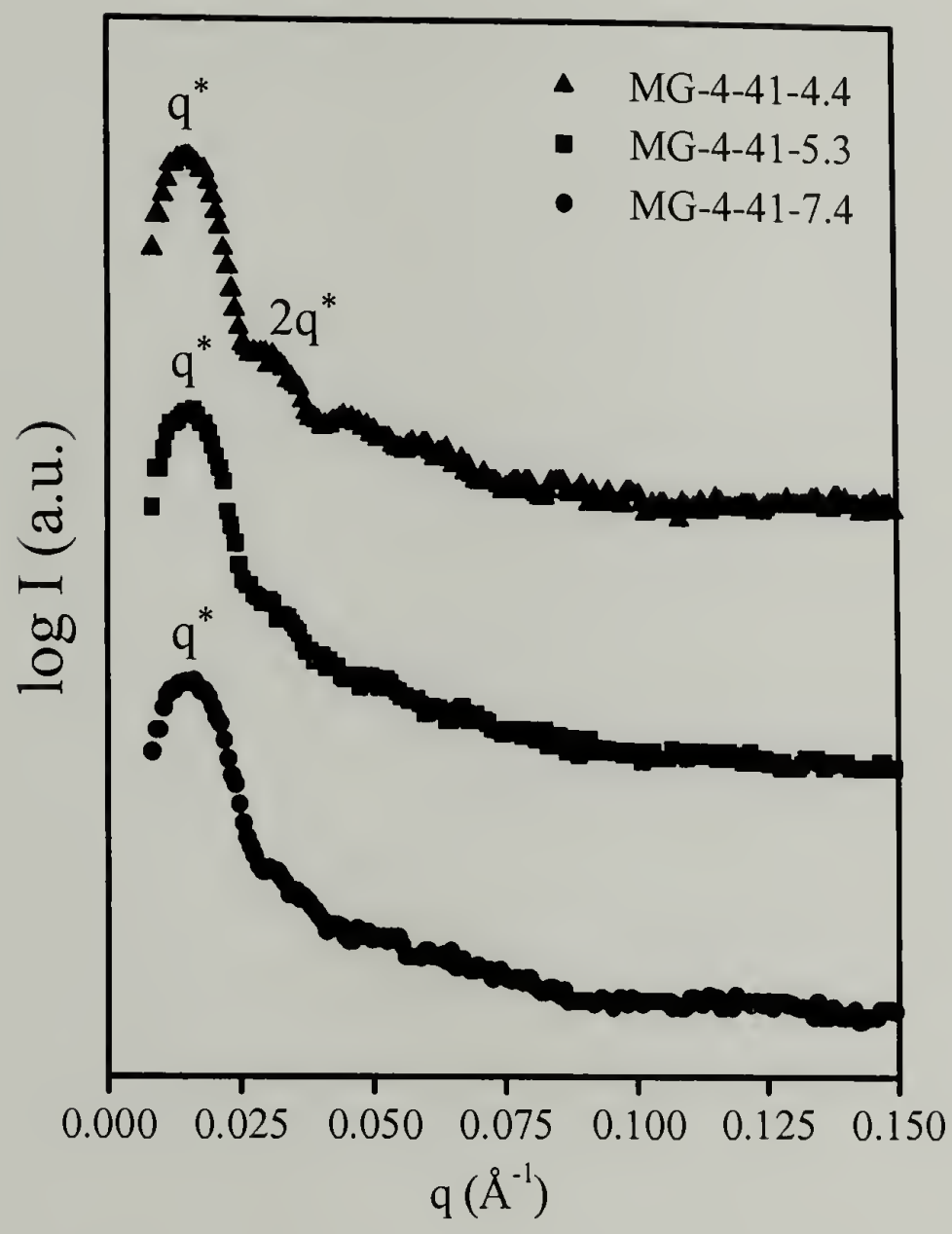

Figure 4.11 Small angle X-ray scattering profiles of MG-4-41 fractions.

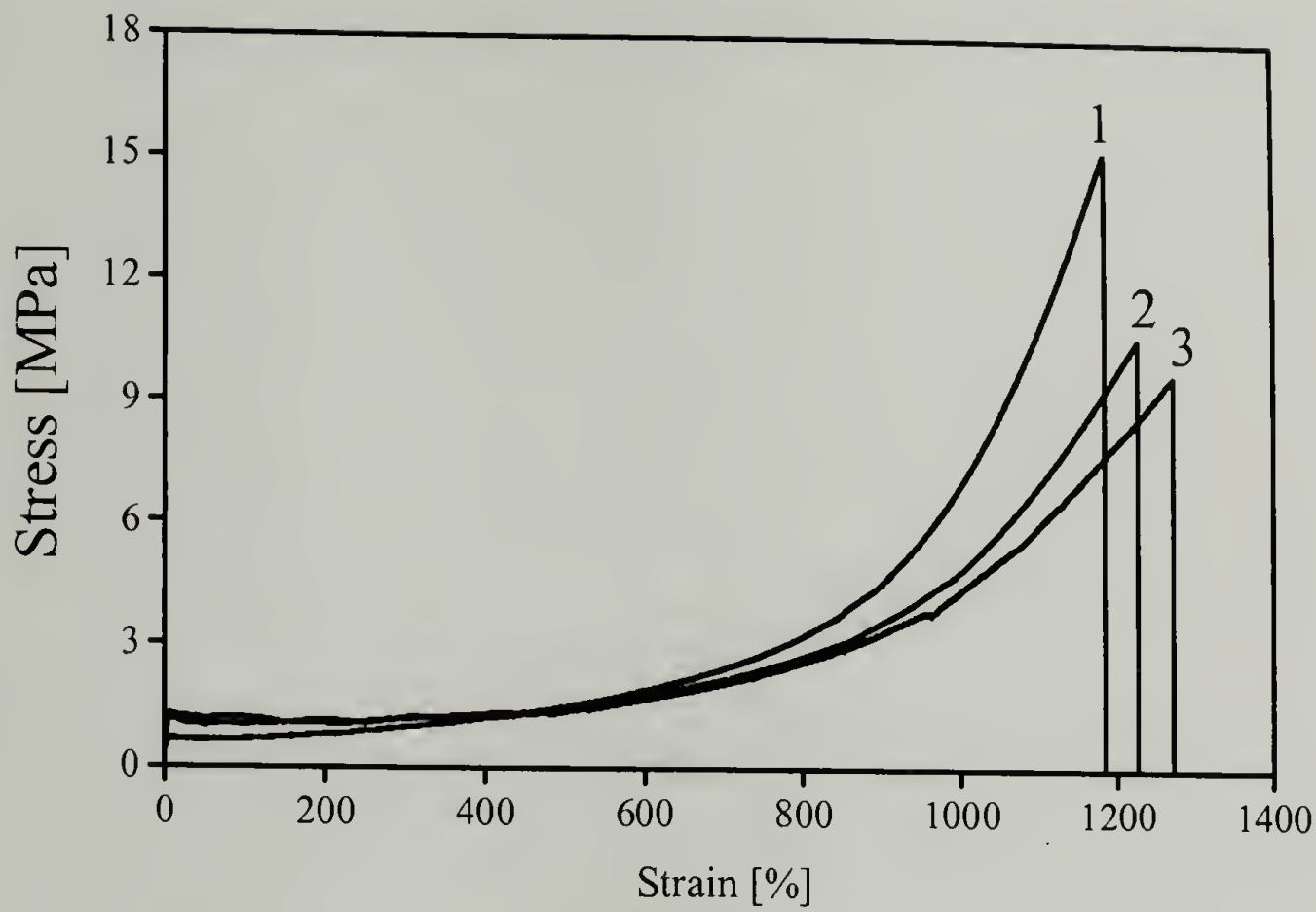

Figure 4.12 Comparison of stress vs. strain behavior of MG-6-21 with average number of junction points per molecule of (1) 5.2, (2) 3.6, and (3) 2.7 respectively.

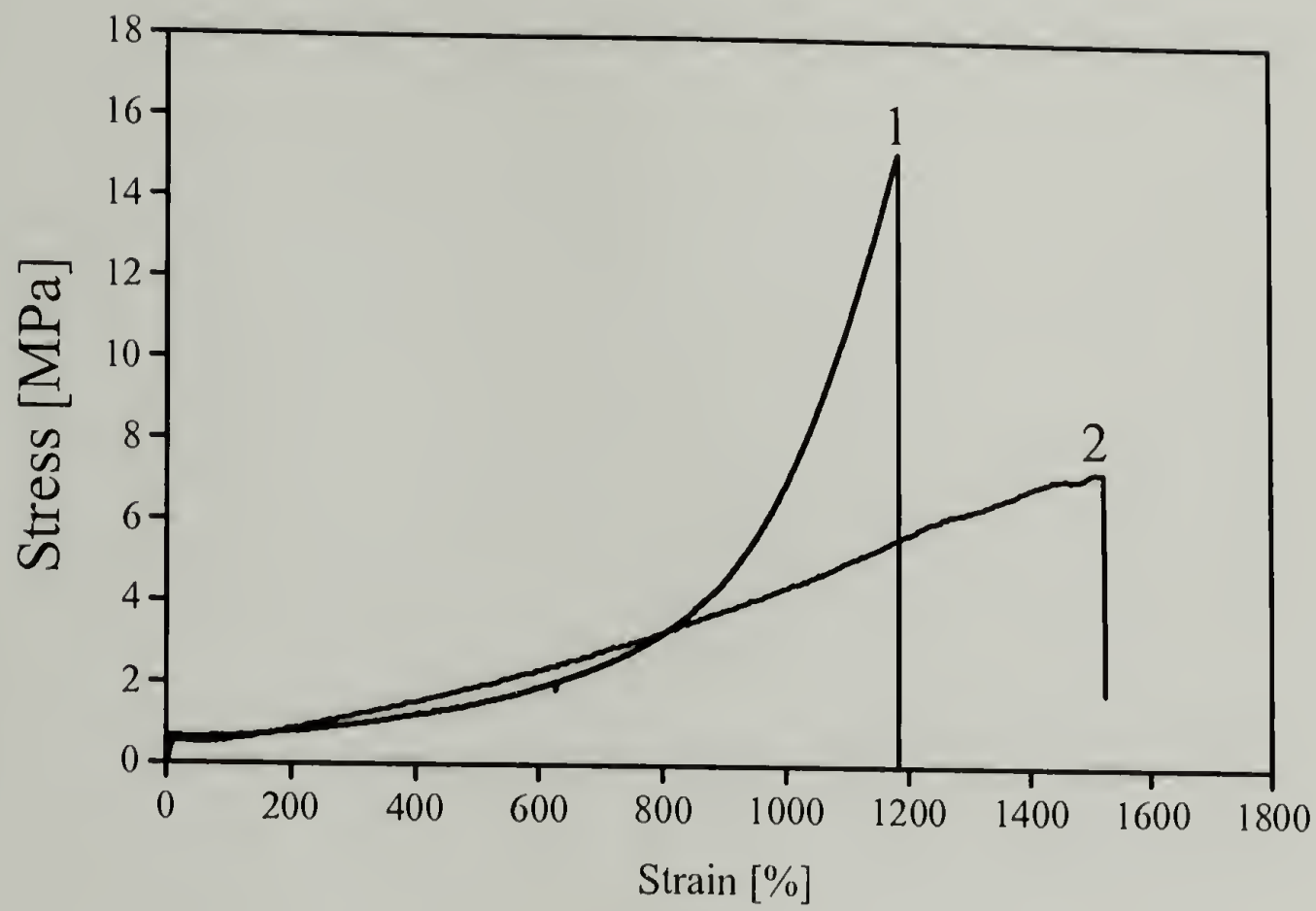

Figure 4.13 Comparison of stress vs. strain behaviors of multigraft copolymers with 21% of PS, and 5 junction points per molecule. (1) MG-6-21-5.2, and (2) MG-4-21-5.0.

CHAPTER 5

MORPHOLOGIES AND TENSILE PROPERTIES IN A SERIES OF BLOCK-DOUBLE-GRAFT (BDG) COPOLYMERS AND TERPOLYMERS

5.1 Abstract

Morphological characteristics and mechanical properties of a series of block-double-graft (BDG) copolymers and terpolymers polystyrene-[1,2-polybutadiene-*g*-X_2] (X = 1,4-polybutadiene, polyisoprene, polystyrene, and polystyrene-*b*-polyisoprene diblocks) were investigated by transmission electron microscopy (TEM), small angle X-ray scattering (SAXS), and tensile testing. All BDG materials have linear polystyrene-1,2-polybutadiene (PS-*b*-1,2-PBD) diblock copolymer backbones. Two identical branches are grafted at every randomly distributed tetrafunctional junction point on the 1,2-PBD part of the backbone. Standard microstructures, such as body-center-cubic spheres, hexagonally packed cylinders and lamellae, are obtained at different total PS volume fractions. It is found that when the branches are polydienes, the BDG molecules form the same morphologies as their linear diblock counterparts. In such cases, phase separation occurs between the polystyrene domain and a combined diene microdomain formed by the backbone 1,2-PBD part and the polydiene branches. In BDG materials in which the branches are polystyrene-polyisoprene diblock copolymers, lamellae are obtained at a total PS volume fraction close to 0.50. It is found that the domain spacings of these materials are predominately determined by molecular weights of the diblock branches instead of the backbones. A lamellae-forming BDG terpolymer with an average

of three tetrafunctional junction points per molecule exhibited characteristic thermoplastic elastomer properties with its stress at break at 32 M Pa and strain at break of 1000%. It is proposed that the high strength of this BDG terpolymer is attributed to the chain conformation in the microphase-separated state. The elastic PBD blocks of the backbone bridge adjacent PS domains through multiple junction points, resulting in the enhanced elastomeric properties. Several parameters are found to influence the mechanical properties of these BDG materials: (1) The existence of backbone PS; (2) The molecular weight of the branches; (3) The number and functionality of branch points on the 1,2-PBD part of the backbone.

5.2 Introduction

Molecular architecture plays an important role in determining morphology, phase behavior and material properties of block copolymers. While the morphology of linear, conformationally symmetric diblock copolymers relies entirely on the volume fraction of the respective blocks,[23,32,58,59] the morphology of single graft and A_mB_n star block copolymers also depends on an additionally factor - the molecular asymmetry parameter, $\varepsilon = (n_A/n_B)(l_A/l_B)^{1/2}$. The ratio of number of arm of the two block types (n_A/n_B) represents the asymmetry due to the architecture. The conformational asymmetry between the two block materials is expressed by the ratio $(l_A/l_B)^{1/2}$, where l_i is the ratio of segmental volume to the square of statistical segment length for the block material i.[32] At $\varepsilon = 1$, conformationally symmetric, AB diblock behavior is observed with the morphology windows being symmetric around 0.5 volume fraction. However, as one increases the arm number of one species relative to the other, the morphological behavior may become

strongly asymmetric with respect to volume fraction. Hence, branched block copolymers are able to yield morphologies that cannot be formed by linear diblock copolymers at the same volume fractions.

In linear ABC triblock copolymer systems, the molecular architecture, the three interaction parameters between different pairs of polymer blocks, and the volume fraction of each block, combine to yield fascinating nanoscale morphologies.[7-10,60,61] While most studies on block copolymers are focused on the influence of chain architecture on phase behavior and morphology, far fewer have focused on the correlations among molecular architecture, the microstructure thus obtained, and the resulting mechanical properties.[62-67] This lack of well-controlled studies linking molecular architecture to mechanical properties no doubt is the result of the difficulties inherent in synthesizing even small amounts of molecules of highly controlled yet complex molecular architecture. While such small quantities of material are sufficient for morphological study they are generally not sufficient for mechanical properties evaluation.

The influences of molecular architecture on mechanical properties of block copolymers can be demonstrated by the higher tensile strength obtained by triblock copolymers with a glassy-rubbery-glassy block sequence compared to diblocks of similar composition and molecular weight.[68] The rubbery middle block of a triblock copolymer produce bridges between glassy domains, thereby creating a physically crosslinked nanocomposite system which can be processed at elevated temperatures. The rubbery block of diblock copolymers, on the other hand, possesses a covalent bond to only one of

the adjacent glassy domains and thus is not able to form this physically crosslinked network. Similar conclusions have been reached comparing weakly segregated poly(styrene-*b*-butylmethacrylate) (PS-PBMA) diblocks and PBMA-PS-PBMA triblock copolymer systems. Recently, mechanical properties of a group of tetrafunctional multigraft PI-*g*-PS_2 copolymers, with the molecular architecture illustrated in Figure 5.1a, have been studied by *Weidisch*.[55] These results indicate that higher numbers of junction points per molecule, as well as the fact that there are two PS branches per junction point, enhances energy transfer from the rubbery matrix to the glassy domains. Molecular architecture is not the only factor that can affect material properties. Since the glassy domains act as the reinforcing component, their shape, orientation and connectivity with respect to the loading direction significantly influence mechanical properties. Block copolymers with the three-dimensional gyroid morphology were found to have enhanced tensile properties compared to block copolymers with other morphologies.[69] In this case, this phenomenon was attributed to the specific gyroid microdomain geometry rather than the PS content, molecular architecture, or molecular weight. Additionally, a PS-PBMA diblock copolymer material with PBMA cylinders was found to exhibit higher tensile strength than pure polystyrene.[64] This phenomenon was credited to the phase behavior and interface formation in the diblock copolymer. All these results indicate that by tailoring molecular architecture, which in turn controls morphology and microstructure, mechanical properties of block copolymers can be controlled and enhanced.

Recently, a series of A-(B-*g*-X_2) block-double-graft (BDG) copolymers and terpolymers have been synthesized by using chlorosilane coupling strategies.[70] The

molecular architectures of these materials are illustrated in Figure 5.1b-d. These molecules have low polydispersity polystyrene-1,2-polybutadiene (PS-1,2-PBD) backbones. On the 1,2-PBD part of the backbone, two branches are grafted at each junction points. Different branch materials were used in the various samples of this study including 1,4-PBD (b); PI (b); PS (c); and PS-PI linear diblock copolymers with the PS block grafted directly to the backbone (d). The placement of the junction points along the 1,2-PBD part of the backbone is determined by the hydrosilylation reaction of vinyl groups of 1,2-PBD part of the backbone. Coupling of two living branches to each of these hydrosilylated groups leads to the formation of randomly located tetrafunctional junction points. The architecture combines features of linear diblock and graft block copolymers, offering novel opportunities to study the influence of polymer molecular architecture on morphology and in turn on material properties. The present study focuses on the influence of architecture on morphology and on the tensile properties of copolymers and terpolymers of BDG architecture. For comparison, a homo-double-graft (HDG) terpolymer 1,2-PBD-*g*-$(PS\text{-}PI)_2$ is also studied. The molecular architecture of this material is shown in Figure 5.1e. It consists of the same 1,2-PBD backbone with grafted PS-PI diblocks as in Figure 5.1d, but it lacks the PS backbone block.

5.3 Experimental

5.3.1 Synthesis and Molecular Characterization

The synthesis of these block-double-graft copolymers and terpolymers was described in an early paper.[70] Polymerization and linking reactions were carried out in evacuated, *n*-BuLi-washed, and solvent-rinsed glass reactors. The purification of the

monomers, solvents, and linking and terminating agents to the standards required for high-vacuum techniques and the controlled hydrosilylation reaction has been described elsewhere.[50] In order to obtain the 1,2-microstructure and thus facilitate the hydrosilylation of the 1,2-PBD blocks, polymerization of butadiene was carried out in the presence of dipiperidinoethane.[70-72]

Molecular characteristics of BDG copolymers and terpolymers, the HDG terpolymer, and precursor intermediate building blocks of these structures are listed in Table 5.1. Membrane osmometry (MO) was performed in toluene at 35 °C, and vapor pressure osmometry (VPO) was performed at 35 °C in toluene. Size-exclusion chromatography (SEC) analysis with both refractive index and UV detectors ($\lambda = 262$ nm) were performed in tetrahydrofuran (THF) at 30 °C. Microstructures of polydiene blocks were obtained from ^{1}H-NMR in $CDCl_3$ at 30 °C. These results are as follows: 100 wt% 1,2-addition for 1,2-PBD backbone blocks; 92 wt% 1,4-addition and 8 wt% 1,2-addition for all 1,4-PBD branches; and 93 wt% 1,4-addition and 7 wt% 3,4-addition for PI branches.

All the BDG materials in this study were synthesized from three PS-1,2-PBD backbones which are listed in Table 5.1 as backbone-1 to 3. In the Table, each backbone is followed by the BDG material(s) that was/were synthesized from it. A PS-[1,2-PBD-*g*-(1,4-PBD)$_2$] material was produced based on each of the three backbones. These molecules have different branch molecular weight, number of branches, and total PS volume fractions; they are labeled PS-[1,2-PBD-*g*-(1,4-PBD)$_2$]-1 to 3 according to their

respective backbones. Two different BDG terpolymer molecules that were synthesized based on PS-1,2-PBD backbone-3 have the same molecular structure but different branches and total PS volume fractions. They are labeled PS-[1,2-PBD-*g*-(PS-PI)$_2$]-1 and 2 respectively.

5.3.2 Morphological characterization and tensile testing

Detail description of morphological characterization can be found in section 1.3. Small Angle X-ray Scattering (SAXS) measurements were also carried out at the National Synchrotron Light Source (NSLS) at Brookhaven National Laboratory (BNL) beamline X27C, Upton, NY and at University of Massachusetts-Amherst (UMass). The wavelength of the X-ray beam used in BNL was 1.307 Å and sample-to-detector distance was determined to be 1513 mm. Two-dimensional scattering patterns were recorded on Fujitsu HR-V image plates and were digitized using a Fujitsu BAS 2000 image plate reader. Background was subtracted, circular averaging was performed, and the data were plotted as Log I vs. q.

Details of tensile testing is described in section 1.4.

5.4 Results and discussion

5.4.1 Morphologies

Morphological results of BDG, HDG copolymers and terpolymers reveal the formation of standard microstructures (Table 5.2). In order to discuss their morphologies and tensile behaviors, these materials are separated into three groups according to the

type of their branches.

The first group of BDG molecules consists of BDG1 though BDG4, whose branches are either 1,4-PBD (BDG1 through BDG3) or PI (BDG4) homopolymers. Based on TEM images, it is found that BDG1 and BDG3 form hexagonally packed PS cylinders, and BDG2 forms body-center-cubic (BCC) PS spheres. TEM results of BDG4 are consistent with microphase separated PS spheres in a polydiene matrix, without long-range lattice order. Figure 5.2 presents representative TEM images of BDG2 (a), BDG3 (b) and BDG4 (c). TEM images of BDG1 are similar to those of BDG3. In Figure 5.3, multiple higher order reflections can be readily observed in SAXS profiles of BDG1, BDG2, and BDG3. BDG1 exhibits Bragg reflections with ratios q_n/q^*, of the *n*th reflection scattering vector to the scattering vector of the primary peak, of 1, $\sqrt{3}$, $\sqrt{4}$, $\sqrt{7}$, $\sqrt{9}$, $\sqrt{12}$, $\sqrt{16}$ and $\sqrt{19}$, indicative of a hexagonal morphology. The (100) interplanar spacing in BDG1 is calculated to be 381 Å. BDG3 exhibits a similar sequence of scattering vector ratios suggestive of hexagonal morphology, except that the $\sqrt{3}$ peak is missing. The comparison to TEM images confirms the hexagonal packed cylindrical structure and we thus conclude that the missing $\sqrt{3}$ peak is due to a minimum in the form factor at the volume fraction of the sample.[73] BDG3 has a (100) spacing of 335 Å. BDG2 gives relative positions of primary and higher order reflections at 1, $\sqrt{2}$, $\sqrt{3}$, $\sqrt{5}$, $\sqrt{6}$ and $\sqrt{7}$, consistent with BCC spherical structure. Based on the data the primary scattering peak gives a (110) interplanar spacing of 230 Å, which corresponds to a cubic lattice parameter of 325 Å. Scattering data of BDG4, shown in Figure 5.3, displays a broad primary peak and an additional broad, higher angle peak due to the form factor. This

scattering profile is consistent with its TEM image in Figure 5.2, which shows a microphase-separated morphology that lacks long-range lattice order. The primary scattering peak suggests an average correlation length of 268 Å for BDG4 and the broad higher q reflection is consistent with form factor scattering from spherical domains. The TEM image of BDG4 in Figure 5.2 is similar to previously reported images of microphase separated spherical domains without lattice order.[18]

The morphological behaviors of BDG1 - BDG3 are similar to those of their respective linear diblock copolymer counterparts with the same PS volume fractions. The PS volume fractions of the cylinder-forming BDG samples BDG1 and BDG3 are 0.23 and 0.27 respectively, falling in the same range where linear diblocks would also form cylinders.[23,58,73] BDG2, which forms a spherical microstructure, has a PS volume fraction 0.13, falling in the same range where linear diblocks would also form spheres. The fact that these BDG molecules behave as their linear counterparts with similar PS volume fraction suggests that microphase separation is occurring between PS and a mixed matrix of 1,2-PBD and 1,4-PBD.

A simple χN calculation confirms the miscibility between 1,2-PBD and 1,4-PBD inside the matrices phases of BDG1 - BDG3. The 1,2-PBD/1,4-PBD part of molecule has the architecture of a multigraft copolymer 1,2-PBD-*g*-(1,4-PBD)$_2$ with 1,2-PBD as its backbone, and two 1,4-PBD homopolymer branches grafted at every randomly spaced junction point. It has been shown experimentally[18,33,34] and theoretically[74] that the appropriate basis for calculating the χN of a graft copolymer is the *constituting unit*

composed of the average structure per junction point. Accordingly, the constituting block copolymer units in BDG1, BDG2, and BDG3 are four-arm, *miktoarm* stars of the type $(1,2\text{-PBD})_2$-$(1,4\text{-PBD})_2$. Roughly speaking a symmetric four-arm *miktoarm* star will display morphological and phase segregation characteristics similar to the corresponding (1,2-PBD)-(1,4-PBD) diblock where the block lengths are equal to those of the various star arms.[13,14,17,18,35,74] Thus the calculation of χN for a $(1,2\text{-PBD})_2$-$(1,4\text{-PBD})_2$ is approximated by the χN of this corresponding diblock. The interaction parameter χ between 1,2-PBD and 1,4-PBD can be calculated based on the equation derived by *Sakurai* and coworkers.[75]

$$\chi_{1,2\text{-}1,4} = 2.69 \times 10^{-3} + 1.87/T$$

Based on this expression for χ and the degrees of polymerization of the various diblocks, χN values at 25 °C are as follows: 1.1 (BDG1), 0.82 (BDG2), and 0.53 (BDG3). These χN values clearly indicate that the 1,2-PBD backbone and 1,4-PBD branches in these three molecules are highly miscible. On the other hand, a calculation of the χN at 25 °C between PS and a mixed PBD domain type indicates relatively strong segregation.[76] These values are as follows: 90 (BDG1), 61 (BDG2), and 88 (BDG3).

A similar approach can also be applied to the evaluation of block miscibility and/or degree of segregation for BDG4. In the graft part of this molecule the branches are PI homopolymers and the constituting block copolymer unit is $(1,2\text{-PBD})_2$-PI_2. Based on the interaction parameter between isoprene and butadiene reported by *Floudas*,[77] χN

of eonstituting block eopolymer in the graft part of BDG4 is found to be 0.27. Furthermore, it is well known that miscibility of PBD with PI increases with inereasing vinyl eontent (1,2-addition) in PBD.[78] The blend of PI and PBD even exhibits a negative χ parameter when the vinyl eontent of PBD is over 90%.[79,80] Our well-eontrolled synthetic teehnique allows strict 1,2-addition of butadiene monomers onto the backbone and thus the vinyl eontents of baekbone 1,2-PBD in all BDG moleeules approach 100%. This process will produee a very low enthalpie interaction between isoprene and butadiene. Based on these arguments, we believe that the two rubbery eomponents in BDG4 are also miseible with eaeh other. Again, if we ean lump together PI and baekbone 1,2-PBD and ealeulate the χN between PS and the eombined rubbery phase, we find that the system has an χN of 188 at the annealing temperature of 120 °C. The total volume fraetion of PS in BDG4 is only about 0.076 so a dibloek analog would form PS spheres in a polydiene matrix. Our data suggest that the spherieal domains are indeed formed, but that they are unable or organize themselves onto a lattice. Previous work[13,17] has shown examples of other multigraft eopolymers in whieh the expeeted (based on component volume fraetions) mierophase separated domain shape forms, but long-range lattice order is suppressed.

BDG1 through BDG4 all share the same general molecular arehiteeture shown in Figure 5.1b. The moleeular weight of the PI braneh es in BDG4 (13,200 g/mol) is significantly higher than that of the PBD braneh es in BDG1 through BDG3 (3,000 g/mol maximum). This moleeular weight information is listed in Table 5.1. The molecular weight of the PI braneh es in BDG4 is higher than the eritieal moleeular weight for PI

entanglement,[45] while the moleeular weights of the grafted braneh es in BDG1 though BDG3 are eonsiderably lower than the eorresponding PBD entanglement moleeular weight. It is suspeeted that the longer graft ehains hindered the kineties of mierophase separation in BDG4. Extending the annealing time to 10 days and inereasing the annealing temperature to 140 °C failed to produee an improvement in the long-range order of the BDG4 morphology.

The seeond sample grouping eonsists of BDG5 only. It eontains a PS-1,2-PBD baekbone with two PS braneh es grafted at every junetion point along the PBD part of the baekbone. TEM results on BDG5 indieate a totally disordered state, consistent with the small angle X-ray seattering data shown in Figure 5.4. The backbone to whieh the grafts are attaehed eomprises the only 1,2-PBD in the moleeule. This 1,2-PBD is only 11 volume pereent of the material. There are on average 12 junetion points along this PBD bloek and thus the average moleeular weight of the PBD conneetor between junction points is only 1300 g/mol. The χN value per junction point in the graft part of this moleeule (eonstituting bloek eopolymer unit) is 2.8 at the annealing temperature of 120 °C, and 3.8 at room temperature. For sueh an asymmetrie PBD volume fraction, this plaees the material deep in the disordered region of the morphology diagram. Thus the laek of mierophase-separated strueture is not surprising.

The third group of samples eonsists of BDG6, BDG7 and HDG terpolymers. The braneh es are PS-PI linear dibloek eopolymers with the PS bloeks of these braneh es grafting directly onto the PBD parts of the baekbones. Lamellae are observed in TEM

images of all three materials. Figure 5.5 shows the TEM images of HDG. Small angle scattering data from BDG6 and BDG7 in Figure 5.6 display Bragg reflections at integer multiples of the primary reflection q^*, which is consistent with lamellar morphologies. Higher order reflections in the scattering data from HDG are hard to identify, but TEM micrographs of HDG show well-ordered lamellar structures. Lamellar long periods of BDG6 and BDG7 are 175 and 244 Å respectively, while that of HDG is 167 Å.

It is found in all TEM micrographs of the materials in the third group that the volume fractions taken by PS phase (as compared the combined osmium stained polydiene segments) are close to 0.50. This is consistent with their total PS volume fractions, from backbone and from branches. The observed domain volume fractions suggest that the backbone 1,2-PBD and the PI blocks of the branches remain in the same combined rubbery domain while the PS blocks from both the backbone and branches reside in the other domain. Figure 5.7a shows some possible chain conformations for BDG6 and BDG7 that arrange the various PS and polydiene blocks among the microphase-separated lamellae of the morphology. Clearly, many possible conformations can occur, and are statically represented in the material. In some conformations a single molecule can span up to two full long periods of the lamellar structure. This is in contrast to diblocks which only span half a long period and to triblocks which can at most span a full long period. Figure 5.7b illustrates an alternative morphology in which the backbone 1,2-PBD and branch PI blocks form different domains separated by PS domains. However, for BDG and HDG molecules, the volume percents of the backbone 1,2-PBD blocks are less than 8%. Most of the polydiene

content is in the branches. Thus the formation of separate PBD and PI domains would yield a -PI-PS-PBD-PS-PI- alternating structure, with dramatic domain thickness differences between PBD and PI layers.[81,82] The TEM and scattering results indicate a single type of combined polydiene lamellar layer.

Figure 5.8 illustrates the differences between BDG6 (a) and BDG7 (b). Both molecules are based on the same PS-1,2-PBD backbone, but the molecular weight of the branches is 14,000 g/mol in BDG6, and is 32,800 g/mol in BDG7. The number of junction points on the backbone 1,2-PBD block is 9 in BDG6 and 3 in BDG7. The lamellar spacing of BDG7 (244 Å) is significantly larger than that of BDG6 (175 Å). We find that the lamellar spacings of BDG6 and BDG7 are comparable to those reported for diblocks of similar molecular weight to those of the diblock branches in BDG6 and BDG7.[48] It seems that the domain spacings of BDG6 and BDG7 are predominately determined by molecular weights of the branches instead of the backbones since BDG6 and BDG7 are built on the same backbone. HDG is very similar to BDG6 in molecular characteristics except that HDG does not have a backbone PS block. The fact that the HDG lamellar spacing (167 Å) is very similar to that of BDG6 supports the assertion that the characteristics of the grafted diblocks determine this spacing.

5.4.2 Tensile properties

Figure 5.9 compares the stress-strain behavior of BDG6, BDG7 and HDG terpolymers, a PI-*g*-PS_2 multigraft copolymer, and a commercial thermoplastic elastomer (TPE) - Shell Kraton® D1101. The PI-*g*-PS_2 multigraft copolymer has a total molecular

weight of 994,000 g/mol with an average of nine tetrafunctional branch points per molecule and a PS volume fraction of 0.22. It was found to have worm-like cylindrical domains (not ordered on a lattice) of PS in a PI matrix. The morphology and tensile properties of this material have been reported previously.[55] The Kraton used for comparison is a polystyrene-polyisoprene-polystyrene linear triblock copolymer and forms hexagonal PS cylinders in a PI matrix. Styrene mass content is reported by the manufacturer to be 31%. The number average molecular weight of this Kraton determined via GPC in our laboratory is 1.05×10^5 g/mol. The PI-*g*-PS_2 multigraft copolymer and Kraton were prepared and tested under the same conditions used for BDG6, BDG7 and HDG. Figure 5.9 shows that HDG displays low strength and a low stain at break. On the other hand, BDG6, BDG7 and Kraton exhibit a large increase of stress at higher strains, typical tensile behavior of thermoplastic elastomers (TPE). BDG7 exhibits higher strength and higher strain at break than BDG6. Its strain at break is a little lower than that of Kraton but its strength is considerably higher. As previously reported,[55] the PI-*g*-PS_2 multigraft copolymer displays very high strain at break and moderately high strength.

Both BDG6 and BDG7 show excellent TPE properties resulting from the ability of individual molecules to participate in multiple physical crosslinks (provided by the PS domains) as illustrated in Figure 5.7a. Such chain conformations resemble those of PS-PI-PS triblock copolymer TPEs in which the rubbery middle block bridges two glassy domains. In the BDG materials, however, a single molecule provides multiple connections between different glassy PS domains, thus resulting in an improvement in

strength.

Compared to BDG7, BDG6 displays lower strength and strain at break. While BDG7 has a lower number of junction points than BDG6, its PS-PI branches have higher molecular weight than those in BDG6. While it was previously found[55] that a higher number of branch points per molecule improves strength and elongation at break, it is also clear from the results on BDG6 and BDG7 that the molecular weight of grafts must be sufficiently high to entangle and not pull out of the crosslinking domains in order to improve properties. The molecular weights of the PS blocks on the BDG6 branches are lower than the critical molecular weight M_c to achieve chain entanglement (M_c = 17,000 g/mol for PS). For BDG7, on the other hand the PS blocks on the grafts are 16,000 g/mol, approaching the entanglement molecular weight. This is apparently enough to provide enhancement of properties.

5.5 Conclusions

For the type of BDG terpolymers, we found two parameters that can adjust material properties - molecular weight of the branches and molecular architecture. Branches must exceed the entanglement molecular weight in order to provide effective physical crosslinks. In terms of molecular architecture, the presence of PS block in the branch provides multiple coupling points between PS and rubbery domains, which appears to enhance properties. The number of junction points and the functionality of these junction points are also very important aspects for energy transfer between different domains.

Table 5.1 Molecular characteristics of the precursors and the fractionated BDG copolymers and terpolymers.

Sample		Branches			BDG copolymers or terpolymers			
		M_n ($\times 10^3$)		M_w/M_n	M_n ($\times 10^3$)	M_w/M_n	wt% PS ^{1}H-NMR	c
	PS-1,2-PBD backbone-1	20.5 [a]	56.0 [b]	1.03			36	
BDG1	PS-[1,2-PBD-*g*-(1,4-PBD)$_2$]-1	3.0		1.06	84.2	1.05	35	5
	PS-1,2-PBD backbone-2	7.30 [a]	24.6 [b]	1.02			30	
BDG2	PS-[1,2-PBD-*g*-(1,4-PBD)$_2$]-2	3.0		1.06	53.1	1.05	19	5
	PS-1,2-PBD backbone-3	24.5 [a]	39.9 [b]	1.04			62	
BDG3	PS-[1,2-PBD-*g*-(1,4-PBD)$_2$]-3	2.30[b]		1.07	84.2	1.05	32	10
BDG4	PS-[1,2-PBD-*g*-(PI)$_2$]	13.2		1.04	288	1.05	11	9
BDG5	PS-[1,2-PBD-*g*-(PS)$_2$]	5.0[b]		1.08	157	1.06	89	12
BDG6	PS-[1,2-PBD-*g*-(PS-PI)$_2$]-1	14.0		1.06	280	1.08	52	9
BDG7	PS-[1,2-PBD-*g*-(PS-PI)$_2$]-2	32.8		1.04	226	1.06	48	3
	1,2-PBD backbone	17.5		1.03				
HDG	1,2-PBD-*g*-(PS-PI)$_2$							

a: Molecular weight of PS part of the backbone.
b: Total molecular weight of PS-1,2-PBD backbone.
c: Number of junctions per molecule: $[(M_n)_{BDG} - (M_n)_{backbone}]/[2 \times (M_n)_{branch}]$.

Table 5.2 Morphological characteristics of BDG and HDG materials.

Sample		Morphology	d* (Å)	Vol% PS	Vol% PBD	Vol% PI
BDG1	PS-[1,2-PBD-*g*-(1,4-PBD)$_2$]-1	PS Cylinders	381	22.5	77.5	
BDG2	PS-[1,2-PBD-*g*-(1,4-PBD)$_2$]-2	PS Spheres	230	12.6	87.4	
BDG3	PS-[1,2-PBD-*g*-(1,4-PBD)$_2$]-3	PS Cylinders	335	27.0	73.0	
BDG4	PS-[1,2-PBD-*g*-(PI)$_2$]	Random PS Spheres	268	7.60	5.30	87.1
BDG5	PS-[1,2-PBD-*g*-(PS)$_2$]	Disordered		89.2	10.8	
BDG6	PS-[1,2-PBD-*g*-(PS-PI)$_2$]-1	Lamellae	175	48.8	5.70	45.5
BDG7	PS-[1,2-PBD-*g*-(PS-PI)$_2$]-2	Lamellae	244	44.9	7.10	48.0
HDG	1,2-PBD-*g*-(PS-PI)$_2$	Lamellae	167	41.9	7.7	50.4

*: domain spacing calculated based on primary SAXS reflection q^*, $d = 2\pi/q^*$.

(a)

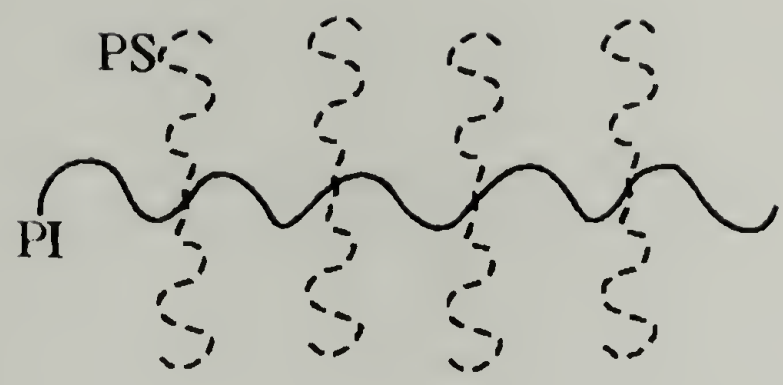

(b)

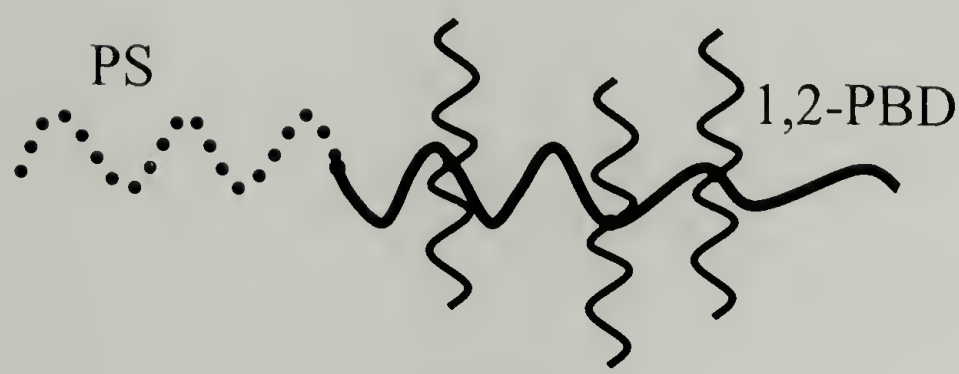

(c)

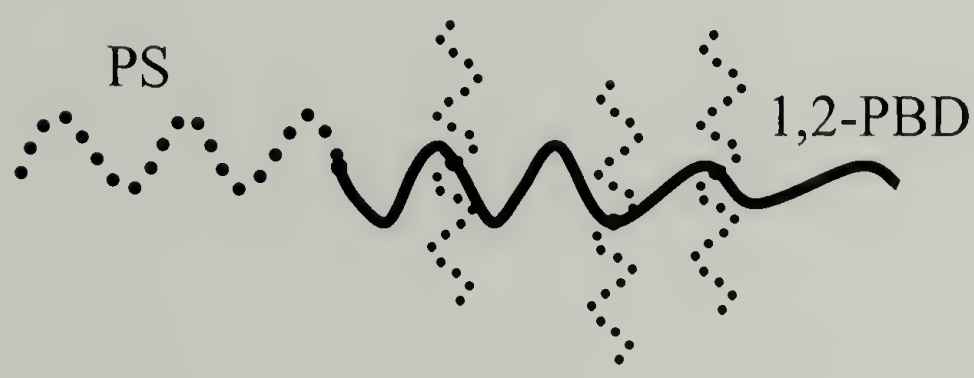

Figure 5.1 Illustrations of (a) a multigraft copolymer PS-*g*-PI_2 with regularly spaced, tetrafunctional junction points; (b) a BDG copolymer with branch X = 1,4-PBD or PI; (c) a BDG copolymer with branch X = PS; (d) a BDG terpolymer with branch X = PS-PI; (e) a HDG terpolymer having a 1,2-PBD backbone and PS-PI branches. Continued next page.

(d)

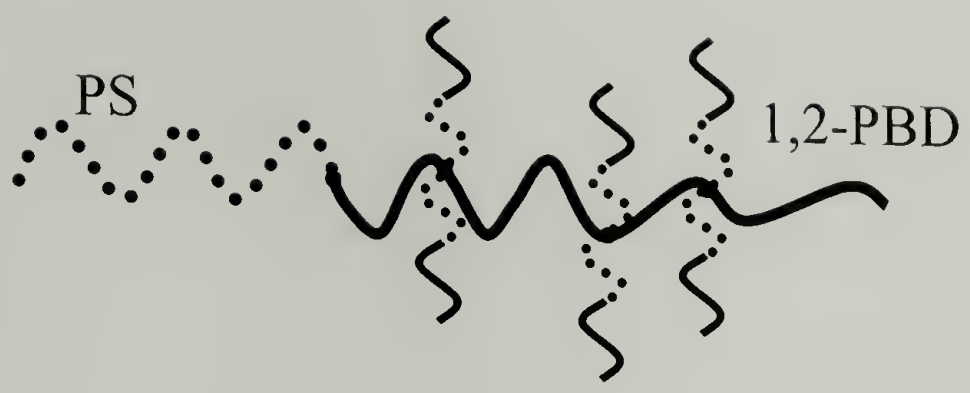

(e)

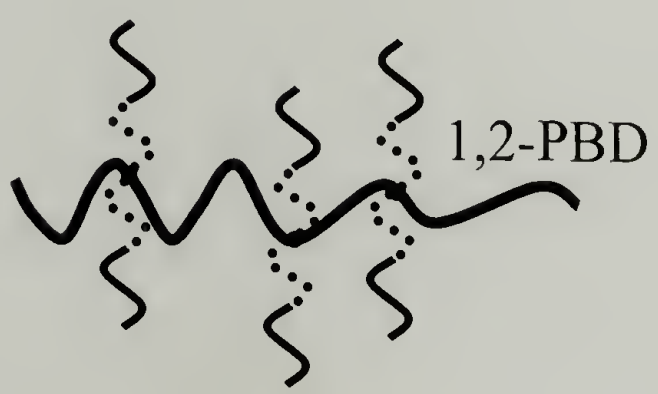

Figure 5.1 Continued.

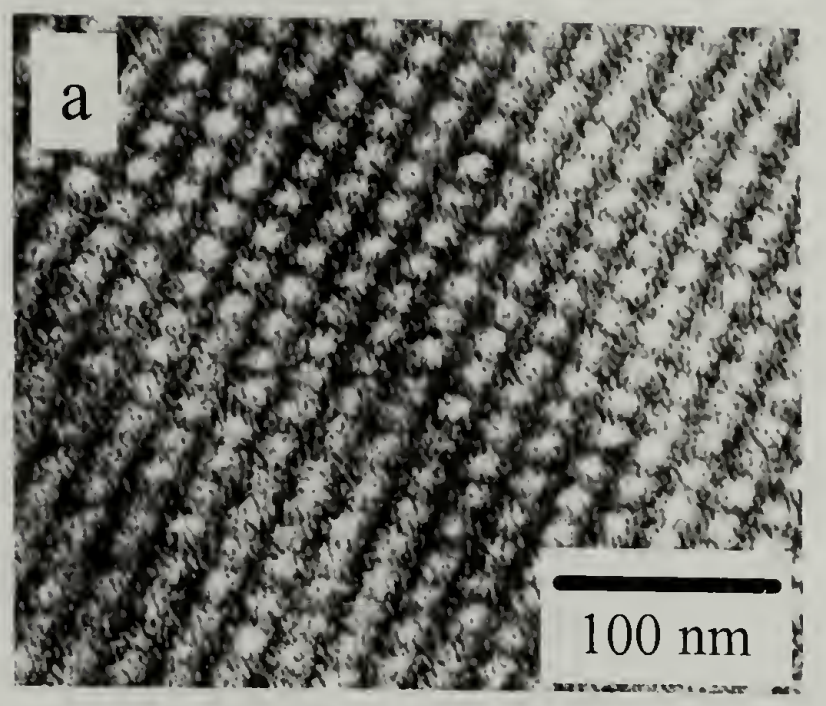

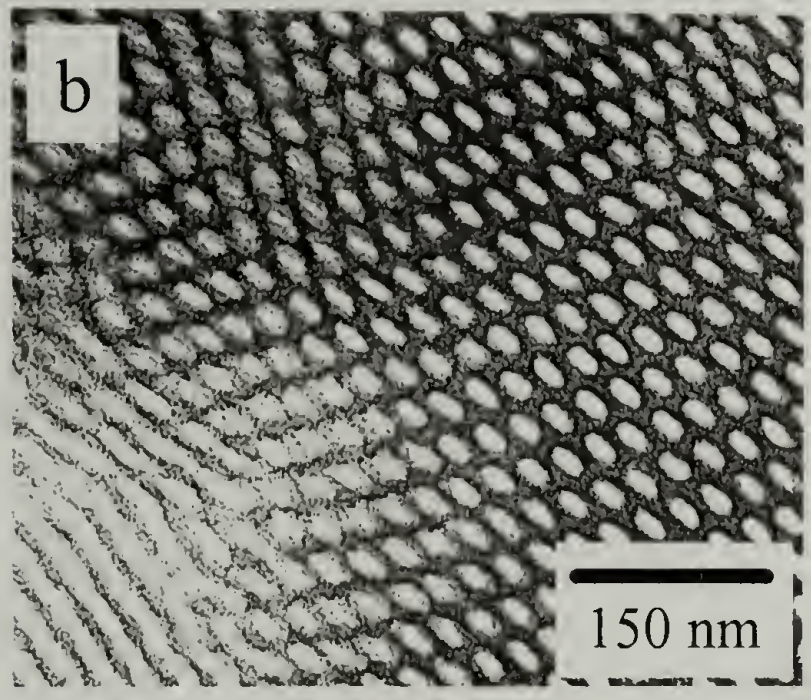

Figure 5.2 TEM images of (a) BDG2, (b) BDG3, and (c) BDG4.

Continued next page.

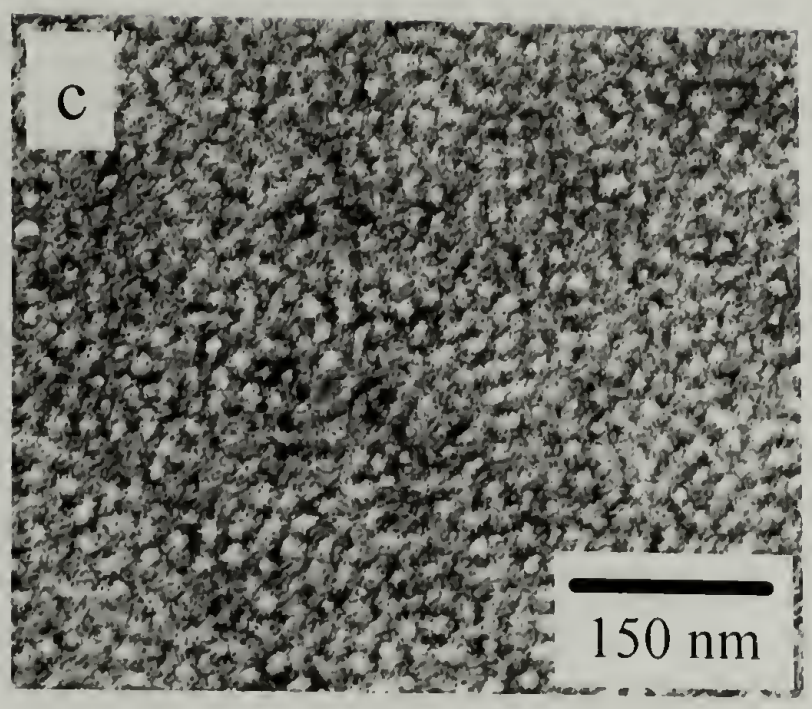

Figure 5.2 Continued.

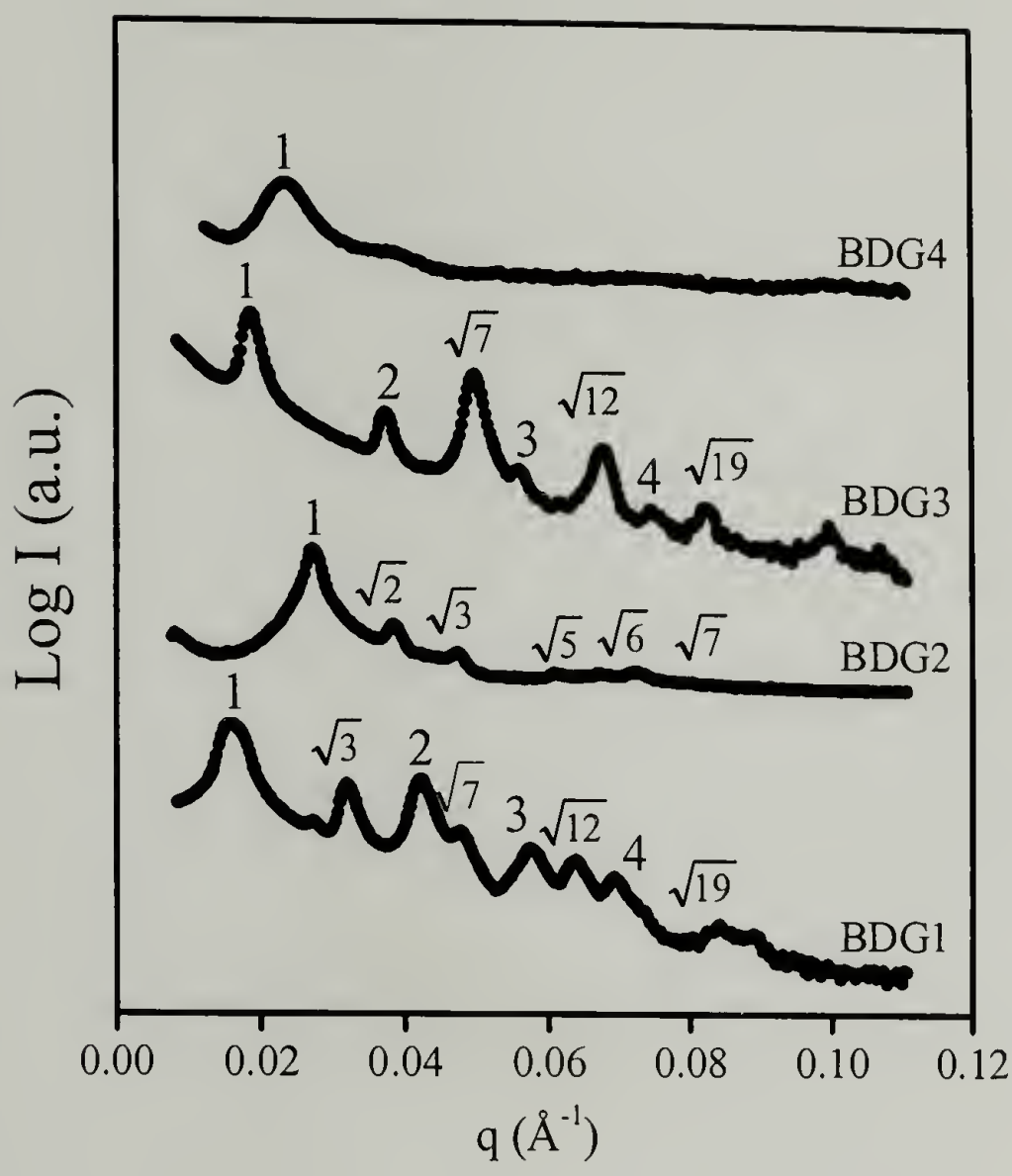

Figure 5.3 Small angle X-ray scattering data of (a) BDG1; (b) BDG2; (c) BDG3 and (d) BDG4.

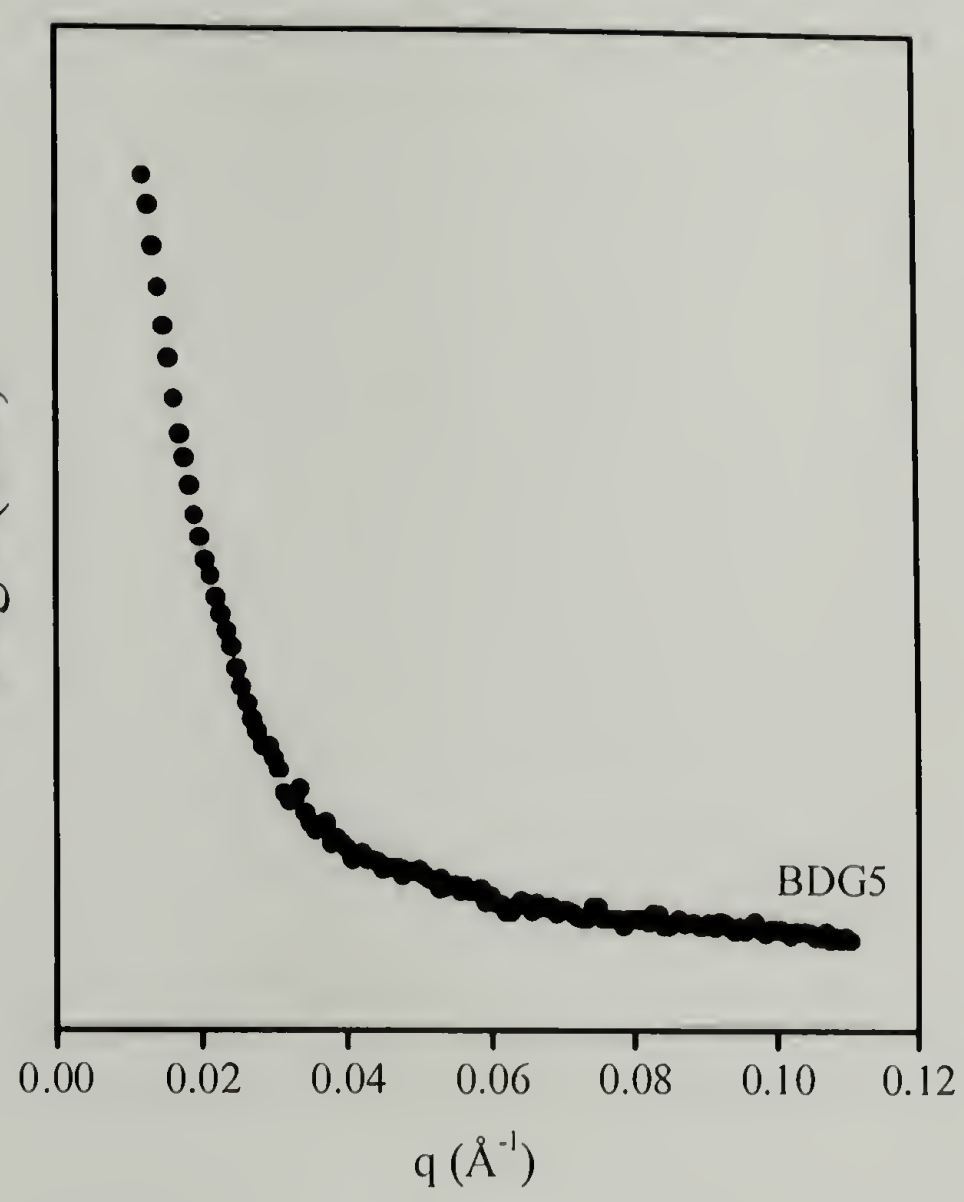

Figure 5.4 Small angle X-ray scattering profiles for BDG5.

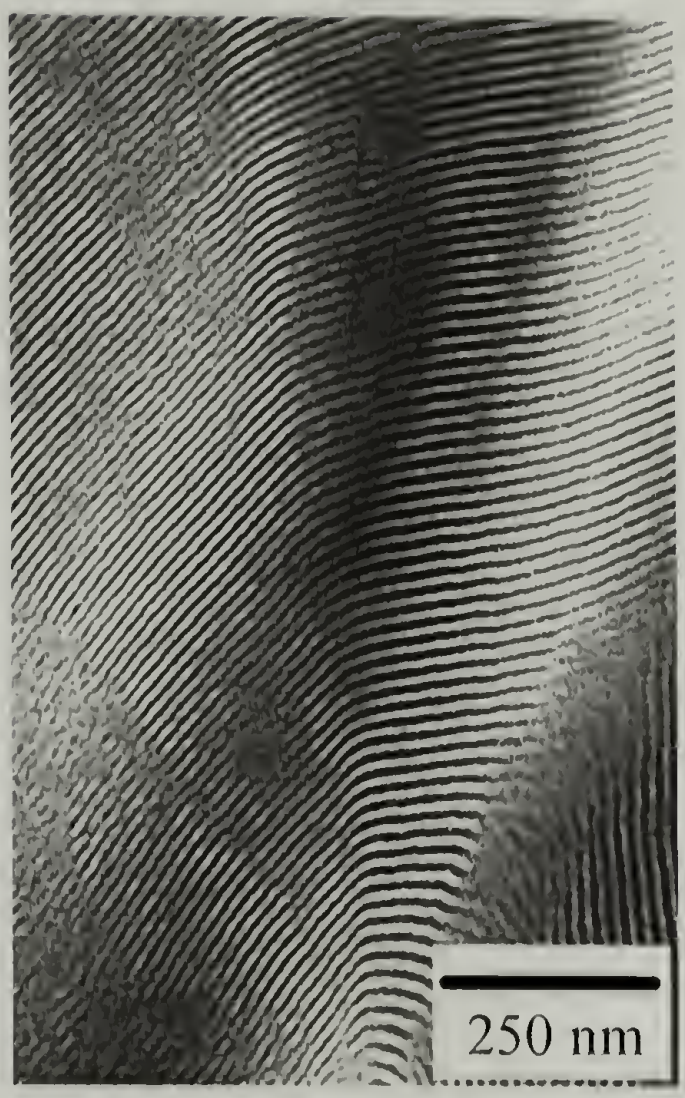

Figure 5.5 TEM micrograph of HDG, showing well ordered lamellar structures.

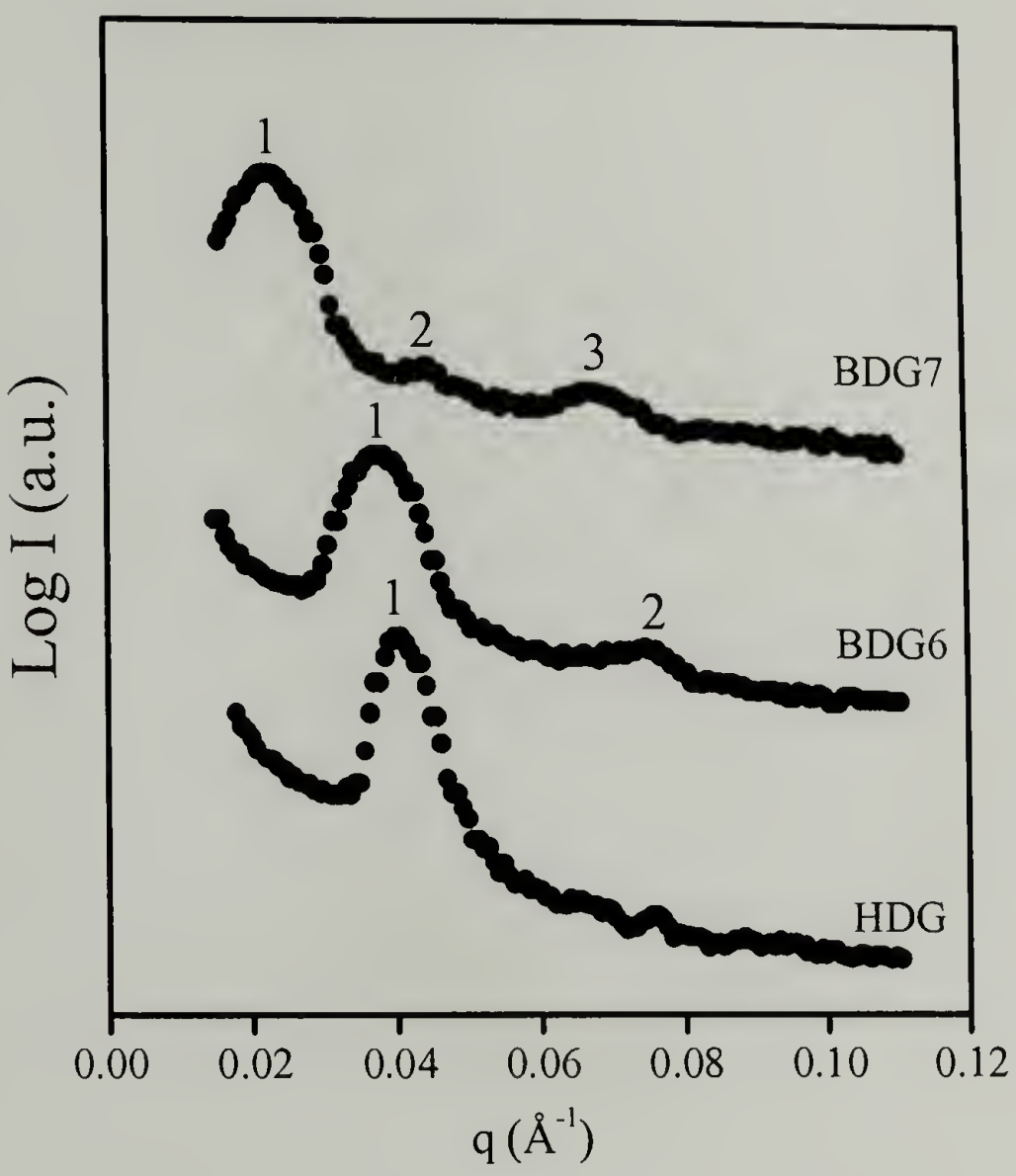

Figure 5.6 Small angle X-ray scattering profiles of (a) HDG, (b) BDG6 and (c) BDG7.

(a)

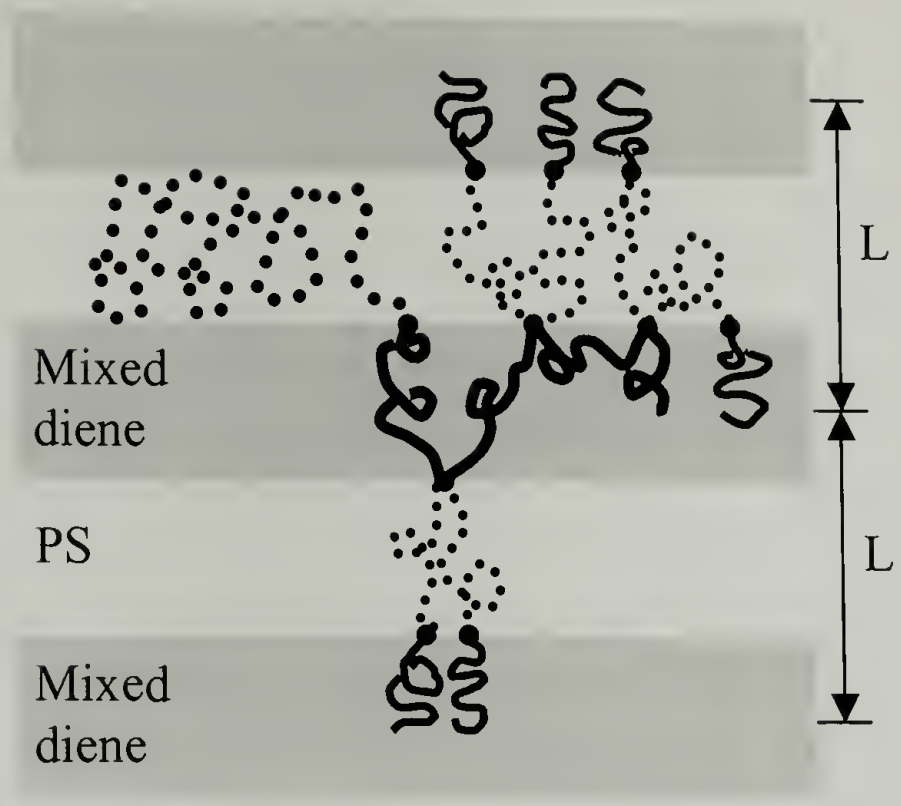

(b)

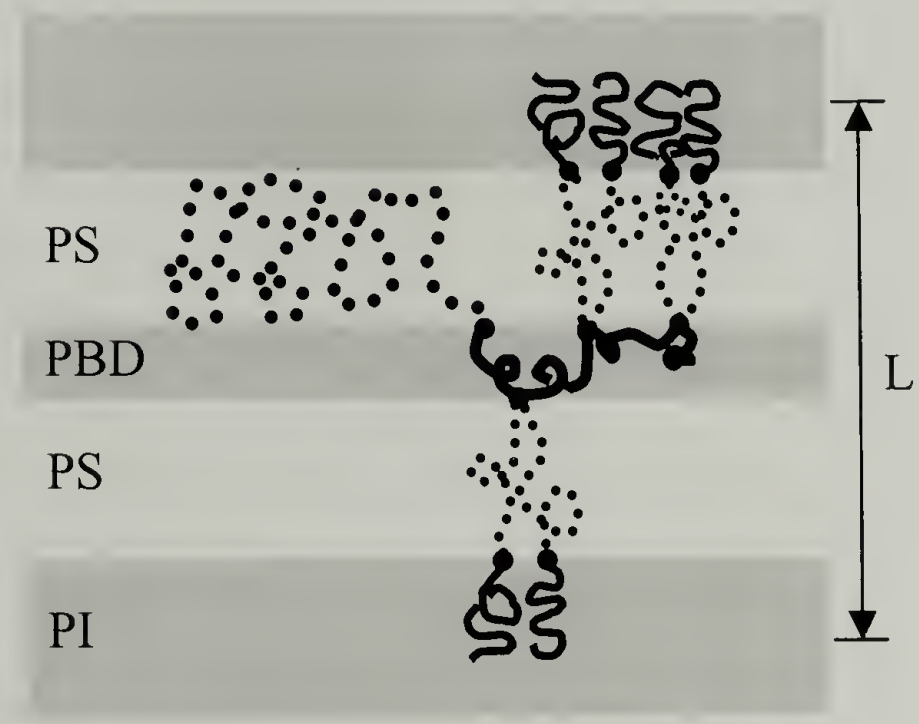

Figure 5.7 (a) Chain conformation of BDG6 and BDG7 in the microphase separated state; (b) Illustration of an alternative morphology in which the backbone 1,2-PBD and branch PI blocks form different domains separated by PS domains.

(a)

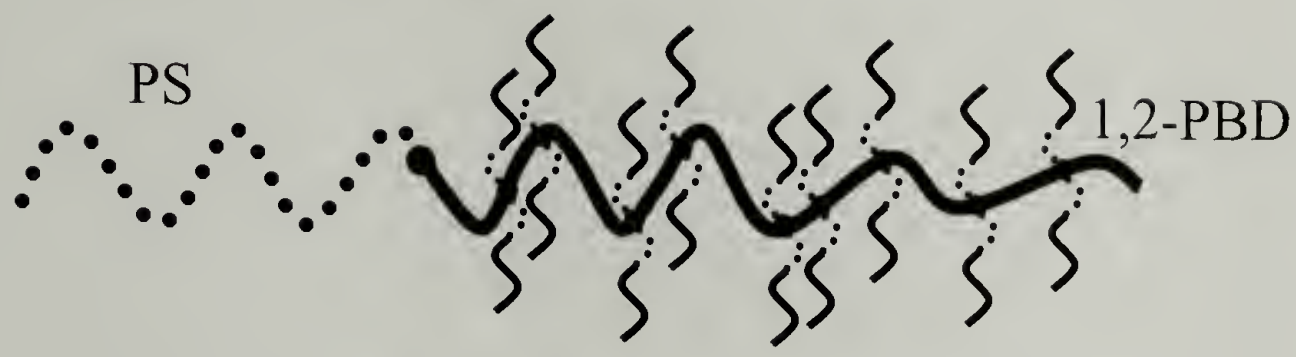

(b)

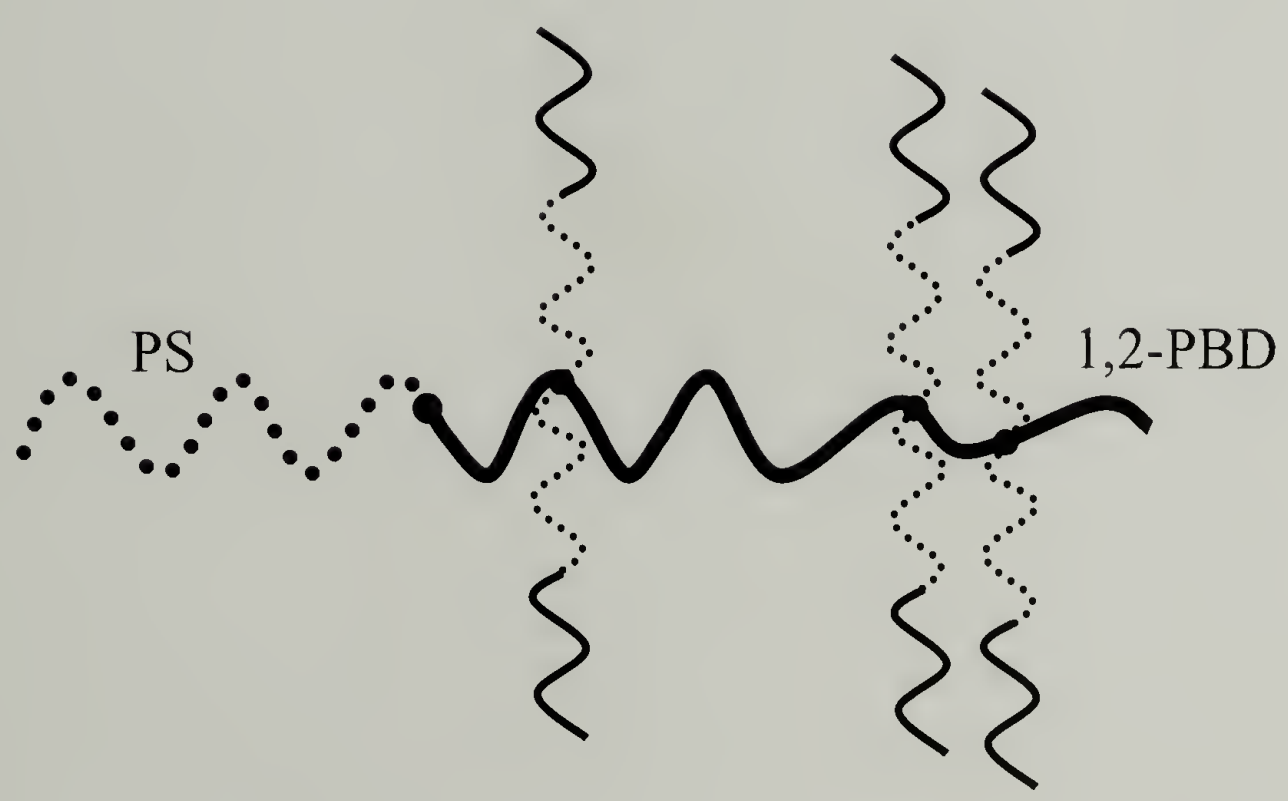

Figure 5.8 Molecular architectures of (a) BDG6 and (b) BDG7.

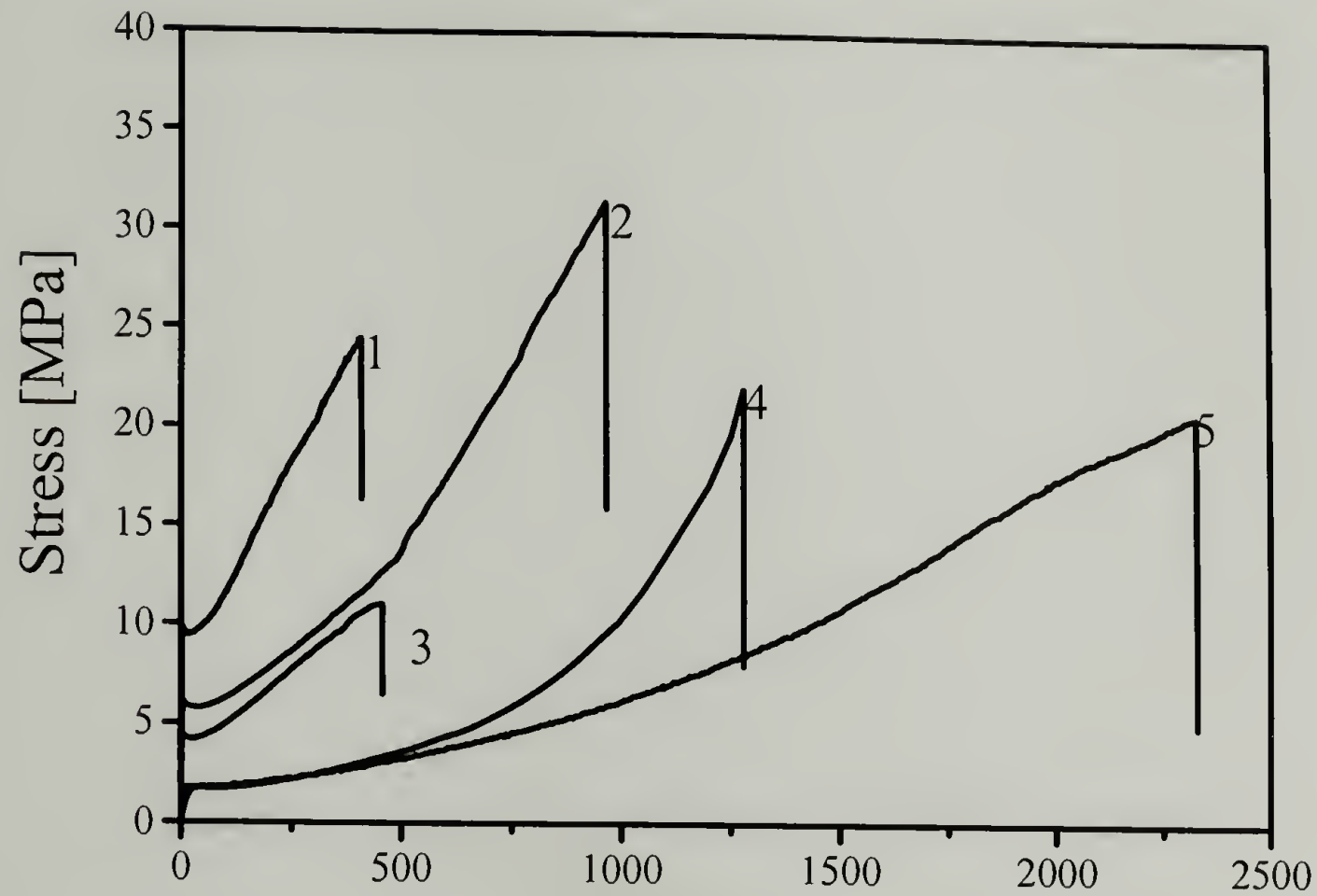

Figure 5.9 Stress-Strain curves for (1) BDG6, 9 junction points, and the branch M_n is 14 kg/mole; (2) BDG7, 3 junction points, and the branch M_n is 32.8 kg/mole; (3) HDG, 9 junction points, and the branch M_n is 12.5 kg/mole; (4) Kraton® D1101; (5) PI-g-PS_2 multigraft copolymer with 9 junction points at branch M_n of 13 kg/mole.

BIBLIOGRAPHY

(1) Matsen, M. W.; Bates, F. S. *Macromolecules* **1996**, *29*, 1091-1098.

(2) Strobl, G. *The Physics of Polymers*, 2nd ed.; Springer, 1997.

(3) Likhtman, A. E.; semenov, A. N. *Macromolecules* **1994**, *27*, 3103-3106.

(4) Hajduk, D. A.; Harper, P. E.; Gruner, S. M.; Honeker, C. C.; Kim, G.; Thomas, E. L.; Fetters, L. J. *Macromolecules* **1994**, *27*, 4063-4075.

(5) Hajduk, D. A.; Takenouchi, H.; Hillmyer, M. A.; Bates, F. S.; Vigild, M. E.; Almdal, K. *Macromolecules* **1997**, *30*, 3788-3795.

(6) Matsen, M. W.; Schick, M. *Physical Review Letters* **1994**, *72*, 2660-2663.

(7) Stadler, R.; Auschra, C.; Beckmann, J.; Krappe, U.; Voigt-Martin, I.; Leibler, L. *Macromolecules* **1995**, *28*, 3080-3097.

(8) Zheng, W.; Wang, Z. *Macromolecules* **1995**, *28*, 7215-7223.

(9) Gido, S. P.; Schwark, D. W.; Thomas, E. L. *Macromolecules* **1993**, *26*, 2636-2640.

(10) Mogi, Y.; Kotsuji, H.; Kaneko, Y.; Mori, K.; Matsushita, Y.; Noda, I. *Macromolecules* **1992**, *25*, 5408-5411.

(11) Pochan, D. J.; Gido, S. P.; Pispas, S.; Mays, J. W. *Macromolecules* **1996**, *29*, 5099-5105.

(12) Pochan, D. J.; Gido, S. P.; Pispas, S.; Mays, J. W.; Ryan, A. J.; Fairclough, J. P. A.; Hamley, I. W.; Terrill, N. J. *Macromolecules* **1996**, *29*, 5091-5098.

(13) Beyer, F. L.; Gido, S. P.; Uhrig, D.; Mays, J. W.; Beck Tan, N.; Trevino, S. F. *Journal of Polymer Science: Part B: Polymer Physics* **1999**, *37*, 3392-3400.

(14) Beyer, F. L.; Gido, S. P.; Poulos, Y.; Avgeropoulos, A.; Hadjichristidis, N. *Macromolecules* **1997**, *30*, 2373-2376.

(15) Matsen, M. W.; Gardiner, J. M. *Journal of Chemical Physics* **2000**, *113*, 1673-1676.

(16) Grayer, V.; Dormidontova, E. E.; Hadziioannou, G. *Macromolecules* **2000**, *33*, 6330-6339.

(17) Xenidou, M.; Beyer, F. L.; Hadjichristidis, M.; Gido, S. P.; Beck Tan, N. *Macromolecules* **1998**, *31*, 7659-7667.

(18) Beyer, F.; Gido, S. P.; Buschl, C.; Iatrou, H.; Uhrig, D.; Mays, J. W.; Chang, M.; Garetz, B. A.; Balsara, N.; Beck Tan, N.; Hadjichristidis, N. *Macromolecules* **2000**, *33*, 2039-2048.

(19) Matsen, M. W.; Schick, M. *Macromolecules* **1994**, *27*, 4014-4015.

(20) Matsen, M. W.; Bates, F. S. *Journal of Polymer Science B: Polymer Physics* **1997**, *35*, 945-952.

(21) Bates, F. S.; Frerickson, G. H. *Macromolecules* **1994**, *27*, 1065-1067.

(22) Melenkevitz, J.; Muthukumar, M. *Macromolecules* **1991**, *24*, 4199-4205.

(23) Helfand, E.; Wasserman, Z. R. *Macromolecules* **1976**, *9*, 879-888.

(24) Jo, W. H.; Jang, S. S. *Journal of Chemical Physics* **1999**, *111*, 1712-1720.

(25) Morozov, A. N.; Fraaije, J. G. E. M. *Macromolecules* **2001**, *34*, 1526-1528.

(26) Marko, J. F. *Macromolecules* **1993**, *26*, 1442-1444.

(27) Matsen, M. W.; Thompson, R. B. *Journal of Chemical Physics* **1999**, *111*, 7139-7146.

(28) Matsen, M. W. *Journal of Chemical Physics* **2000**, *113*, 5539-5544.

(29) Mayes, A. M.; Olvera de la Cruz, M. *Journal of Chemical Physics* **1989**, *91*, 7228-7235.

(30) Matsen, M. W.; Schick, M. *Macromolecules* **1994**, *27*, 187-192.

(31) Watanabe, H. *Macromolecules* **1995**, *28*, 5006-5011.

(32) Milner, S. *Macromolecules* **1994**, *27*, 2333-2335.

(33) Gido, S. P.; Lee, C.; Pochan, D. J.; Pispas, S.; Mays, J. W.; Hadjichristidis, N. *Macromolecules* **1996**, *29*, 7022-7028.

(34) Lee, C.; Gido, S. P.; Poulos, Y.; Hadjichristidis, N.; Beck Tan, N.; Trevino, S. F.; Mays, J. W. *Polymer* **1998**, *39*, 4631-4638.

(35) Olvera de la Cruz, M.; Sanchez, I. C. *Macromolecules* **1986**, *19*, 2501-2508.

(36) Amis, E. J.; Hodgson, D. F.; Wu, W. *Journal of Polymer Science: Part B: Polymer Physics* **1993**, *31*, 2049-2056.

(37) Yu, G.; Yang, Z.; Attwood, D.; Price, C.; Booth, C. *Macromolecules* **1996**, *29*, 8479-8486.

(38) Lescanec, R. L.; Hajduk, D. A.; Kim, G. Y.; Gan, Y.; Yin, R.; Gruner, S. M.; Hogen-Esch, T. E.; Thomas, E. L. *Macromolecules* **1995**, *28*, 3485-3489.

(39) Ryan, A. J.; Mai, S.; Fairclough, J. P. A.; Hamley, I. W.; Booth, C. *Physical Chemistry Chemical Physics* **2001**, *3*, 2961-2971.

(40) Mai, S.; Mingvanish, W.; Turner, S. C.; Chaibundit, C.; Fairclough, J. P. A.; Heatley, F.; Matsen, M. W.; Ryan, A. J.; Booth, C. *Macromolecules* **2000**, *33*, 5124-5130.

(41) Li, B.; Ruckenstein, E. *Macromolecular Theory and Simulations* **1998**, *7*, 333-348.

(42) Iatrou, H.; Hadjichristidis, N.; Meier, G.; Frielinghaus, H.; Monkenbusch, M. *Macromolecules* **2002**, *35*, 5426-5437.

(43) Oster, G.; Riley, D. P. *Acta Crystallographica* **1952**, *5*, 1-6.

(44) Alward, D. B. In *Polymer Science & Engineering*; University of Massachusetts: Amherst, 1985; p 235.

(45) Buzza, D. M. A.; Fzea, A. H.; Allgaier, J. B.; Young, R. N.; Hawkins, R. J.; Hamley, I. W.; McLeish, T. C. B.; Lodge, T. P. *Macromolecules* **2000**, *33*, 8399-8414.

(46) Turner, C. M.; Sheller, N. B.; Foster, M. D.; Lee, B.; Corona-Galvan, S.; Quirk, R. P.; Annis, B.; Lin, J. S. *Macromolecules* **1998**, *31*, 4372-4375.

(47) Daoud, M.; Cotton, J. P. *Journal de Physique* **1982**, *43*, 531-538.

(48) Hashimoto, T.; Shibayama, M.; Kawai, H. *Macromolecules* **1980**, *12*, 1237-1247.

(49) Hadjichristidis, N.; Iatrou, H.; Pispas, S.; Pitsikalis, M. *Journal of Polymer Science: Part A: Polymer Chemistry* **2000**, *38*, 3211-3234.

(50) Morton, M.; Fetters, L. J. *Journal of Rubber Chemistry technology* **1975**, *48*, 359-409.

(51) Iatrou, H.; Hadjichristidis, N. *Macromolecules* **1992**, *25*, 4649-4651.

(52) Roovers, J.; Toporowski, P. M. *Macromolecules* **1983**, *16*, 843-849.

(53) Zhou, L.; Roovers, J. *Macromolecules* **1993**, *26*, 963-968.

(54) Zhu, Y.; Weidisch, R.; Gido, S. P.; Velis, G.; Hadjichristidis, N. *Macromolecules* **2002**, *35*, 5903-5909.

(55) Weidisch, R.; Gido, S. P.; Uhrig, D.; Iatrou, H.; Mays, J.; Hadjichristidis, N. *Macromolecules* **2001**, *34*, 6333-6337.

(56) Uhrig, D.; Mays, J. W. *Macromolecules* **2002**, In press.

(57) Oster, G.; Riley, D. P. *Acta Crystallographica* **1952**, *5*, 272-276.

(58) Helfand, E. *Macromolecules* **1975**, *8*, 552-556.

(59) Helfand, E.; Wasserman, Z. R. *Macromolecules* **1980**, *13*, 994-998.

(60) Krappe, U.; Stadler, R.; Voigt-Martin, I. *Macromolecules* **1995**, *28*, 4558-4561.

(61) Breiner, U.; Krappe, U.; Stadler, R. *Macromolecular Rapid Communications* **1996**, *17*, 567-575.

(62) Alward, D. B.; Kinning, D. J.; Thomas, E. L.; Fetters, L. J. *Macromolecules* **1986**, *19*, 215-221.

(63) Kinning, D. J.; Thomas, E. L.; Alward, D. B.; Fetters, L. J.; Handlin, D. L. *macromolecules* **1986**, *19*, 1288-1290.

(64) Weidisch, R.; Michler, G. H.; Arnold, M.; Fisher, H. *Journal of Materials Science* **2000**, *35*, 1257-1268.

(65) Weidisch, R.; Schreyeck, G.; Ensslen, M.; Michler, G. H.; Stamm, M.; Schubert, D. W.; Budde, H.; Horing, S.; Arnold, M.; Jerome, R. *Macromolecules* **2000**, *33*, 5495-5504.

(66) Weidisch, R.; Michler, G. H.; Arnold, M. *Polymer* **2000**, *41*, 2231-2240.

(67) Sakurai, S.; Sakamoto, J.; Shibayama, M.; Nomura, S. *Macromolecules* **1993**, *26*, 3351-3356.

(68) Holden, G.; Legge, N. R. In *Thermoplastic Elastomers*, 2nd ed.; Holden, G.; Legge, N. R.; Quirk, R.; Schroeder, H. E., Eds.; Hanser: Munich Vienna, 1996; pp 47-71.

(69) Dair, B. J.; Honeker, C. C.; Alward, D. B.; Avgeropoulos, A.; Hadjichristidis, N.; Fetters, L. J.; Capel, M.; Thomas, E. L. *Macromolecules* **1999**, *32*, 8145-8152.

(70) Velis, G.; Hadjichristidis, N. *Journal of Polymer Science: part A: Polymer Chemistry* **2000**, *38*, 1136-1138.

(71) Halasa, A. F.; Lohr, D. F.; Hall, J. E. *Journal of Polymer Science: Polymer Chemistry Edition* **1981**, *19*, 1357-1360.

(72) Bywater, S.; Mackerron, D. H.; Worsfold, D. J. *Journal of Polymer Science: Polymer Chemistry Edition* **1985**, *23*, 1997-2003.

(73) Funaki, Y.; Kumano, K.; Nakao, T.; Jinnai, H.; Yoshida, H.; Kimishima, K.; Tsutsumi, K.; Hirokawa, Y.; Hashimoto, T. *Polymer* **1999**, *40*, 7147-7156.

(74) Shinozaki, A.; Jasnow, D.; Balazs, A. *Macromolecules* **1994**, *27*, 2496-2502.

(75) Sakurai, S.; Hasegawa, H.; Hashimoto, T.; Hargis, I. G.; Aggarwal, S. L.; Han, C. C. *Macromolecules* **1990**, *23*, 451-459.

(76) Wolff, T.; Burger, C.; Ruland, W. *Macromolecules* **1993**, *26*, 1707-1711.

(77) Floudas, G.; Hadjichristidis, N.; Iatrou, H.; Pakula, T.; Fisher, E. W. *Macromolecules* **1994**, *27*, 7735-7746.

(78) Trask, C. A.; Roland, C. M. *Polymer Communications* **1988**, *29*, 332-334.

(79) Roland, C. M. *Macromolecules* **1987**, *20*, 2557-2563.

(80) Tomlin, D. W.; Roland, C. M. *Macromolecules* **1992**, *25*, 2994-2996.

(81) Gido, S. P. *Nature* **1999**, *398*, 107-108.

(82) Goldacker, T.; Abetz, V.; Stadler, R.; Erukhimovich, I.; Leibler, L. *Nature* **1999**, *398*, 137-139.